ANCIENT SOILS OF EARTH AND MARS

by

ADRIAN P. BROZ

A DISSERTATION

Presented to the Department of Earth Sciences
and the Division of Graduate Studies of the University of Oregon
in partial fulfillment of the requirements
for the degree of
Doctor of Philosophy

December 2022

DISSERTATION APPROVAL PAGE

Student: Adrian Broz

Title: Ancient Soils of Earth and Mars

This dissertation has been accepted and approved in partial fulfillment of the requirements for the Doctor of Philosophy degree in the Department of Earth Sciences by:

Dr. Josh Roering	Chairperson
Dr. Lucas C.R. Silva	Advisor
Dr. Carol Paty	Core Member
Dr. Matt Polizzotto	Institutional Representative

and

Krista Chronister	Vice Provost for Graduate Studies

Original approval signatures are on file with the University of Oregon Division of Graduate Studies.

Degree awarded December 2022

DISSERTATION ABSTRACT

Adrian Broz

Doctor of Philosophy

Department of Earth Sciences

December 2022

Title: Ancient Soils of Earth and Mars

Three to four billion years ago the surface of Mars may have been habitable. Ancient martian rocks that were subject to aqueous alteration in near-surface environments may store a record of this habitable paleoclimate, and they may also be favorable environments for the preservation of biosignatures. Some of the oldest altered rocks on Mars appear to be similar in mineralogy and geochemistry to ancient, buried soils (paleosols) on Earth. By using terrestrial paleosols as an analog for Mars, this dissertation seeks to constrain the organic preservation potential of martian paleosols. This is a first step towards understanding if putative martian paleosols should be considered high priority targets for *in-situ* drilling campaigns and sample return to Earth.

The objectives of this work were to a) identify the factors that have led to enhanced preservation of organic matter in terrestrial paleosols from throughout Earth's 3.7 billion year old geological record; b) determine if the mineralogy and alteration history of Eocene (33 million-year-old) paleosols from eastern Oregon can be identified with Mars rover-like instruments; and c) determine if trace amounts of organic carbon in the Oregon paleosols can be detected with evolved gas analysis (EGA), a technique currently employed by the NASA *Curiosity* Mars Rover to search for past signs of life on Mars. A data compilation of previously published organic matter content of paleosols spanning ~3 billion years of Earth history showed that soil redox

state before burial was a major factor that was associated with enhanced preservation of organic matter in paleosols. Chemically reduced paleosols were found to preserve organic carbon at abundances two to three orders of magnitude greater than oxidized paleosols. Next, evolved gas analysis, spectroscopy, and x-ray diffraction were determined to be suitable techniques for constraining the mineralogy and alteration history of 33-million-year-old paleosols from Oregon. Very low amounts of organic carbon (~0.01 wt. %) and fragments of organic molecules in oxidized paleosols were able to be observed with EGA, suggesting these techniques may be suitable for detecting low amounts of organic carbon in similar materials on Mars. This work indicates that putative paleosols / weathering profiles on Mars should be considered high priority targets for *in-situ* biosignature detection and eventual sample return to Earth.

CURRICULUM VITAE

NAME OF AUTHOR: Adrian Broz

GRADUATE AND UNDERGRADUATE SCHOOLS ATTENDED:

University of Oregon, Eugene, OR
California Polytechnic State University, San Luis Obispo, CA

DEGREES AWARDED:

Doctor of Philosophy, Earth Sciences, University of Oregon, Eugene, OR
Master of Science, Agricultural Soil Science, California Polytechnic State University, San Luis Obispo, CA
Bachelor of Science, Earth Science, California Polytechnic State University, San Luis Obispo, CA

AREAS OF SPECIAL INTEREST:

Planetary Geology

Astrobiology

Soil and Water Chemistry

Isotope Geochemistry

Botany and Plant Ecology

PROFESSIONAL EXPERIENCE:

Mars 2020 Perseverance Rover Postdoctoral Scientist, 2022 - present
Purdue University / NASA JPL

Mars Research Intern, 2019
Jacobs JETS contract / NASA Johnson Space Center

Graduate Teaching Fellow, University of Oregon, 2017- present
Soil-Plant-Atmosphere Laboratory

Graduate Student Research Assistant, California Polytechnic State University, 2014-2017; Soil and Water Chemistry Laboratory

GRANTS, AWARDS, AND HONORS:

Selected Participant, NASA International Astrobiology Summer School, Santander, Spain, 2022

Encompass Fellow, Soil Science Society of America, 2021

Graduate Student Research Grant, Geological Society of America, 2021

Graduate Student Research Grant, Clay Minerals Society, 2020

Roscoe G. Jackson II Award for graduate research in sedimentology, Geological Society of America, 2019

Graduate Student Research Grant, Society for Sedimentary Geology, 2019

Margaret Thayer Graduate Student Research Grant, University of Oregon, 2018

Outstanding Graduate Student Award, California Polytechnic State University, San Luis Obispo, 2017

PUBLICATIONS:

Broz, A., and Petersen., D.P. An Eocene (50-55 Ma) greenhouse climate recorded in nonmarine rocks of San Diego, CA, USA**.** *Geology* (In preparation).

Bradák, B., Kereszturi, A., **Broz, A.**, Gomez, C., Hyodo, M, Szeberényi, J., Medveďová, S. and Rostinsky, P. 2022. Magnetic properties of Pleistocene paleosols from loess successions and astropedological implications for Mars. *Icarus* (In review).

Broz, A., Aguilar, J., Xu, X., and Silva, L.C.R. 2022. Accumulation of radiocarbon in ancient terrestrial landscapes. *Nature Geoscience* (In review). Preprint link: https://doi.org/10.31223/X52P9B

Broz, A. and Silva, L.C.R. 2022. Pedogenic processes and the drying of Mars. *Nature Communications* (In review). Preprint link: https://doi.org/10.31223/X5NG9J

Broz, A, Clark, J.V., Archer, P.D., Sutter, B, Ming, D.W., Horgan, B.H., and Silva, L.C.R. 2022. Detection of organic carbon in Mars-analog paleosols with thermal and evolved gas analysis. *Journal of Geophysical Research: Planets* https://doi.org/10.1029/2022JE007340

Broz, A, Clark, J.V., Sutter, B., Ming, D.W., Tu, V., Horgan, B.H., and Silva, L.C.R. 2022. Mineralogy and diagenesis of Mars-analog paleosols from eastern Oregon, USA. *Icarus* 380: 114-128 https://doi.org/10.1016/j.icarus.2022.114965

Broz, A.**,** Retallack, G., Maxwell, T., and Silva, L.C.R. 2021. A record of vapour pressure deficit stored in wood and soil across biomes. *Nature Scientific Reports* https://doi.org/10.1038/s41598-020-80006-9

Chafe, O.E., **Broz, A.,** Anderson, R. O., Levinson, E.S., Farinacci, M.D., and L.C.R. Silva. 2021. The spatial and temporal domains of natural climate solutions. *Plant and Soil* (In review), Preprint link: https://doi.org/10.31223/X5CD2Q

Broz, A. 2020**.** Organic matter preservation in ancient soils of Earth and Mars. *Life* **2020**, *10*(7), 113; https://doi.org/10.3390/life10070113

Retallack, G., **Broz, A**., Lai, S.H., and K. Gardner. 2020. Neoproterozoic marine chemostratigraphy or glacioeustatic sea level change? *Palaeogeography, Palaeoclimatology, Palaeoecology* 562; https://doi.org/10.1016/j.palaeo.2020.110155

Retallack, G. and **Broz**, A. 2020. *Arumberia* and other Ediacaran–Cambrian fossils of central Australia. *Historical Biology* 2020 https://doi.org/10.1080/08912963.2020.1755281

Retallack, G., and **Broz**, A. 2020. Ediacaran and Cambrian paleosols from central Australia. *Palaeogeography, Palaeoclimatology, Palaeoecology* 560 https://doi.org/10.1016/j.palaeo.2020.110047

Retallack, G., Martin, J., **Broz**, A., N. Matthews and D. Walton. 2018. Late Pleistocene mammoth trackway from Fossil Lake, Oregon. *Palaeogeography, Palaeoclimatology, Palaeoecology* 496: 192-204. https://doi.org/10.1016/j.palaeo.2018.01.037

Broz, A., P. Verma, C. Appel, J. Yost and S. Hurley. 2017. Strawberry growth, nitrogen dynamics and nitrate leaching in vermicompost-amended media. *Journal of Compost Science and Utilization* 25: 194-205. https://doi.org/10.1080/1065657X.2016.1277806

Broz, A., P. Verma and C. Appel. 2016. Nitrogen dynamics of vermicompost use in sustainable agriculture. *Journal of Soil Science and Environmental Management* 7: 173-183. https://doi.org/10.5897/JSSEM2016.0587

ACKNOWLEDGMENTS

I was allowed unusual academic freedom to pursue a wide range of interdisciplinary projects during my graduate career, one of which is the focus of this dissertation. Many incredible humans contributed to the success of this project. From a fundamental standpoint, Dr. Briony Horgan's inspiring work on paleosols and ongoing mentorship played a major role in the direction and overall success of this dissertation.

I am grateful for Dr. Greg Retallack's guidance in support of this project, and am thankful for his deep knowledge of paleosols, a small fraction of which was passed to me during the course of this dissertation.

Drs. Elizabeth Rampe, Joanna Clark, Brad Sutter and Doug Ming at NASA Johnson Space Center provided constant guidance and expertise in support of this project. This work would not have been possible without their involvement.

My undergraduate and M.S. degree advisor Dr. Chip Appel showed me how incredibly fulfilling a life in science/academia can be. His unwavering guidance, patience and friendship, as well as "surf office hours" where we would go surfing and talk science, was integral for my academic and personal success. Chip also revealed to me the expansive world of soil and water chemistry, a gift for which I am forever grateful.

Much of this project would also not have been possible without the help of Barry Hugues, who on one occasion overnighted a 20 kg box of paleosol samples to Texas that had been left behind in Oregon. During the following days most of the analyses that compose Chapters 2 and 3 were performed on these samples.

I would also like to thank all the members of my dissertation committee who were always available for assistance and answering questions. Many thanks to Dr. Carol Paty, and members of her lab group including Joe Caggiano, Paul Regensberger, and Angela Olson. Dr. Lucas Silva was my pillar of support over the course of this dissertation. His expertise, passion, humor, and kindness were passed to me during my tenure in his incredible lab at the University of Oregon. As a direct result of this mentorship, I conclude this dissertation with a sense of exuberance and enthusiasm for the next chapter.

My fiancée and life partner Dr. Kendall Smith deserves the grandest of accolades for sharing with me a life in paradise, forever supporting me, and moving to Oregon during the course of this dissertation. My success is derived from her unique ability to stoke creativity, scientific curiosity, adventure, healing and focus.

I would be lost without the love, dedication, patience and motivation from my parents, Christine and Lawrence. Lastly, always remember it is a big world out there, folks!

This work is dedicated to my grandmother, Carmen Morán Broz

TABLE OF CONTENTS

LIST OF FIGURES

Figure Page

CHAPTER II

CHAPTER III

Figure Page

CHAPTER IV

LIST OF TABLES

Table Page

CHAPTER I

INTRODUCTION

Decades of space exploration have shown that Mars billions of years ago was a habitable place. Pedogenic (soil-forming) alteration of rocks and sediments with liquid water may have been widespread in the Noachian (4.1-3.7 billion years ago), which could have subsequently led to the formation of ancient, buried soils (paleosols) on Mars. On Earth, soils are highly habitable environments, and after rapid burial can also preserve organic carbon and other past signs of life (biosignatures) for millions or even billions of years. In addition to the preservation of biosignatures, the mineralogy and geochemistry of paleosols can also provide a detailed fingerprint of the climate conditions during formation. Therefore, targeting putative martian paleosols for future exploration may be useful for estimating the extent and duration of habitable conditions on Mars, and they may also be sites of enhanced organic matter preservation.

This dissertation is divided into two parts, the first of which is a literature review of the factors leading to enhanced organic preservation in terrestrial paleosols from the geological record on Earth (Chapter II), and the second being a field and laboratory study of Eocene (33-million-year-old) Mars-analog paleosols from eastern Oregon, USA (Chapters III and IV). Both approaches are a first step towards constraining the organic preservation potential of putative paleosols on Mars.

Dissertation Research

The objectives of this dissertation were to 1) identify the factors that have led to enhanced preservation of organic matter in terrestrial paleosols from throughout Earth's 3.7 billion year old geological record; 2) determine if the mineralogy and alteration history of

Eocene (33 million-year-old) paleosols from eastern Oregon can be identified with Mars rover-like instruments; and 3) determine if trace amounts of organic carbon in the Oregon paleosols can be detected with evolved gas analysis (EGA), a technique currently employed by the NASA *Curiosity* Mars Rover to search for past signs of life on Mars.

In order to identify the factors that can lead to enhanced organic carbon preservation in paleosols, I first performed a data compilation from previously published work that reported total organic carbon (TOC) in paleosols from the Holocene (~5 Ka) to the Archean (2.7 Ga) (Chapter II). I also gathered data on geochemical parameters of each paleosol profile where TOC was reported. These data included bulk chemical composition, molecular weathering ratios, redox state, clay mineralogy and abundance, and the degree of diagenesis, which allowed for evaluation of statistical relationships between paleosol TOC and geochemical/ mineralogical variables.

A major finding of Chapter II is that paleosol redox state before burial was a major factor related to enhanced preservation of organic carbon. Other variables that were related to high TOC values in paleosols were clay mineralogy and abundance, sulfur speciation and abundance, and the degree of diagenesis. However, it was determined redox state before burial, inferred by the ratio of reduced iron to oxidized iron (FeO/Fe_2O_3) in bulk samples, was most often associated with exceptional organic preservation in paleosols. For example, Histosol paleosols (strongly reducing swamp soils), which are commonly associated with coal seams in Earth's geological record, have high FeO/Fe_2O_3 ratio (>1) indicative of strongly reducing conditions before burial, and they commonly preserve organic carbon at abundances greater than 35 wt. %. Additionally, an Archean (2.7) Ga paleosol profile that appears to have formed under an anoxic atmosphere had TOC of 0.4 wt. %. The surface horizon (e.g., the paleosurface) had higher TOC relative to

deeper layers in the profile, suggesting these paleosols, like modern soils, are enriched towards the surface (A) horizon. Exceptionally preserved filamentous organic matter in this profile is thought to have been derived from cyanobacterial mats living on the soil surface between 2.6 and 2.7 billion years ago. Further evidence for oxidation state as a first order control on paleosol TOC was the significant positive relationship between the FeO/Fe_2O_3 and TOC content of Permian (261 Ma) and Triassic (250 Ma) paleosols from Antarctica. Across ~35 samples from three individual paleosol profiles, samples with higher FeO/Fe_2O_3 had significantly higher amounts of TOC. There was a marked increase in the slope of the regression at $FeO/Fe_2O_3 = 1$ that was associated with an increase in TOC values to > 0.1 wt. %, suggesting that $FeO/Fe_2O_3 \sim 1$ may be a threshold associated with enhanced organic preservation in paleosols containing Fe-bearing clays and/or oxyhydroxides. These findings thus achieved the objective to identify several factors related to enhanced organic preservation in paleosols. Chapter II is titled "Organic matter preservation in ancient soils of Earth and Mars" and is published in *Life* (2020). I am the sole author of this publication.

Chapter III performed a field and laboratory study of 33-million-year-old paleosols from the Eocene-Oligocene John Day Formation in Eastern Oregon, USA, which were selected as an analog for putative paleosol sequences on Mars. A major objective of this work was to determine if instruments calibrated to operate like those onboard the NASA *Curiosity* Mars Rover could constrain the mineralogy and alteration history of paleosols. This objective provides the first comprehensive analysis of terrestrial paleosols with a suite of Mars-rover instruments. For this work, performed in the field and at NASA Johnson Space Center (JSC), we analyzed paleosol samples with visible/near infrared (VNIR) spectroscopy, an x-ray diffraction (XRD) instrument calibrated to operate like the CheMin instrument onboard the *Curiosity* Mars Rover, and an

instrument calibrated to operate like the Sample Analysis at Mars Evolved Gas Analysis (SAM-EGA) instrument also onboard the *Curiosity* Mars Rover. Handheld VNIR spectroscopy of three different paleosol profiles showed strong absorbance features that were diagnostic of mixtures of Al and Fe smectite, hematite, and zeolites. A clay mineral "doublet" absorbance feature between 2.20 and 2.25 microns was noted in most samples and was possibly related to isomorphic substitution of Fe for Al in the crystalline structure of phyllosilicates that formed via pedogenic weathering.

X-ray diffraction performed at NASA JSC confirmed VNIR detections of clay minerals, Fe oxides and hematite. XRD diffractograms showed strongly crystalline clay minerals dominated all samples (Figure 7, Table 1). Major phases identified in all samples (> 5 wt. %) were montmorillonite (Al smectite) and nontronite (Fe smectite) while minor phases (< 5 wt. %.) identified from patterns in all samples were clinoptilolite, cristobalite, Opal-CT, quartz, andesine, orthoclase, gypsum and jarosite. The zeolite mineral clinoptilolite was identified from patterns in all paleosol samples, which likely formed from post-burial alteration of volcanic glass, weakly crystalline smectite, or other poorly ordered phases during Miocene-age burial recrystallization. Lastly, when the samples were analyzed with a SAM-EGA analog instrument, the evolutions of volatiles (H_2O and SO_2) were consistent with mixed amounts of Al and Fe smectite and small amounts of sulfates and/or sulfides. This result confirmed the VNIR and XRD detections of the same phases and thus achieved the objective of this Chapter to determine if the mineralogy and alteration history of Mars-analog paleosols can be evaluated with Mars-rover-like instrumentation. Chapter III is titled "Mineralogy and Diagenesis of Mars-analog Paleosols from Eastern Oregon, USA and is published in *Icarus* (2022). It is coauthored by me, Joanna Clark, Brad Sutter, Doug Ming, Valerie Tu, Briony Horgan, and Lucas C.R. Silva.

The final chapter of this dissertation (Chapter IV) dives deeper into the SAM-EGA analysis of the Oregon paleosol samples. In addition to H_2O and SO_2, the SAM-EGA analog instrument at NASA JSC can monitor evolutions of other volatiles such as CO_2 and organic fragments that form as a result of the thermal decomposition of organic carbon. A major goal of Chapter IV was to determine if the SAM-EGA analog instrument can detect low abundances of organic carbon (~0.01 wt. %) in strongly oxidized paleosol samples. A secondary goal was to determine if the paleosurface horizons of each profile had significantly higher TOC relative to deeper layers, a trend that is common in modern soil profiles. In order to constrain the age and sources of organic carbon composing the paleosol TOC pool observed with EGA, a third goal was to perform radiocarbon dating of bulk samples, followed by the application of a two-endmember isotopic mixing model for radiocarbon activity to estimate the amount of modern organic carbon in ancient paleosol samples. We determined that the Oregon paleosols contain trace amounts of organic carbon (0.008 - 0.04 wt. %) that was able to be detected and quantified by a SAM-EGA analog instrument. A major result of Chapter IV was that the paleosurface horizons of each individual profile (e.g., A-horizon) were enriched in organic carbon content relative to deeper layers in the profile, similar to a modern soil profile. Lastly, radiocarbon dating of bulk samples showed calibrated radiocarbon dates of ~7,000- 14,000 years before present, suggesting there had been inputs of recent/modern organic carbon to the paleosol organic carbon pool. A two-endmember mixing model suggested these dates could be explained by the mixing of small amounts (0.5-3.5%) of modern organic carbon with larger amounts of potentially ancient radiocarbon-dead organic material. These results achieved our final objective to determine if low levels of organic carbon in Mars analog paleosols can be detected with evolved gas analysis. Chapter IV is titled “Detection of organic carbon in Mars-analog paleosols with

thermal and evolved gas analysis" and is published in *The Journal of Geophysical Research: Planets* (2022). It is coauthored by me, Joanna Clark, Brad Sutter, Doug Ming, Briony Horgan, Paul Douglas Archer, Jr., and Lucas C.R. Silva.

CHAPTER II
ORGANIC MATTER PRESERVATION IN ANCIENT SOILS OF EARTH AND MARS

Published as A. P. Broz, Organic Matter preservation in ancient soils of Earth and Mars. *Life*. **10** (2020), doi:10.3390/life10070113.

Introduction

Paleosols are ancient, fossil soils, created by removal from their soil-forming factors, either because of change in those factors, or by burial. Modes of burial range from the deposition of volcanic ash, lava flows, rapid sedimentation from flooding, or landslides. Paleosols are a geological record on Earth of the atmospheric composition, climate, topography and organisms present before soil burial [1]. Importantly, some of the oldest fossils of life in terrestrial environments are found in paleosols [2,3]. Soils and life have coevolved with one another over geological time scales, because organisms alter the structure, mineralogy function, and morphology of the soil. Modern soils are saturated with a diverse array of microscopic life, often averaging 10^{10}-10^{11} bacterial cells and 10^{3} and 10^{4} species per gram of soil [4]. Life leaves trace or body fossils in paleosols, and other biosignatures like isotopically light carbon [5] and complex organic matter [2] as evidence of their ancient relationship with soils, which may have extended well back into the Archean [6–9]. The intrinsic value of paleosols is now realized across the disciplines of soil and planetary sciences: Paleosols on Mars were recently named a high priority location for in-situ biosignature investigation [10,11] and Mars Sample Return [12,13].

Recently there has been increasing consideration of the abiotic pathways of pedogenesis (soil creation) on planets other than Earth. These include chemical alteration through leaching of layered sedimentary rocks in subaerial settings on Mars [14–16] and a variety of photochemical

reactions that create soil minerals [17,18]. If life does not define soil, then the key questions now are when and how did life appear in soils, and what evidence for life can be preserved in paleosols? Some paleosols such as Histosols and gleyed Entisols preserve organic matter beautifully with microscopic details of plant structure [19], but oxidized paleosols contain much less organic carbon than comparable modern soils [1].

The purpose of this paper is not to determine the nature and properties of organic matter in paleosols of Earth, because one cannot determine the nature of the inputs (e.g., type and amount) of organic materials from the study of paleosol organic matter alone. Instead, the focus here is on the "results" of life on land, which includes the emplacement and storage of highly recalcitrant (resistant to decay) organic matter in paleosols for millions or even billions of years. More specifically this paper is a first step to prioritize and select locations within potential paleosols for in-situ biosignature investigation (with *Curiosity* Rover, Mars 2020 *Perseverance* Rover; ExoMars 2020) and Mars Sample Return.

Whether molecular in size or larger, biosignatures are at the mercy of numerous preservation and degradation mechanisms, most often regulated by redox chemistry, the surfaces of minerals, diagenesis, and depth in the soil profile. This review is a first step to identify the factors responsible for organic matter preservation and degradation in Earth's paleosol record from the Pleistocene to the Archean and seeks to provide insight into similar phenomena which may influence organic matter storage in Noachean (4.1-3.7 Ga) subaerial paleoenvironments on Mars.

Paleosols on Mars?

There is mounting evidence that paleosols may be preserved in the geological record on Mars [14,20–24]. One problem inhibiting discussion of paleosols on Mars is that they could not

be true soils because a biological component has not yet been proven. However, the Soil Science Society of America in 2017 updated their definition of soil to include abiotic soils on planetary bodies: “The layer(s) of generally loose mineral and/or organic material that are affected by physical, chemical, and/or biological processes at or near the planetary surface and usually hold liquids, gases, and biota and support plants”[25]. This updated definition reflects a modern understanding of abiotic pedogenic pathways, which include subaerial low temperature water-rock interactions (hydrolysis), physicochemical weathering phenomena, and photochemical creation of soil minerals [17], all of which have been documented on Mars [14,26]. **Table S1** discusses Mars-relevant pedogenic features and scales of observation (in-situ to orbital).

Mars is cold, dry and barren today, but there is extensive evidence that liquid water was stable on the surface of the planet in the geologic past. Geomorphic evidence of liquid water includes deltas, valley networks, and dendritic channels [27] compliment *in-situ* and orbital detections of phyllosilicates and other hydrated minerals and indicate surface weathering occurred under an early Mars climate. The conditions for surface weathering were better in the past than on Mars today [14,28]. Several climate models favor a wet but cold surface on early Mars [29], but the volumetric and temporal occurrence of liquid water markedly decreased [30]. Thus during most of Martian history only microscopic liquid water may have been present [31,32], though chemical alteration involving perchlorate brines and microscopic liquid films may have been common [33,34]. Importantly, ultraviolet and ionizing radiation can degrade biosignatures at the surface [35] and subsurface [36] of Mars, respectively, and surface oxidizing salts including perchlorate can encourage complete combustion of organic carbon during thermal and evolved gas analysis [37,38], which is currently the only method employed for the detection of organic carbon on Mars.

Both in-situ [39,40] and orbital remote sensing [22] techniques have been employed for the investigation of sedimentary rocks and potential paleosols on Mars. In-situ examinations focus on geochemical interrogation of samples (e.g., Mars Science Laboratory (MSL) instrument suite onboard *Curiosity* rover), while remote sensing techniques [41] examine mineralogical reflectance and absorbance spectroscopy of the Martian surface, primarily in the visible/near infrared (VNIR) range [15,20]. Hawaiian surface weathering studies and speculation about the Martian climate led Ming et al. (1988) to predict the presence of kaolinite on Mars, which has now been confirmed from orbit [22] and from *in-situ* x-ray diffraction [42]. Chemical analysis and imaging of a late Noachean (3.7 Ga) potential paleosol in the Sheepbed mudstone at Yellowknife Bay, Gale Crater reveals phosphorus depletion, vesicular structure, potential periglacial sand wedges, nodularized instead of crystalline sulfate grouped into a gypsic (By horizon), and ptygmatic folding of a deep sulfate dike, which are compatible with soil formed under a hyperarid frigid climate and later buried by approximately 5 km of overburden [26]. However, the interpretation of this unit as a potential paleosol has been disputed by MSL sedimentologists, who argue the Sheepbed mudstone is a lacustrine sedimentary deposit with subsequent diagenetic alteration, which are consistent with the observed chemical and physical features of the unit.

Sequences of candidate paleosols can also be observed from orbit with visible/near infrared spectroscopy (VNIR). The Compact Reconnaissance Spectrometer for Mars (CRISM, [41]) onboard the Mars Reconnaissance Orbiter is a high-resolution (~18 m/pixel) VNIR (0.35-3.92 μm) imaging spectrometer which has detected what appear to be dioctahedral phyllosilicates in thousands of locations across the surface of the planet [14]. Noachean (4.1-3.7 Ga) terrains at Mawrth Vallis have vertical sequences of dioctahedral phyllosilicate clays which resemble

sequences of paleosols on Earth [15]. Paleosols are generally recognized based on clay mineralogy and the stratigraphic distribution of clay minerals, which are sensitive to VNIR spectroscopy [20,43]. Fortunately, many pedogenic minerals are recognized with VNIR spectroscopy due to strong absorption of the overtones of SO_4^{2-}, CO_3^{2-} and OH^-, and combinations of H_2O and CO_2 [44]. Common soil and paleosol minerals include hydrated dioctahedral phyllosilicate clays (montmorillonite, illite, nontronite) and amorphous or poorly crystalline phases (e.g., imogolite, ferrihydrite and allophane). Dioctahedral Fe/ Mg smectite clays including montmorillonite have characteristic absorption features at 1.9 and 2.3 μm [45,46], and similarities between terrestrial paleosols and subaerial clay deposits on Mars are known from these absorbance features **(Figure 1).**

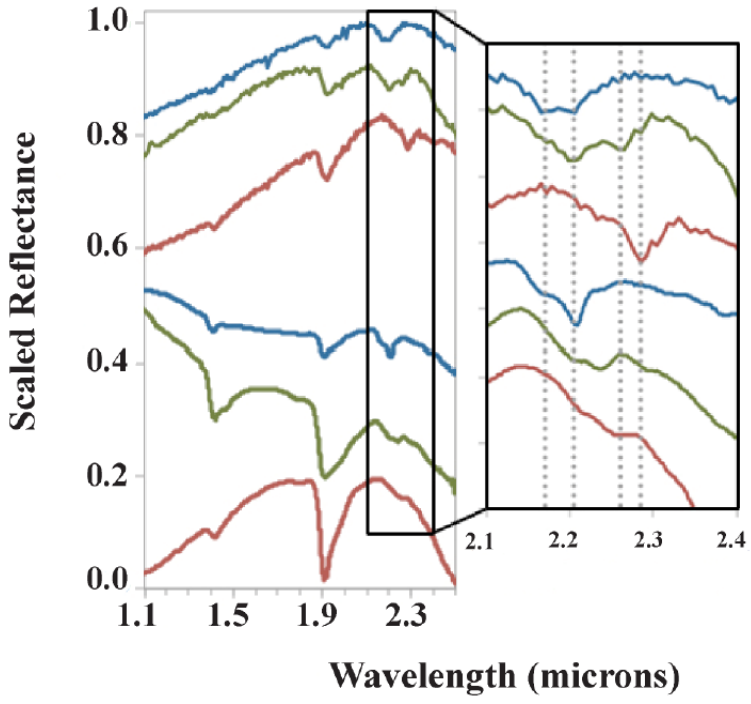

Figure 1. Spectral comparisons of minerals in terrestrial and Martian subaerial paleoenvironments. Compact Reconnaissance Spectrometer for Mars (CRISM) spectra (FRT863E) from Mawrth Vallis compared with laboratory spectra of a volcaniclastic paleosol from the Oligocene (33 Ma) John Day formation in Oregon with enlarged area to right (adapted from [20]). Top three: CRISM kaolinite, Al/Si doublet, and nontronite dominated spectra. Bottom three: John Day paleosol spectra with varying contributions of kaolins/illite/smectites/silica as interpreted from both near and thermal IR spectra (adapted from [20]).

Orbital remote sensing of the Martian surface has shown stratigraphic distribution of what appear to be pedogenic minerals similar to those observed in terrestrial sequences of paleosols or leaching profiles **(Figure 2)** [20,24,47,48]**.** Potential paleosol sequences in the Arabia Terra region have been documented, and feature layered dioctahedral clay units up to 200 m in thickness [14,23,48], now known as the Mawrth Vallis Group [46]. Some areas show spectral evidence of sediments so intensely weathered they resemble lateritic soils because of inferred abundances of oxides and Al-rich clays [49]. Post-depositional leaching profiles rarely exceed 100m in thickness, but the upper limit on the thickness of paleosol sequences on Earth may be 9 km in paleosols of the Neogene Siwalik Group of India and Pakistan [1]. One hypothesis to explain the exceptional thickness of the Mawrth Vallis clays is that it may be a Fe/Mg-smectite paleosol sequence formed under a semi-arid climate, overlain by a subsequent and thinner Al-rich leaching profile, and topped with an igneous caprock [23,24]. This stratigraphy is consistent with current climate hypotheses for early Mars, including a Noachian hyperarid frigid paleoclimate, alternating with warmer and wetter conditions [14,26] or the possibility of a wetter but cold surface with a warm subsurface [50,51]. Additional evidence for widespread aqueous surface weathering on Mars is known from targeted CRISM observation of Al clays (~1 m thickness) overlying Fe/ Mg smectite (>10 m thickness) clays near Valles Marinerias, which could have formed from leaching by several hundred meters of highly acidic fluids [48]. More details may be forthcoming from the ExoMars 2020 rover landing at at Oxia Planum, which is a westward extension of the lowest portions of the Mawrth Vallis stratigraphy, and host to one of the largest clay units on Mars [23,52,53].

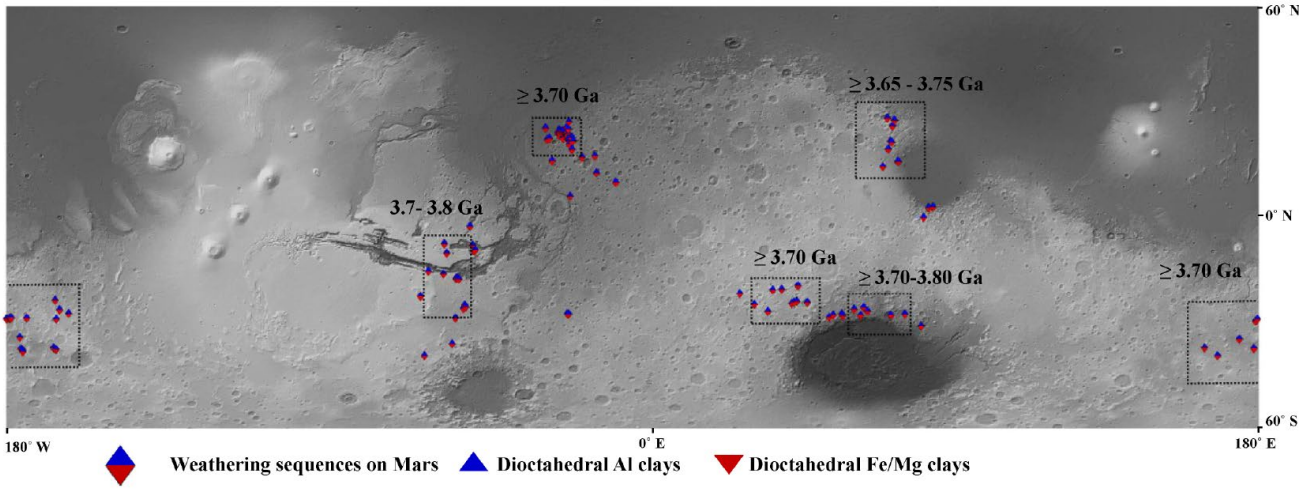

Figure 2. Vertical stratigraphies of dioctahedral Al overlying Fe/Mg clays from CRISM spectra indicating possible weathering sequences or paleosols (e.g., Al clays stratigraphically above Fe/Mg clays and never in the opposite sequence) across the surface of Mars, with boxes indicating the regions for which the likely age of weathering is constrained (adapted from [23]).

One feature of Mars that both in-situ and orbital investigations observe is the widespread abundance of phyllosilicates **(Figure 2).** Phyllosilicates probably formed during transient warm and wet conditions during the Noachian (4.1 – 3.7 Ga), and are common across the surface of the planet [15,47,54]. Furthermore, these clays are not from deeply buried sedimentary rocks because they show hydration and crystalline disorder incompatible with deep burial diagenesis [55].

On Earth, clay mineralogy is often determined by factors other than general temperature and water conditions, most notably the composition of the parent material. Soils derived from the weathering of ultramafic rocks like serpentinite can exhibit mixed di-trioctahedral clay composition [56]. Trioctahedral serpentine, although uncommon, has been detected on Mars [57] though trioctahedral clays have not been observed in layered vertical sequences [14]. Hence, potential paleosol sequences on Mars exhibit dominant spectral signatures of dioctahedral phyllosilicates in layered vertical profiles and do not have signatures of trioctahedral

phyllosilicates [22,46], suggesting that parent materials of these potential paleosols may have lacked an ultramafic component.

Two hypotheses to explain the formation and distribution of phyllosilicate clays on Mars are (1) subsurface hydrothermal activity and/or diagenesis [58–60] and (2) surface chemical weathering [10,14,23,61]. Hydrothermalism and/or diagenesis most often forms trioctahedral clay deposits exhibiting lateral variations in Al and Fe/Mg smectites intermixed with chlorite, serpentinite, talc and zeolite [14]. In contrast, dioctahedral smectite-rich outcrops with extensive vertical profiles of Al-smectites overlain by Fe/Mg smectites and then amorphous materials suggest subaerial formation in poorly-drained surface environments [14], consistent with pedogenesis.

The study of fossil soils has historically drawn upon features of modern soils for the interpretation of paleosols and paleoenvironments, including the unique geochemistry of soils, soil horizons, soil structure, and fossil root traces [1]. Because many paleosols are found in sedimentary rocks, and constitute alterations after deposition, formation of paleosols in sedimentary rocks has traditionally been considered early diagenesis. This is distinct from late diagenesis, which is alteration after burial. Soils also are subject to alteration shortly after burial under low confining pressures and still in communication with groundwater and air, which need to be distinguished from deep burial diagenetic and metamorphic alterations; however, there appears to be an impressive lack of diagenetic maturation of chemical sediments across the surface of Mars [55]. Common diagenetic alterations to soils and their effects on indigenous organic matter preservation are outlined in the following paragraphs and provide guidelines for investigation of biosignatures in subaerial paleoenvironments of Mars.

Burial decomposition of organic matter

Many paleosols have significantly less organic carbon than their modern soil counterparts **(Figure 3)**. The loss of paleosol organic carbon is facilitated by aerobic microbial decomposers that inhabit the overlying burial layer as part of the ecosystem forming soil on the sediment that buried the soil, or by facultative aerobic microbial communities which persist in the original soil after burial [1]. Both communities metabolize organic C to CO_2, and are significant contributors to the decomposition of organic matter in paleosols. Other losses of organic matter may occur during deep burial and the generation of oil and gas, or after paleosol exhumation and exposure to photodissolution of organic matter [17], which in modern soils causes rapid losses up to several percent of soil organic matter in the top 10 cm over 10^1 - 10^2 yrs [62].

Burial decomposition of organic matter is especially obvious in Neogene (20 - 2.5 Ma) paleosols which are sufficiently similar to modern soils for comparison [1,63,64]. Despite the loss of organic matter, paleosols still show surface or shallow subsurface enrichment of organic carbon **(Figure 3).** Burial decomposition of organic matter is attenuated in soils that formed under reducing and waterlogged conditions, such as Permian (254 Ma) [65] and Oligocene (33 Ma) [66] coals, which are Histosols in the U.S Soil Taxonomy.

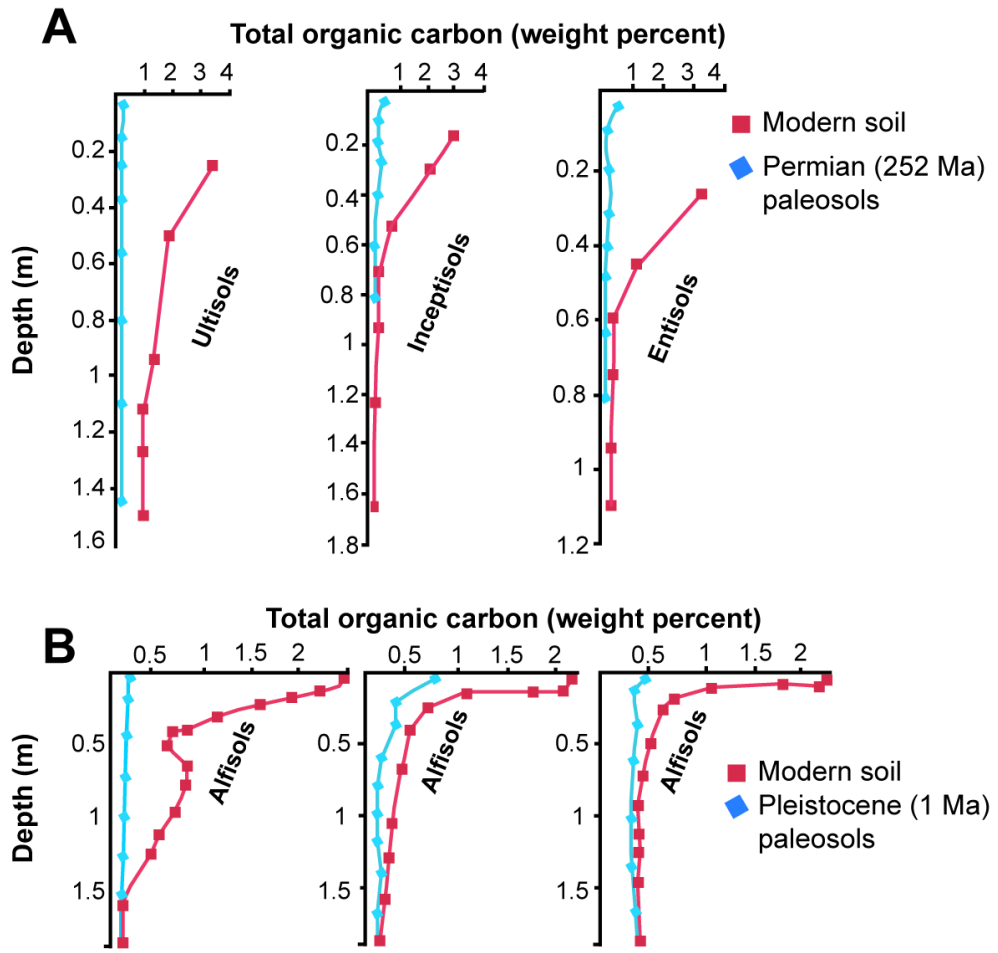

Figure 3. Depth profiles showing burial decomposition of organic matter in Permian (A) and Pleistocene (B) paleosols, and comparisons to modern soils. (A) Permian (252 Ma) paleosols from Graphite Peak, Antarctica (blue lines) and comparison with modern soil equivalents (red lines); (B) Pleistocene (0.2 - 1 Ma) paleosols (blue lines) compared to overlying modern soils (red lines) from the Midwest United States (Adapted from [1])

Illitization of smectites

A common diagenetic alteration of paleosols is the burial-induced conversion of smectite to illite [67]. Diagenetic conditions that encourage illitization (1.2–3.2 km overburden and 55–100° C) result in loss of cations other than potassium (Ca^{2+}, Mg^{2+}, Na^{+}) in expelled formation waters that would presumably also carry away organic matter. Illitization of smectite kinetics is partly controlled by temperature, but also by availability and thus ion activity of potassium and ammonium, which are rate-limiting [68].

The crystal structure and surface charge of soil smectites encourages the formation of organo-mineral complexes [69], which are presumably altered or removed after illitization. Some paleosols may have been originally illitic in composition, like some desert soils of regions with strong seasonality effects, and lower productivity soils of the Paleozoic and Precambrian may have been illitic in composition [70]. However, mounting evidence from laboratory studies [71–73] and paleosol observations [70,74] suggest that illitization of smectite is common in the geological record.

It is commonly assumed that solid state-transformation or dissolution–recrystallization reactions (e.g., Ostwald ripening, the minimization of free energy by formation of progressively larger crystal faces) drive the smectite-illite conversion [71] but the presence of organo-mineral complexes, or microbes themselves, may influence illitization. The maturation of organic matter has been implicated in accelerating the conversion rate of smectite to illite by increasing the Gibbs free energy of illite growth [75]. Microbial mediation of illitization in dioctahedral smectites has been documented [73] and the desorption or decomposition of organic matter adsorbed in smectite interlayers at temperatures above 350° C may control the degree of smectite illitization [71]. Similarly, common organic acids like acetate and oxalate can liberate Al and K ions to pore fluids by dissolution of smectites, K-feldspar and muscovites [72]. The associated pH changes, along with increased amounts of K in pore solutions, have been documented to partially control smectite illitization in laboratory studies [71]. Thus organic carbon itself may influence the degree of alteration in paleosols subject to burial temperatures above 200° C.

Certain clayey paleosols exhibit resistance to illitization of smectite. Clay-rich (> 80 wt % smectite) Alfisols and Inceptisols of Oligocene (33 Ma) age from the middle Big Basin Member of the John Day formation in eastern Oregon [66] have resisted illitization despite burial

by 1 km of overburden, likely aided by high clay content **(Figure 4).** Strikingly, the Inceptisols (Yellow paleosols, **Figure 4)** forming under reducing conditions have black iron manganese nodules (up to 1 m diameter) in subsurface (Bg) horizons, which are typical of seasonally waterlogged modern soils (Aquepts) and preserve higher amounts of organics relative to the bulk soil matrix. A lack of diagenetic illitization in these paleosols may be related to the preservation of these iron manganese nodules. Stratigraphically above, amorphous-rich (> 30 wt %) and less clayey (< 60 wt %) Aridisols and Andisols of the late Oligocene (26 Ma) Turtle Cove member show evidence of severe diagenetic alteration, including illitization of smectites [20] and celadonization from Ostwald ripening of an iron-rich smectite, exhibited by striking lime-green color of these paleosols. These green paleosols exhibit more extensive burial illitization relative to older and more deeply buried paleosols, because they were Andisols with unstable, non-crystalline colloids from weathering of vitric volcanic ash, unlike the smectite paleosols lower in the succession [66]. Therefore, certain clay-rich soils may be more resistant to diagenetic alteration relative to less clayey paleosols, even when buried by upwards of 1 km of overburden.

Figure 4. Early Oligocene (33 Ma) Mars-relevant paleosols in the middle Big Basin Member of the John Day Formation, eastern Oregon, USA. Repeating sequences of yellow clayey soils (Inceptisols) rich in Al-smectite formed under chemically reducing conditions and have horizons of abundant large (up to 1 m diameter) black iron manganese nodules associated with organic matter, while red soils (Alfisols) with abundant Al smectite and Fe oxides formed under oxidizing, well-drained conditions. Both paleosols exhibit minimal or absent illitization of smectite

Type, structure and function of organic matter in modern and fossil soils

A wide variety of organic compounds with variable structures, sizes, functions and reactivities have been documented in soils and paleosols. In modern soils, soil organic matter is a continuum of organic fragments that are progressively decayed by soil decomposers [76,77] which are then selectively preserved and altered after burial in paleosols. Progressive decreases in molecular size increases the number of polar and ionizable functional groups, thus increasing solubility in water of soil organic matter [77]. Progressive decay to smaller molecules also encourages sorption of organic matter to mineral surfaces which often leads to long-term recalcitrance [78]. However, many differences exist between the types of organic matter in soils and paleosols. The following paragraphs identify these differences and discuss implications for organic carbon preservation on Mars.

In the modern soil environment a continuum of organic molecules exists, which are variable in size, structure, function, reactivity, and resistance to degradation [77]. The largest of these pools is fragments from plants and microbial tissues which are predominantly composed of carbohydrate C, with lesser amounts of protein, lignin, and alkyl-C. Smallest and most "recalcitrant" are chemical structures dominated by alkyl-C [77]. Such recalcitrant compounds include long-chained *n*-alkanes with predominant odd-over-even chain length which are considered biomarkers of land plant leaf waxes [79].

Carbon from microbial biomass and/or metabolites can compose a high proportion of the total organic carbon in paleosols. Biomarker ratios have been used to examine the proportion of C derived from plant versus microbial compounds in modern soils [80] and paleosols [78]. Quaternary (< 2.5 Ma) paleosols typically have relatively low amounts of organic matter from plant biopolymers and instead a dominance of N compounds and carbohydrates from microbial

cells [81]. Biomarkers of chitin are abundant in Quaternary paleosols, a common cell wall component of insects and fungi, known from the presence of 3-acetamidofuran, 3-acetamide-5-methylfuran, 3-acetamido-2-pyrone and oxazoline compounds [81].

The clay-size fraction of modern soils [82] and Holocene paleosols [78] is dominated by aliphatic compounds from plant biomass, microbial biomass and /or metabolites, which are considered highly recalcitrant [83]. Holocene (~15 Ka) paleosols buried by loess in the Midwest of the United States have clay-size fractions with higher proportions of aliphatic compounds from microbial biomass (n-C_{14} alkanoic acid) relative to the overlying modern soil [78]. Biomarkers of the clay-sized fraction of much older Devonian (360 Ma) paleosols from Russia show organic carbon (0.5 – 5 wt %) composed mainly of carbon from aryls, acetyls and O-alkanes [64]. Selective preservation may be a result of paleosol mineralogy: smectite-dominated mineral matrices appear to preferentially preserve aliphatic structures compared to kaolinite or palygorskite dominated matrices [64]. The clay-size fraction of smectite-rich potential Martian paleosols thus offers the tantalizing prospect of being a favorable location for the retention of indigenous and highly recalcitrant organic carbon. However, exposure to ionizing radiation at the Martian surface and subsurface (0 - 500 cm) [36] can degrade organic carbon and other biosignatures like microbial carotenoids [84]. The duration of surface exposure and depth in the profile should be strongly considered when determining a sufficient location to sample the clay-sized fraction of potential Martian paleosols.

Broadly, paleosols preserve highly recalcitrant organic carbon with a significant fraction derived from microbial biomass (e.g., iso-Alkanoic acids, [80]) but this does not include Histosols, which as paleosols offer exceptional preservation of plant-derived organic matter as coal seams. More likely to be encountered on Noachean (4.1-3.7 Ga) terrains of Mars are Fe/Mg

smectite-rich paleosol sequences with evidence of variable redox conditions [14] which are now considered a potential high-priority target for in-situ biosignature detection [11] and Mars Sample Return [12,13]. However, it is important to note that exogenous organic carbon could have been delivered to the surface of early Mars by interplanetary dust particles, and could be a significant component of Noachian and pre-Noachian sediments [85].

The nature of organic matter in Precambrian (> 541 Ma) paleosols

For the first two billion years of life on Earth, the main organisms contributing to the terrestrial organic carbon pool were microbes and microbial consortia, not plants. Microbes have left a record in organic carbon with a variety of life-like isotopic ratios in Precambrian paleosols [5,8,86,87], which indeed may be the best analogs for potential Martian paleosols because they probably formed in the presence of microscopic organisms [88]. There are relatively few studies about the nature and composition of organic matter in Precambrian and older paleosols, and more research is warranted. However, it is clear that soil formation during the Precambrian probably involved a biological component, in contrast to speculation that Precambrian terrestrial weathering proceeded exclusively as an abiotic process [74].

Paleosols that formed after the evolution of land plants in the Ordovician (~470 Ma) were modernized by plant inputs of organic matter. In modern soils, a significant proportion of plant organic matter passes through microbial biomass before becoming recalcitrant soil organic matter [89]. In any case, the organic matter in Precambrian paleosols is derived from a diverse suite of terrestrial microorganisms. Signatures of life in these ancient subaerial environments are

known from isotope ratios, biomarkers and / or microfossils of terrestrial organisms, including cyanobacteria [90], actinobacteria [5,91,92], methanogens [6], and fungi [93,94].

Precambrian (> 541 Ma) paleosols on Earth have been subject to significant alteration after burial. Alterations include metamorphism [95], deformation [96], hydrothermal graphitization during serpentinization [8], illitization of smectite [67], and burial decomposition of organic matter [97]. Precambrian metamorphosed paleosols have been confused with upward-fining fluvial sequences, mudflow deposits, fault mylonites, marine hardgrounds, ash beds, or zones of groundwater or hydrothermal alteration [5,70]. Fortunately, there is no evidence of metamorphic alteration to potential paleosols at Gale Crater or possible sequences of paleosols at Mawrth Vallis on Mars [22,26,55]. Noachian surface paleoenvironments on Mars may therefore offer exceptional preservation of biosignatures.

Factors influencing organic matter preservation in paleosols

Redox chemistry

The most obvious control on organic matter preservation and degradation in paleosols is the redox state of the bulk soil prior to burial, especially evident from coals. Histosols are organic-rich soils with thick peaty horizons that typically form in low-lying, swampy, and boggy areas with a shallow groundwater table, predominantly under anoxic and reducing conditions (Eh < -100 mV). Upon burial these soils form coal seams, retaining organic carbon in amounts similar to the original soil (> 25 wt % TOC), suggesting prolonged conditions that limit burial decomposition of organic matter. Microbial degradation is retarded under perpetually reducing conditions because anaerobic decomposition of organic carbon is much slower than aerobic

decomposition. As is common with shallow or deep marine black shales, anoxic conditions of paleosols prior to burial provide a first order control on the preservation of organic matter.

Archean (2.3 Ga) paleosols with prominent reduced horizons from an anoxic atmosphere have organic matter concentrations ranging from 0.014-0.25% in the upper 2 m [74], possibly from microbial crusts [88,92], suggesting that clayey, poorly-drained soils preserve organic matter over geologic time scales [11]. Similar anoxic atmospheres may have been the rule for Mars over all of its known history [26], but the oxidation state of an early Mars atmosphere is not well constrained [28]. It is highly unlikely that paleosols as rich in organic matter as coals will be discovered on the surface of Mars, given satellite reconnaissance so far [46], but discovery of carbonaceous layers in boreholes is possible.

Molecular weathering ratios are a useful tool for estimating the redox state of a paleosol. The molecular ratio of ferrous to ferric iron (FeO / Fe_2O_3) can serve as a proxy for bulk redox state of a soil prior to burial [1]. Paleosols that formed under well-drained and strongly oxidizing conditions (Eh > +600 mV) have a characteristic FeO / Fe_2O_3 ratio of < 1. Variable redox conditions have FeO/Fe_2O_3 of ~ 0.5 - 1, while waterlogged soils of coal measures (Eh < -25 mV) have a FeO/Fe_2O_3 ratio of > 1, indicating prolonged anoxic conditions. These chemically reduced paleosols can often have orders of magnitude more organic carbon (TOC > 1 wt %) relative to oxidized paleosols. Soils of intermediate redox status (Eh ~ 0 mV) may have experienced partial water logging or periodic flooding [1]. The influence of variable redox state on organic preservation in paleosols is not well understood, but it has been shown that certain types of organic matter can be preserved within the interlayers of smectite clay minerals against a changing redox environment [98]. Additionally, modern Ultisols with prominent redoximorphoic features exhibit depth-dependent crystallinity of iron oxides [99], which may

influence organic matter preservation and degradation. Lower crystallinity phases are generally more reactive as sorbents for organic compounds and electron acceptors for organic matter mineralization relative to strongly crystalline iron oxides [99]. Certain intermediate-redox state paleosols exhibit strong redoximorphic features like mottling (spots or blotches of different color), probably from hydrolytic liberation of drab-colored (dull olive-green) Fe(II) during reducing conditions which upon seasonal drying of the soil oxidize to Fe (III) hydroxides including goethite. A compilation of FeO/Fe_2O_3 of Permian (260 Ma) paleosols from Antarctica show a significant ($R^2 = 0.6$) relationship between redox state and total organic carbon preserved in the soil profile **(Figure 5).**

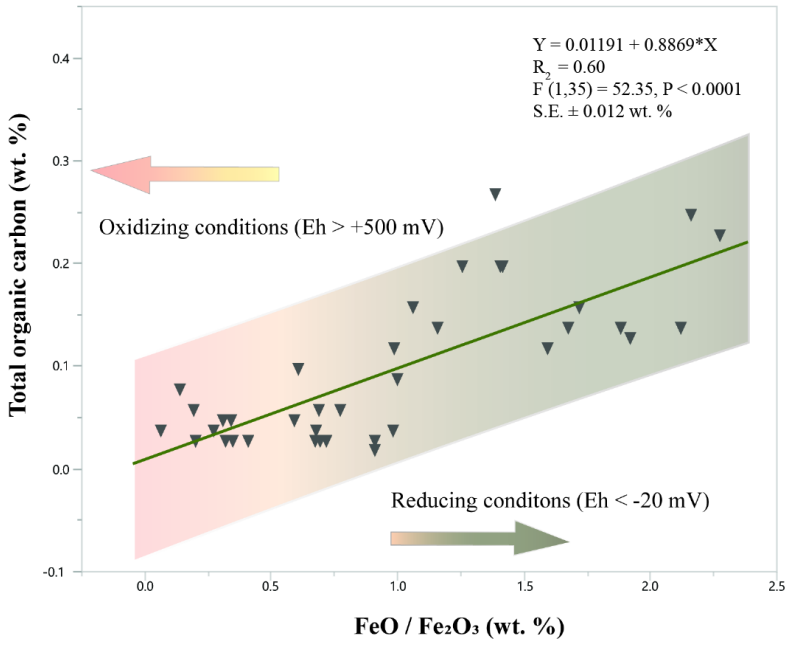

Figure 5. Relationship between total organic carbon and moecular ratio of FeO/Fe_2O_3 in Permian (260 Ma) and Triassic (251) paleosols from Antarctica. Values of FeO/Fe_2O_3 greater than one generally suggest reducing conditions during soil formation; values less than one are associated with oxidizing conditions during soil formation. Data are from [65] and included as supplementary data

It is broadly assumed that clay minerals can aid in the preservation of organics in redox-active soils. However, the oxidation state of iron in clay minerals may play a key role in the

preservation of organics in clayey paleosols of variable redox state. The Fe (III) reducing bacteria *Shewanella putrefaciens* can liberate intercalated organic matter upon reductive dissolution of small and poorly crystalline phases of nontronite, a Fe (III) dioctahedral smectite clay whose formation is typically associated with anoxic conditions, but this does not occur in larger and more crystalline nontronite phases [98]. Variable redox state may indeed encourage the preservation of organic matter in strongly crystalline Fe/Mg smectites, which appear to be common across Noachian (4.1-3.7 Ga) subaerial paleoenvironments of Mars [24]. Strongly crystalline nontronite, however, has been experimentally shown to form under highly oxidizing (> 800 mV) conditions from solutions containing Fe (III) and Mg (II) under Mars-like temperatures and pressures [100]. Strongly oxidizing conditions do not typically favor the preservation of organics intercalated in the interlayer spaces or on mineral surfaces of smectites, so the presence of dioctahedral smectites alone may not necessarily lend high organic preservation potential. Instead, reliance on discreet molecular weathering ratios like FeO / Fe_2O_3 can be used to target high-priority locations for biosignature investigation in ancient subaerial paleoenvironments of Mars.

Depth

Similar to modern soils, many paleosols exhibit a surface enrichment of organic matter relative to lower horizons [8]. Depth functions for organic carbon content are variable but are at least one order of magnitude lower in Precambrian (> 541 Ma) paleosols when compared with modern or Pleistocene paleosols, probably due to extended burial decomposition of organic matter and / or diagenesis. Despite presumed low biomass of Precambrian organisms per soil volume unit, even the most ancient putative soil organisms were likely concentrated in surface horizons [74,88].

Analysis of total organic carbon from Eocene (33 Ma) paleosols of the John Day Fossil Beds National Monument in eastern Oregon show a marked surface enrichment of organic carbon in two of three profiles examined **(Figure 6).** Although these soils formed under oxidizing conditions and most indigenous organic matter has been removed, the surface horizons of the uppermost soil had the highest amounts of organic carbon of any location in any of the three paleosols. Thus, the depth in profile which to sample is an important feature to consider when prioritizing locations for biosignature investigation on Mars. When faced with a sequence of bedded rocks overlying gradationally altered soil below, the samples most likely to be rich in organic matter will be just below the upper contact.

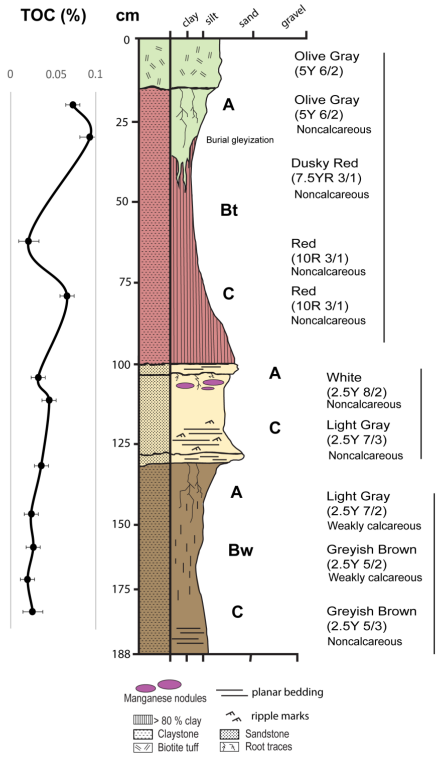

Figure 6. Total organic carbon (TOC), lithology and morphology of three paleosols from the John Day Fossil Beds National Monument, Oregon, USA showing surface enrichment of organic carbon. Error bars (n=2) were constructed using one standard deviation from the mean.

Clay mineralogy

Relationships between organic matter content and mineral surface area have been widely reported across terrestrial and marine settings. Mineral surface area and cation exchange capacity are dictated by clay mineralogy, so natural differences arise between different types of clays and their affinities to form organo-mineral complexes. However, the influence of clay mineralogy on the stability and persistence of organo-mineral complexes through deep time is poorly understood [101]. Organic compounds are well-preserved in the interlayer spaces of certain phyllosilicate clay minerals because the charged surface area of these minerals sorbs and retains organic matter [102,103] and can be extremely resistant to desorption [104], making separation of organics and clays rather difficult. Interlayer binding acts as a retention mechanism for the sorption of organic compounds [105], including amino acids onto phyllosilicates [106], which may shelter organic matter from oxidation [98] and radiation exposure [14,59].

The surfaces of soil clay minerals are favorable locations for organic carbon preservation, and several pathways have been identified which can preserve organic molecules through geologic time. These include occlusion (physical protection) of organic matter, organo-mineral sorption to phyllosilicate surfaces, crystal edges, and interlayer spaces, and/or the establishment of chemically reducing microenvironments that shelter organic matter from degradation [107]. Mineral sorption is especially effective in fixing labile soluble organic matter, including amino acids, carbohydrates, fatty acids, and RNA oligomers.

Clay mineralogy is generally reflected in the degree of weathering of a soil. High kaolinite content of soils and paleosols is characteristic of highly weathered soils including Ultisols and Oxisols which accumulate Al and Fe at the expense of soluble cations as a result of sustained hydrolytic weathering **(Figure 7).** Smectites are a group of 2:1 clay minerals which are common in moderately weathered soils and paleosols and are thought to be more favorable for the preservation of organics relative to 1:1 kaolinitic clay minerals, discussed below.

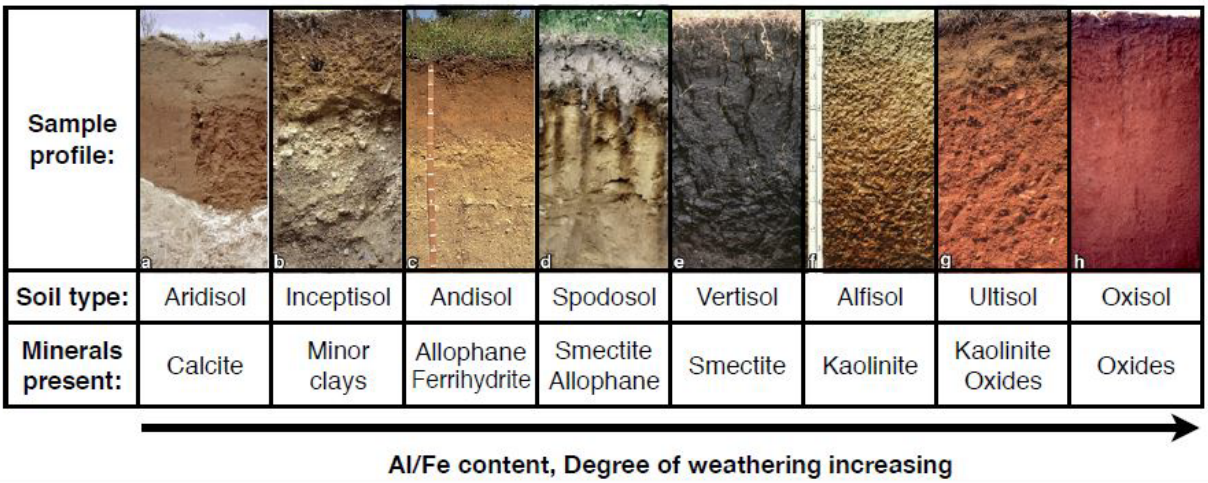

Figure 7. Dominant mineralogy of eight modern soil types (A-H) as a function of weathering. Minimally weathered soils include Aridisols and Inceptisols, while highly weathered soils include Ultisols and Alfisols (From [108], used with permission.)

In clayey (> 80 wt % clay) paleosols, the molecular ratio of bases to alumina (CaO + MgO / Al_2O_3) is a proxy for smectite to kaolinite clay mineralogy [1]. Values of > 1 for bases / alumina suggest smectite as the principal clay mineral, while low (< 0.5) values (increasing Al_2O_3) indicate increasing kaolinite content. However, it is not suitable to apply this proxy for less clayey soils (< 60 wt. %) because values can be compromised if there are still a significant fraction of unweathered primary minerals, characteristic of less mature and thus less clayey soils. A compilation of Cenozoic paleosols with greater than 60 wt. % clay shows that organic C is related to the molecular ratio of CaO + MgO / Al_2O_3 **(Figure 8).** Early Eocene (55 Ma) clay-rich acid-sulfate paleosols from Big Bend National Park, Texas show chemical index of alteration (CIA) ranging from 78-80, indicating extreme weathering conditions and resulting in kaolinite as the principal clay mineral [109]. Extreme weathering is characteristic of Ultisols, which form in humid, tropical settings [110]. These kaolinite-bearing Ultisols have bases / alumina ratio of 0.08 – 0.1 and low (< 0.2 wt %) TOC **(Figure 8).** In contrast, less-weathered Miocene (8.5 Ma) Alfisols (clayey, forest soils [110]) from Pakistan [111] have bases / alumina of ~ 0.3 - 0.8 and higher TOC values (0.22 – 0.8 wt %, **Figure 8)** which reflects the smectite composition and

moderate weathering during soil formation. Considerably less-weathered Miocene (8.5 Ma) Inceptisols also from the Siwaluk formation in Pakistan show bases/ alumina of > 0.6 and the highest TOC (0.1-0.3 wt. %). These soils probably formed in perennially saturated conditions because they are classified as "aquic Inceptisols" [110] implying groundwater presence within 100 cm of the soil surface for some part of the year. Inceptisols forming under perennially saturated conditions often have higher TOC relative to well-drained Inceptisols of similar mineralogy. As such, it is important to consider clay mineralogy in conjunction with redox state (Figure 6).

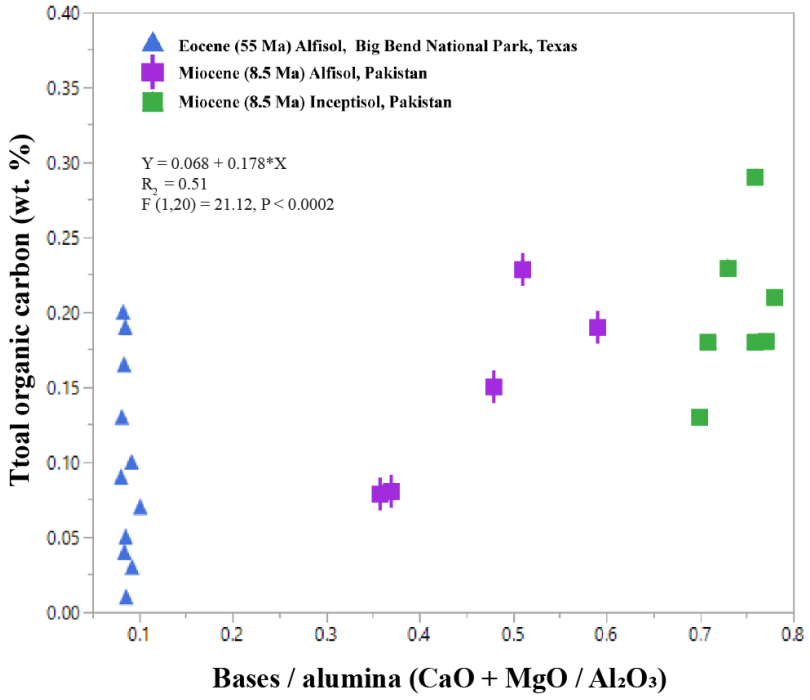

Figure 8. Total organic carbon (wt. %) versus the molecular ratio of bases to alumina (CaO + MgO / Al_2O_3, wt. %) in Cenozoic (55 – 8.5 Ma) clayey paleosols. Bases / alumina is a proxy for kaolinite to smectite clay mineralogy of clay-rich > 60 wt. % paleosols: values of < 0.1 suggest kaolinite and values of > 0.1 suggest smectite mineralogy

Smectites have the highest mineral surface area and cation exchange capacity of all phyllosilicates [112], so they are broadly considered a favorable clay mineral group for preservation of organo-mineral complexes and other biosignatures. However, there are many factors that influence organo-mineral

stability and persistence, including pH-dependent surface charge and ionic strength of pore waters. For example, pedogenic smectites can be stripped of their organic carbon upon deposition in distal marine settings, probably due to changes in ionic composition and strength once submerged in seawater [101].

Wattel-Koekkoek et al. [104] studied differences in organic matter residence time in modern pedogenic smectite versus kaolinite and found large differences in residence time of organic C in kaolinite (360 years) relative to smectite (1100 years), concluding that clay mineralogy is the main factor explaining differences in extracted organic C levels (**Table 1**).

Table 1. Mean residence time of organic carbon in modern kaolinitic and smectitc soils (data from [104]

Site	MAT (C)	MAP (mm/y)	Soil type[φ]	Clay (g/kg)	TOC (g/kg)[ʊ]	Kaolinite (%)[†]	Mica (%)	Sme (%)	Mean age of org. C (yr)[‡]
Kaolinitic									
Brazil	23	1317	Haplic Lixisol	150	10	92	8	0	187
Brazil	23	1234	Haplic Lixisol	260	10	98	2	0	487
Mali	27	1087	Ferric Acrisol	230	9	96	4	0	162
Mozam-bique	24	932	Ferric Acrisol	270	23	100	0	0	545
Smectitic									
Kenya	18	504	Pellitic Vertisol	600	14	1	0	99	1368
Nicara-gua	27	1184	Pellitic Vertisol	790	11	0	0	100	629
South Africa	19	928	Pellitic Vertisol	460	24	21	0	79	903
South Africa	19	928	Pellitic Vertisol	570	16	21	0	79	1302

φ Soil type is after USDA Keys to Soil Taxonomy, 2014
† Clay mineralogy determined by XRD and displayed as relative peak area of diffractograms (%)
‡ Age of organic C determined by ^{14}C analysis and corrected for Suess and Bomb effects, respectively
ʊ Total organic carbon (TOC) determined by combustion on an Interscience elemental analyzer EA 1108

This may be a result of cationic bridging of organic matter in smectite, not thought to be common in organic matter associated with kaolinite, where instead organics are free or sorbed to the aluminum

hydroxide surface of kaolinite [69]. Thus soils rich in original smectite clays may retain more organic matter than paleosols rich in kaolin clays because of differences in chemical bonding between organic carbon and mineral surfaces. Fortunately, dioctahedral Fe/ Mg smectite clays have been detected from orbit at Jezero Crater, the final landing site for the Mars 2020 mission [113] and at Oxia Planum, the landing site of ExoMars 2020 mission [114].

Clay abundance

The weight percent of clay in a paleosol has also been shown to influence organic matter preservation and susceptibility to diagenesis [10,66]. Paleosols with high (>80 wt %) abundances of smectite clays generally have higher amounts of organic carbon and less diagenetic alteration relative to less clayey paleosols [66]. Importantly, paleosols with high smectite clay content and low abundances of amorphous colloids exhibit resistance to severe diagenetic alteration including illitization, celadonization and zeolitization [10]. This is most noticeable within Mars-relevant paleosols at the John Day Fossil Beds National Monument in eastern Oregon, where less clayey Andisols and Aridisols rich in amorphous colloids (imogolite, allophane) from the late Oligocene (26 Ma) exhibit severe diagenetic alteration relative to older, more developed and clay-rich paleosols (Alfisols and Ultisols) of the early Oligocene (33 Ma) despite greater depths of burial.

Soils and sediments share some characteristics related to the storage of organic matter, despite profound differences in the way clay minerals are delivered, transformed and interact with organics in each system [112]. Detrital minerals in marine sediments are often delivered from sedimentation of terrestrial mineral assemblages, and a significant amount of shallow marine organic carbon can be pedogenic in origin [77], often depending on local uplift rate [101]. Within wetland (saturated) soils and marine environments, concentrations of organic carbon are correlated with the abundance of clay minerals [76,112,115], although temperature and water availability create increased variance in soil environments [115]. In formerly well

drained paleosols, however, even clayey profiles may have little organic matter because of decomposition by aerobic microbes early after burial **(Figure 3).**

Paleosols with higher clay content generally have higher total organic carbon. A compilation of total organic carbon content of five Miocene (16-20 Ma) paleosols from Australia, Pakistan and Kenya show that organic matter content in each soil is related to the percentage of clay in the soil **(Figure 9).** This relationship may be due to the high specific surface area and cation exchange capacity of clayey soils provide more surfaces for the formation of stable organo-mineral complexes, but the redox state of the soil during formation is probably more important for organic carbon preservation. For example, clay-rich tropical rainforest Oxisols are abundant in kaolinite clay but have trace (< 0.1 wt %) amounts of organic carbon, while less-weathered smectitic paleosols (Alfisols, Inceptisols) have preserved much more (> 1 wt. %) organic carbon **(Supplementary data).** Therefore, clay abundance alone may not prove useful for predicting organic carbon, but may be more useful for characterizing subaeriel paleoenvironments with high preservation potential when other factors like redox state and clay mineralogy are considered.

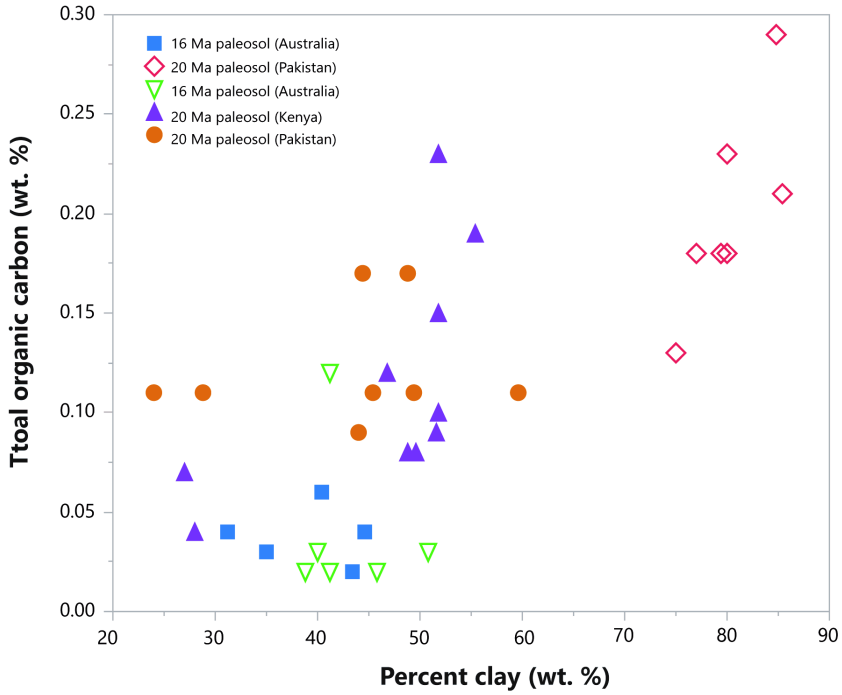

Figure 9. The relationship between clay content and total organic carbon in Miocene paleosols (all Alfisols) from Australia (16-20 Ma), Pakistan (20 Ma), and Kenya (20 Ma). Data are from Metzger and Retallack, 2010 and included as supplementary data

Composition and abundance of amorphous materials

Amorphous phases are formed from primary (e.g.,volcanism, impacts) or secondary processes (e.g., pedogenesis, hydrothermal alteration, radiation damage) [116,117]. Amorphous colloidal non-crystalline phases are abundant in soils when instantaneous weathering rates are high and/or when parent materials are high in amorphous materials, such as volcanic glass [118]. Amorphous materials are a common product of volcanic soils and consist mainly of hydrolyzed Al, Si and Fe, and are characterized by high specific surface area and reactivity. Chemical weathering of volcanic ash begins with the leaching of soluble components (desilication) including H_4SiO_4, Ca^{2+}, Mg^{2+}, Na^+ and K^+ and is accelerated by the presence of carbonic acid, resulting in the accumulation of sesquioxides (e.g., Al_2O_3) and the formation of secondary amorphous minerals from aluminum and silicic acid. In many volcaniclastic soils, amorphous ferrihydrite ripens first to magnetite and/or maghemite then ultimately to hematite [119]. The composition of amorphous materials in volcanic soils is also a function of soil permeability: if soils are well drained, soluble reaction products are removed rapidly from leaching, whereas poorly drained soils accumulate soluble reaction products including Mg^{2+} and in some cases form poorly crystalline smectites including montmorillonite ([119].

Reactive amorphous phases of Al and Fe oxyhydroxides in soils adsorb and retain organic matter [49,102]. Amorphous $Al(OH)_3$ is known to have a strong affinity to chemisorb organic matter and thus provide a strong preservation mechanism in soils [119–121]. Poorly crystalline Fe (oxy)hydroxides are generally more reactive than higher crystallinity phases as sorbents for organic matter [99]. In modern soils, ligand exchange between poorly crystalline mineral surface hydroxyl groups and negatively charged organic functional groups can stabilize and preserve organic matter in subsurface horizons of acid soils [102]. DNA from Holocene volcaniclastic paleosols (Andisols) is often adsorbed, chemisorbed and / or encased in nanopores of amorphous allophane which can be successfully extracted and amplified using wet chemistry methods [122]. Amorphous materials may therefore serve as a repository for organic matter in paleosols, especially those lacking evidence of severe diagenetic alteration.

X-ray amorphous phases have been detected (approximately 15 – 70 wt. %) in all soil and rock samples analyzed by the CheMin x-ray diffractometer at Mars Science Laboratory (MSL) onboard Curiosity rover [123]; however, the composition of these amorphous phases is difficult to constrain, and may range from primary (volcanic glass) and secondary (silica, Fe [oxy]hydroxides) phases alone or in combination [118]. Approaches to resolve the composition of amorphous phases at Gale Crater have employed a combination of bulk mineral abundances from CheMin and bulk chemical composition from the Alpha Particle X-ray Spectrometer (AXPS), also onboard MSL . X-ray diffraction refinements, pattern fitting, and mass-balance calculations applied to terrestrial samples reveal compositional similarities between certain Martian soils and sediments and modern glacial sediments, volcanic soils and volcaniclastic paleosols [124]. Rhyodacitic to andesitic paleosols and modern glacial sediments show abundances of amorphous SiO_2, TiO_2 and Al_20_3 phases similar to those of mudstones at Gale Crater [124].

Amorphous phases in volcaniclastic paleosols commonly include volcanic glass, allophane ($Al_2O_3 \cdot [SiO_2]_{1.3\text{-}2} \cdot 2.5\text{-}3\ H_2O$), nanocrystalline silica, and imogolite ($Al_2SiO_3[OH]_4$). The composition of amorphous phases in vitric tuffaceous soils and paleosols is dominated by aluminum oxides and silicates. These distinctive soils, called Andisols, often have a dark organic surface horizon, known as a melanic epipedon in US Soil Taxonomy. In such soils the decomposition of organic matter is hindered by sorption to amorphous aluminum hydroxides. As these soils mature, the increasing crystallinity of amorphous phases in modern Andisols leads to decreased amounts of TOC (**Figure 10**). The "activity ratio" [119] of active iron oxides to free iron oxides, determined by Mossbauer spectroscopy and expressed in weight percent, is a proxy for the degree of crystallinity of amorphous soil minerals, and is significantly correlated with the total organic carbon in modern soils **(Figure 10).** Ultisols are much more developed soils relative to Andisols with mineralogy dominated by crystalline compounds and lower values of active iron oxides/ free iron oxides (0.15–0.32) than Andisols (0.30–0.99) [119].

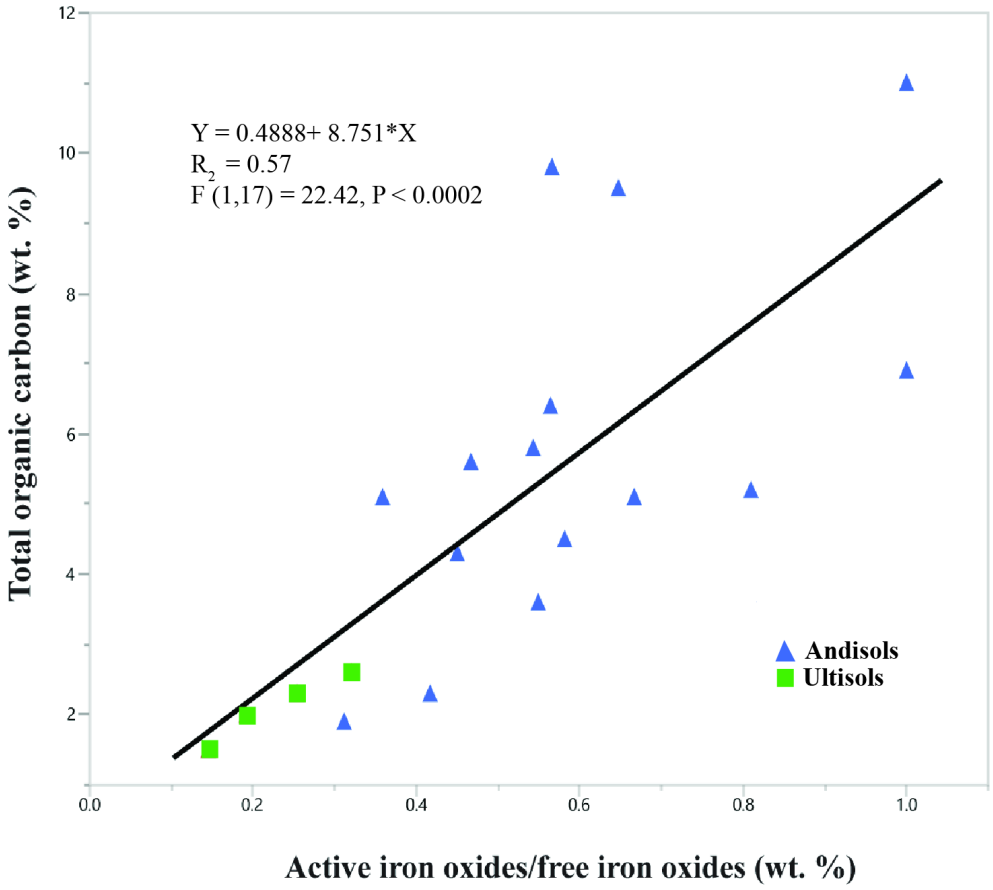

Figure 10. Total organic carbon versus the ratio of active to free iron oxides in modern Andisols (amorphous-rich volcanic soils, blue triangles) and Ultisols (highly weathered, highly crystalline soils, green squares) from Chile. The ratio of active to free iron oxides is a proxy for Fe_2O_3 crystallinity; increasing values of active to free Al_2O_3 are indicative of higher amounts of amorphous Fe_2O_3 (Data from [119]).

Volcaniclastic paleosols formed in volcanic glass are often dominated by imogolite, which can through diagenetic Ostwald ripening transform to celadonite or clinoptilolite [66,118]. These paleosols however are unusually barren of organic matter, presumably lost in water expelled by these diagenetic alterations resulting from deep burial. Such deep burial diagenetic alterations have not been noticed in Martian clays so far [55]. Together, the large specific surface area, high reactivity, and lack of diagenetic alteration suggest that amorphous-rich

volcaniclastic paleosols on Mars are a high-priority target for biosignature investigation [11] and Mars Sample Return [13].

Sulfur aids preservation of organic matter

Interactions between organic matter and sulfur can encourage long-term (10^6-10^9 yr) preservation of organic matter in sedimentary rocks [107,125–128] and paleosols [126]. Sulfurization is the incorporation of reduced inorganic sulfur species into sedimentary organic matter [129] and has been cited as a dominant preservation mechanism for functionalized organic compounds during early diagenesis [130]. The addition of sulfur encourages structural cross-linking of organic components, creating a macromolecular structure [128] which attenuates degradation of organics by addition of an oxidative sink [107] and possibly results in organo-sulfur compounds which are incompatible with exoenzyme degradation [130]. Organic carbon detected at the base of the Murray formation at Gale Grater, Mars is composed of methanethiol, dimethylsulfide, carbonyl sulfide, and carbon disulfide [107], which are common products of early diagenetic sulfurization reactions involving organic carbon. These compounds indicate diagenetic alteration of rocks and organics with acidic fluids in the lower Murray formation [123] was not sufficient to oxidize and remove all organic carbon [107].

Similarly, terrestrial sulfurization reactions documented in Archean rocks has been shown to enhance short-term preservation of organic carbon while encouraging long-term recalcitrance to acid diagenesis, oxidation, and cosmic ray-induced degradation [107]. Potential paleosols of Archean (3.7-2.5 Ga) age show geochemical evidence of formation under an anoxic, reducing atmosphere [5,6,74] even when formed in well-drained settings [95]. Furthermore many Archean paleosols have abundant sulfates including gypsum, barite and perhaps kieserite [5,87] associated with other evidence of sulfur oxidizing photosynthetic bacteria [92]. Geologically

younger paleosols from the upper Triassic (215 Ma) Chinle formation in Arizona [131] contain the sulfate mineral jarosite, which appears to encourage organic matter preservation when forming a rind on calcite-rich nodules [132], while organosulfur compounds including thiophenes and thienothiophenes are common in late Jurassic paleosols from the “dirt beds” near Dorset, UK [126]. Considering these large temporal scales across terrestrial environments, the role of sulfur in the preservation of organic compounds may be a common phenomenon throughout the fossil record of soils.

Sulfur may have played a role in the preservation of organic carbon in potential Archean (3.0 Ga) alluvial paleosols in the Farrel Quartzite of Western Australia (**Figure 11**) [92]. However, the presence of paleosols and the non-marine affinity for carbonaceous microfossils has been disputed [133]. Several lines of evidence support a pedogenic and non-marine hypothesis for the formation of the Farrel Quartzite, which are summarized in [92]. Most notably the presence of replacive barite ($BaSO_4$) sand crystals and silicified pseudomorphs of nahcolite ($NaHCO_3$) grouped into distinct layers resembling a soil gypsic (By) horizon [110] are thought to be diagnostic of a subaerial formation environments [92]. Alternatively, this unit has been interpreted as a microfossil-bearing carbonaceous chert deposited in a shallow marine to subaerial sedimentary setting [134], and accordingly there is an ongoing debate about whether the paleosol hypothesis is correct [133]. From a soil science perspective, the subaerial exposure of marine sediments and the formation of evaporitic sulfate minerals implies extended subaerial chemical weathering and allows for classification as Gypsid soils (salt crusts) in USDA soil Taxonomy [110], though sand-sized barite nodules described as pedogenic features could be reworked grains of hydrothermal barite[133]. Despite disagreement on the origin of the Farrel

Quartzite, the influence of sulfur on the preservation of organic carbon in these rocks requires examination, further discussed below.

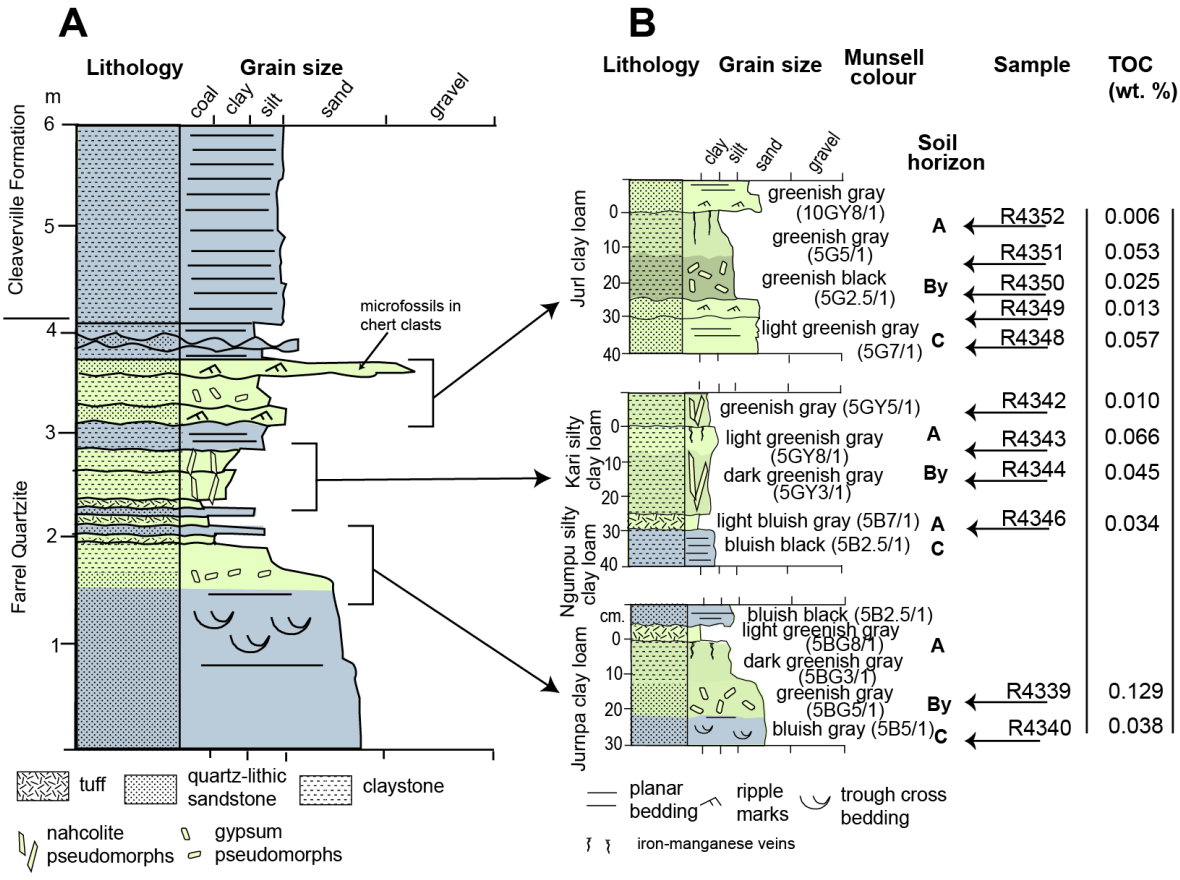

Figure 11. Stratigraphic section (A) and potential paleosol profiles (B) from the 3.0 Ga Farrel Quartzite, Western Australia (redrafted from [92]**). "Sample"** in (B) corresponds to locations where analysis of total organic carbon (TOC) was performed on hand samples previously used to collect oriented thin sections for determination of framboidal pyrite abundance [92]. Determination of TOC was performed by combustion on a Costech ECS 4010 elemental analyzer. Samples were pre-treated with HCl to remove inorganic carbonates. Total organic carbon values displayed are average of two replicates. All samples are in the Condon Collection of the Museum of Natural and Cultural History of the University of Oregon. All data are included as supplementary data

In what has been interpreted as the gypsic (By) horizon, abundant pyrite (FeS) framboids were associated with spheroidal and spindle-like carbonaceous microfossils which are putatively identified as *Archaeosphaeroides* and *Eopoikilofusa,* respectively, possibly representing a terrestrial consortium of actinobactera, purple sulfur bacteria and methanogens [92]. In contrast, carbonaceous microfossils in the Farrel Quartzite were first described as aquatic organisms

based on stratigraphic, petrographic and trace element evidence [135]. Though the affinities remain disputed, there is general agreement that they are putative microfossils and not pseudofossils [136] which is partially supported by their association with sulfur-bearing minerals including pyrite framboids[92]. Pyrite framboids are subspherical to spherical clusters of submicron to micron-sized pyrite crystals packed together in tight association [137] resembling the aggregate of druplets of a raspberry. Photosynthetic sulfur bacteria may have been responsible for accumulation of barite, which then served as the electron acceptor for endolithic sulfate-reducing bacteria whose metabolic activity is represented by clusters of opaque pyrite framboids [92]. Opaque pyrite framboids can represent traces of the activity of sulfur-reducing microbes [138] and are known to grow in association with modern anaerobic microbial biofilms [137]. The abundance of pyrite framboids is related to the organic carbon content of potential paleosols in the Farrel Quartzite (Figure 11) because gypsic (By) horizons with abundant (> 500) pyrite framboids were found to contain higher levels of total organic carbon relative to horizons with lower (< 100) abundances (Figure 12, Supplementary data). It should be noted that only eleven samples were analyzed for this work and thus the data point with the highest TOC (0.12 wt. %) and greatest number of pyrite framboids (866 framboids) (sample R4339, Figure 12) largely controls the slope and significance of the relationship (Supplementary data). Nevertheless these data suggest subaerial or shallow marine Archean rocks with evaporitic sulfate minerals and framboidal pyrite can be conducive to the preservation of organics associated with microbial metabolism, and should be considered a high-priority target for biosignature investigation in sulfur-rich subaerial paleoenvironments on Mars [132].

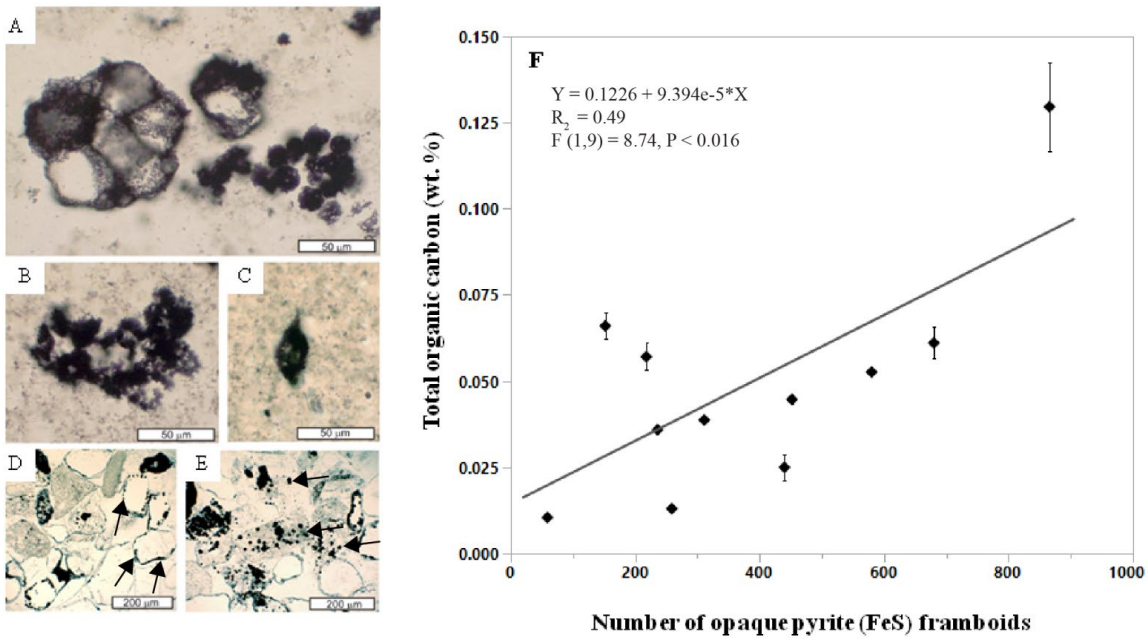

Figure 12. Microfossils and opaque pyrite framboids from Archean (3.0 Ga) potential paleosols in the Farrel Quartzite, Western Australia, and the relationship between total organic carbon and pyrite framboids. (A) clusters of large thick wall spheroid (left: some deformed by crystal growth) and small spheroid (right) morphotypes; **(B)** cluster of small spheroid morphotype; **(C)** spindle morphotype; **(D–E)** sandstone with grains of fossiliferous chert (grey) and quartz (white), including marginal opaque framboids of possible endolithic microbes (black arrows); **(F)** Least-squares regression of mean total organic carbon content (TOC) versus number of opaque pyrite framboids in the clasts and matrix of an Archean (3.0 Ga) coastal-plain paleosol in the Farrel Quartzite, Western Australia. Error bars are constructed using one standard error from the mean. Hand samples and oriented thin sections in the Condon Collection of the Museum of Natural and Cultural History of the University of Oregon are (A–C) F118310B = R4336 from A horizon of Jurnpa clay loam, (D-E) F118310E =R4339 from By horizon of Jurnpa clay loam. All data are included as supplementary data

Conclusion

Ancient soils are subject to a wide range of physical, chemical and biological processes that facilitate organic carbon preservation and degradation over geological time scales. Results of a global compilation of organic matter content of soils and paleosols show that redox state of a paleosol prior to burial is the predominant control on the preservation of organic matter. Paleosols that formed under oxidizing conditions have significantly lower total organic carbon prior to burial and are more prone to burial decomposition of organic matter relative to poorly-drained paleosols that formed under reducing conditions. However, diagenetic alteration, depth

in the soil profile, clay mineralogy, amount of amorphous colloids, and sulfur content are all important factors that influence organic matter preservation and degradation in paleosols Notably, Oligocene (33 Ma) Mars-relevant paleosols with abundant (> 80 wt %) dioctahedral Fe/Mg smectite clays appear to resist severe diagenetic alteration including illitization and celadonization, which may liberate mineral-associated organic carbon from paleosols with lower clay content and higher amounts of amorphous colloids.

Severe diagenetic alteration of Earth's oldest putative soils have transformed original clay minerals and amorphous colloids, and only pseudomorphs of sulfur-bearing evaporite minerals appear to remain, though pyrite framboids persist. Despite diagenetic burial decomposition of organic matter, many Phanerozoic (< 541 Ma) and Precambrian (> 541 Ma) paleosols exhibit surface and shallow subsurface enrichment of organic carbon, similar to modern soils. Additionally, paleosols with smectite clays are more favorable for the preservation of organic carbon relative to paleosols with accumulations of kaolin clays. Importantly, the clay-size fraction of modern soils and paleosols can preserve highly recalcitrant organic matter derived from microbial biomass and/or metabolites which suggests that clay-size fractions of smectite-rich potential Martian paleosols should be prioritized for biosignature investigation. Data also show that amorphous colloids, common in soils and paleosols, are favorable location for the sorption of organic carbon, but diagenetic alteration of amorphous-rich paleosols can remove organic compounds. Finally, putative Archean (3.0 Ga) acid sulfate paleosols show evidence of biomineralized pyrite (FeS) and the possible persistence of organo-sulfur compounds: horizons with accumulations of framboidal pyrite have significantly higher total organic carbon relative to horizons with lower accumulations of framboidal pyrite.

A compilation of organic matter content of paleosols spanning the geological record on Earth show that organic carbon is most abundant in the upper horizons of paleosols that are unoxidized, rich in smectites, amorphous colloids and sulfur. Future approaches to biosignature detection in possible paleosols on Mars should target regions and horizons that fit these criteria. The factors presented here are all aspects of soil science, and therefore soil scientists should continue to be involved in the current and future exploration of Mars.

Acknowledgements

I am grateful for the assistance and motivation provided by my advisors Greg Retallack, Lucas Silva and Matt Polizzotto. Barry Hughes provided thoughtful discussion and assisted with fieldwork. Elizabeth Rampe, Paul Niles, Joanna Hogancamp, Brad Sutter, and Doug Ming provided critical discussion and data review in support of this project. Funding in support of this project was provided by the Geological Society of America and the Society for Sedimentary Geology.

Author Disclosure Statement

No competing financial interests exist.

References

1. Retallack, G. J. *Soil of the Past*. (Wiley Blackwell, 2019).
2. Retallack, G. J. Astropedology: palaeosols and the origins of life. *Geol. Today* **32**, 172–178 (2016).
3. Retallack, G. J., Krinsley, D. H., Fischer, R., Razink, J. J. & Langworthy, K. A. Archean coastal-plain paleosols and life on land. *Gondwana Res.* **40**, 1–20 (2016).

4. Raynaud, X. & Nunan, N. Spatial ecology of bacteria at the microscale in soil. *PLoS One* **9**, (2014).

5. Retallack, G. J. & Noffke, N. Are there ancient soils in the 3 . 7 Ga Isua Greenstone Belt , Greenland ? *Palaeogeogr. Palaeoclimatol. Palaeoecol.* **514**, 18–30 (2019).

6. Rye, R. & Holland, H. Life associated with a 2 . 76 Ga ephemeral pond ?: Evidence from Mount Roe # 2 paleosol. *Geology* **28**, 483–486 (2000).

7. Homann, M. *et al.* Microbial life and biogeochemical cycling on land 3,220 million years ago. *Nat. Geosci.* **11**, 665–671 (2018).

8. Watanabe, Y., Stewart, B. W. & Ohmoto, H. Organic- and carbonate-rich soil formation ~2.6 billion years ago at Schagen, East Transvaal district, South Africa. *Geochim. Cosmochim. Acta* **68**, 2129–2151 (2004).

9. Finke, N. *et al.* Mesophilic microorganisms build terrestrial mats analogous to Precambrian microbial jungles. *Nat. Commun.* **10**, 1–11 (2019).

10. Horgan, B. Strategies for Searching for Biosignatures in Ancient Martian Sub-Aerial Surface Environments. *Biosignature Preserv. Detect. Mars Analog Environ.* 7463 (2016) doi:10.1089/ast.2016.1627.

11. Hays, L. E. *et al.* Biosignature Preservation and Detection in Mars Analog Environments. *Astrobiology* **17**, 363–400 (2017).

12. Bishop, J. L. *et al.* Potential high priority subaerial environments for Mars sample return. *Proc. Second Int. Mars Sample Return Conf.* **2071**, (2018).

13. Beaty, D. W. *et al.* The potential science and engineering value of samples delivered to Earth by Mars sample return. *Meteorit. Planet. Sci.* **671**, 667–671 (2019).

14. Bishop, J. L. *et al.* Surface clay formation during short-term warmer and wetter conditions

on a largely cold ancient Mars. *Nat. Astron.* **2**, 206–213 (2018).

15. Horgan, B., Baker, L., Carter, J. & Chadwick, O. Where is the climate signature in the mineral record of early Mars? *Fourth Conf. Early Mars 2017* **3077**, 2014–2015 (2017).
16. Pajola, M. *et al.* Eridania Basin : An ancient paleolake floor as the next landing site for the Mars 2020 rover. *Icarus* **275**, 163–182 (2020).
17. Doane, T. A. A survey of photogeochemistry. *Geochem. Trans.* 1–24 (2017) doi:10.1186/s12932-017-0039-y.
18. Doane, T. A., Silva, L. C. R. & Horwath, W. R. Exposure to Light Elicits a Spectrum of Chemical Changes in Soil. *J. Geophys. Res. Earth Surf.* **124**, 2288–2310 (2019).
19. Gastaldo, R. A. & Demko, T. M. The Relationship Between Continental Landscape Evolution and the Plant-Fossil Record : Long Term Hydrologic Controls on Preservation. in *Taphonomy: Processes and Bias Through Time* 249–285 (2011). doi:10.1007/978-90-481-8643-3.
20. Horgan, B., Bishop, L., Christensen, P. R. & Bell, J. F. Potential ancient soils preserved at Mawrth Vallis from comparisons with Eastern Oregon paleosols: Implications for Early Martian Climate. *Third Conf. Early Mars* **7074**, 12–13 (2012).
21. Dobrea, E. Z. N. *et al.* Mineralogy and stratigraphy of phyllosilicate - bearing and dark mantling units in the greater Mawrth Vallis / west Arabia Terra area : Constraints on geological origin. *J. Geophys. Res.* **115**, 1–27 (2010).
22. Bishop, J. L. *et al.* What the ancient phyllosilicates at Mawrth Vallis can tell us about possible habitability on early Mars. *Planet. Space Sci.* **86**, 130–149 (2013).
23. Carter, J., Loizeau, D., Mangold, N., Poulet, F. & Bibring, J. Widespread surface weathering on early Mars : A case for a warmer and wetter climate. *Icarus* **248**, 373–382

(2015).

24. Poulet, F. *et al.* Mawrth Vallis, Mars: A Fascinating Place for Future In Situ Exploration. *Astrobiology* **20**, 1–36 (2020).

25. van Es, H. A New Definition of Soil. *CSA News* **62**, 20–21 (2017).

26. Retallack, G. J. Paleosols and paleoenvironments of early Mars. *Geology* **42**, 755–758 (2014).

27. Hynek, B. M., Beach, M. & Hoke, M. R. T. Updated global map of Martian valley networks and implications for climate and hydrologic processes. *J. Geophys. Res.* **115**, 1–14 (2010).

28. Ramirez, R. M. & Craddock, R. A. warmer and wetter early Mars. *Nat. Geosci.* **11**, (2018).

29. Weiss, D. K. & Head, J. W. Crater degradation in the Noachian highlands of Mars: Assessing the hypothesis of regional snow and ice deposits on a cold and icy early Mars. *Planet. Space Sci.* **117**, 401–420 (2015).

30. Kereszturi, A. Review of wet environment types on Mars with focus on duration and volumetric issues. *Astrobiology* **12**, 586–600 (2012).

31. Javier Martín-Torres, F. *et al.* Transient liquid water and water activity at Gale crater on Mars. *Nat. Geosci.* **8**, 357–361 (2015).

32. Pál, B. & Kereszturi. Possibility of microscopic liquid water formation at landing sites on Mars and their observational potential. *Icarus* **282**, 84–92 (2017).

33. Góbi, S. & Kereszturi, Á. Analyzing the role of interfacial water on sulfate formation on present Mars. *Icarus* **322**, 135–143 (2019).

34. Phillips-Lander, C. M., Elwood Madden, A. S., Hausrath, E. M. & Elwood Madden, M. E.

Aqueous alteration of pyroxene in sulfate, chloride, and perchlorate brines: Implications for post-Noachian aqueous alteration on Mars. *Geochim. Cosmochim. Acta* **257**, 336–353 (2019).

35. Dartnell, L. R. & Patel, M. R. Degradation of microbial fl uorescence biosignatures by solar ultraviolet radiation on Mars. *Int. J. Astrobiol.* **13**, 112–123 (2014).

36. Dartnell, L. R., Desorgher, L., Ward, J. M. & Coates, A. J. Martian sub-surface ionising radiation : biosignatures and geology ∗. *Biogeosciences* **4**, 545–558 (2007).

37. Royle, S. H. *et al.* Perchlorate-Driven Combustion of Organic Matter During Pyrolysis-Gas Chromatography-Mass Spectrometry: Implications for Organic Matter Detection on Earth and Mars. *J. Geophys. Res. Planets* **123**, 1901–1909 (2018).

38. Navarro-González, R., Vargas, E., De La Rosa, J., Raga, A. C. & McKay, C. P. Reanalysis of the Viking results suggests perchlorate and organics at midlatitudes on Mars. *J. Geophys. Res. E Planets* **115**, 1–11 (2010).

39. Ming, D. W. *et al.* Volatile and Organic Compositions of Sedimentary Rocks in Yellowknife Bay , Gale Crater , Mars. *Sci. Express* 1–15 (2014).

40. Grotzinger, J. P. *et al.* A Habitable Fluvio-Lacustrine Environment at Yellowknife Bay, Gale Crater, Mars. *Science (80-.).* **321**, 1–15 (2014).

41. Murchie, S. *et al.* Compact Reconnaissance Imaging Spectrometer for Mars (CRISM) on Mars Reconnaissance Orbiter (MRO). *J. Geophys. Res.* **112**, 1–57 (2007).

42. Treiman, A. H. *et al.* Mineralogy, provenance, and diagenesis of a potassic basaltic sandstone on Mars: CheMin X-ray diffraction of the Windjana sample (Kimberley area, Gale Crater). *J. Geophys. Res. Planets* **121**, 75–106 (2016).

43. Bishop, J. . *et al.* Mineralogy of layered outcrops at Mawrth Vallis and implications for

early aqueous geochemistry on Mars. *47th Lunar Planet. Sci. Conf.* **2**, 2–3 (2016).

44. Brown, D. J., Shepherd, K. D., Walsh, M. G., Mays, M. D. & Reinsch, T. G. Global soil characterization with VNIR diffuse reflectance spectroscopy. *Geoderma* **132**, 273–290 (2006).

45. Ehlmann, B. L. *et al.* Clay minerals in delta deposits and organic preservation potential on Mars. *Nature* **1**, 355–358 (2008).

46. Lowe, D. R. *et al.* Deposition of > 3 . 7 Ga clay-rich strata of the Mawrth Vallis Group , Mars , in lacustrine , alluvial , and aeolian environments. *GSA Bull.* 17–30 (2020).

47. Deit, L. Le *et al.* Extensive surface pedogenic alteration of the Martian Noachian crust suggested by plateau phyllosilicates around Valles Marineris. *J. Geophys. Res.* **117**, 1–25 (2012).

48. Loizeau, D. *et al.* Quantifying widespread aqueous surface weathering on Mars : The plateaus south of Coprates Chasma. *Icarus* **302**, 451–469 (2018).

49. Fornaro, T., Steele, A. & Brucato, J. R. Catalytic/protective properties of martian minerals and implications for possible origin of life on mars. *Life* **8**, 1–41 (2018).

50. Kamada, A. *et al.* A coupled atmosphere–hydrosphere global climate model ofearly Mars: A 'cool and wet' scenario for the formation of water channels. *Icarus* **18**, 113567 (2019).

51. Palumbo, A. M., Head, J. W. & Wordsworth, R. D. Late Noachian Icy Highlands climate model : Exploring the possibility of transient melting and fluvial / lacustrine activity through peak annual and seasonal temperatures. *Icarus* **300**, 261–286 (2018).

52. Ivanov, M. A., Slyuta, E. N., Grishakina, E. A. & Dmitrovskii, A. A. Geomorphological Analysis of ExoMars Candidate Landing Site Oxia Planum. *Sol. Syst. Res.* **54**, 1–14 (2020).

53. Kereszturi, A., Bradak, B., Chatzitheodoridis, E. & Újvári, G. Indicators and Methods to Understand Past Environments from ExoMars Rover Drills. *Orig. Life Evol. Biosph.* **46**, 435–454 (2016).

54. Thomas, R. J., Hynek, B. M., Osterloo, M. M. & Kierein-Young, K. S. Widespread exposure of Noachian phyllosilicates in the Margaritifer region of Mars: Implications for paleohydrology and astrobiological detection. *J. Geophys. Res. Planets* **122**, 483–500 (2017).

55. Tosca, N. J. & Knoll, A. H. Juvenile chemical sediments and the long term persistence of water at the surface of Mars. *Earth Planet. Sci. Lett.* **286**, 379–386 (2009).

56. Lee, B. D., Sears, S. K. & Vali, H. Secondary Mineral Genesis from Chlorite and Serpentine in an Ultramafic Soil Toposequence. *Soil Sci. Soc. Am. J.* **67**, 1309–1317 (2003).

57. Ehlmann, B. L., Mustard, J. F. & Murchie, S. L. Geologic setting of serpentine deposits on Mars. *Geophys. Res. Lett.* **37**, 1–5 (2010).

58. Ehlmann, B. L. *et al.* Subsurface water and clay mineral formation during the early history of Mars. *Nature* **479**, 53–60 (2011).

59. McMahon, S. *et al.* A Field Guide to Finding Fossils on Mars. *J. Geophys. Res. Planets* **123**, 1012–1040 (2018).

60. Michalski, J. R. *et al.* Constraints on the crystal-chemistry of Fe / Mg-rich smectitic clays on Mars and links to global alteration trends. *Earth Planet. Sci. Lett.* **427**, 215–225 (2015).

61. Bristow, T. F. *et al.* Clay mineral diversity and abundance in sedimentary rocks of Gale crater , Mars. *Sci. Adv.* **4**, 1–9 (2018).

62. Mayer, L. M., Thornton, K. R., Schick, L. L., Jastrow, J. D. & Harden, J. W.

Photodissolution of soil organic matter. *Geoderma* **170**, 314–321 (2012).

63. Metzger, C. A. & Retallack, G. J. Paleosol record of Neogene climate change in the Australian outback Paleosol record of Neogene climate change in the Australian outback. *Aust. J. Earth Sci.* **57**, 871–885 (2010).

64. Alekseeva, T. V, Zolotareva, B. N. & Kolyagin, Y. G. Nonhydrolyzable Part of Soil Organic Matter in Buried and Modern Soils. *Eurasian Soil Sci.* **52**, 632–643 (2019).

65. Krull, E. S. & Retallack, G. J. 13C depth profiles from paleosols across the Permian-Triassic boundary : Evidence for methane release. *GSA Bull.* **112**, 1459–1472 (2000).

66. Retallack, G. J., Bestland, E. . & Fremd, T. . Eocene and Oligocene Paleosols of Central Oregon. *Geol. Soc. Am. Spec. Pap.* **344**, 1–192 (2000).

67. Novoselov, A. A., Roberto, C. & Filho, D. S. Potassium metasomatism of Precambrian paleosols. *Precambrian Res.* **262**, 67–83 (2015).

68. Elliott, W. C. & Matisoff, G. Evaluation of kinetic models for the smectite to illite transformation. *Clays Clay Miner.* **44**, 77–87 (1996).

69. Wattel-Koekkoek, E. J. ., van Genuchten, P. P. ., Buurman, P. & van Lagen, B. Amount and composition of clay-associated soil organic matter in a range of kaolinitic and smectitic soils. *Geoderma* **99**, 27–49 (2001).

70. Retallack, G. J. Untangling the effects of burial alteration and ancient soil formation. *Annu. Rev. Earth Planet. Sci.* 183–206 (1991).

71. Li, Y., Cai, J., Song, M., Ji, J. & Bao, Y. Influence of organic matter on smectite illitization : A comparison between red and dark mudstones from the Dongying Depression , China. *Am. Mineral.* **101**, 134–145 (2016).

72. Schumann, D. *et al.* THE INFLUENCE OF OXALATE-PROMOTED GROWTH OF

SAPONITE AND TALC CRYSTALS ON RECTORITE : TESTING THE INTERCALATION-SYNTHESIS HYPOTHESIS OF 2 : 1 LAYER SILICATES. *Clays Clay Miner.* **61**, 342–360 (2013).

73. Fang, Q. *et al.* Applied Clay Science New insights into microbial smectite illitization in the Permo-Triassic. *Appl. Clay Sci.* **140**, 96–111 (2017).

74. Gay, A. . & Grandstaff, D. E. Chemistry and mineralogy of precambrian paleosols at elliot lake, ontario, canada. *Precambrian Res.* **12**, 349–373 (1980).

75. Berger, G., Velde, B., Beaufort, D. & Lanson, B. Kinetic constraints on iilitization reactions and the effects of organic diagenesis in sandstone / shale sequences. *Appl. Geochemistry* **12**, 23–35 (1997).

76. Baldock, J. A., Masiello, C. A. & Ge, Y. Cycling and composition of organic matter in terrestrial and marine ecosystems. *Mar. Chem.* **92**, 39–64 (2004).

77. Lehmann, J. & Kleber, M. The contentious nature of soil organic matter. *Nature* 1–9 (2015) doi:10.1038/nature16069.

78. Marin-spiotta, E. *et al.* Long-term stabilization of deep soil carbon by fire and burial during early Holocene climate change. *Nat. Geosci.* (2014) doi:10.1038/NGEO2169.

79. Schobben, M., van de Schootbrugge, B. & Wignall, P. B. Interpreting the Carbon Isotope Record of Mass Extinctions. *Elements* **15**, 331–337 (2019).

80. Otto, A., Shunthirasingham, C. & Simpson, M. J. A comparison of plant and microbial biomarkers in grassland soils from the Prairie Ecozone of Canada. *Org. Geochem.* **36**, 425–448 (2005).

81. Vancampenhout, K., Schellekens, J., Slaets, J., Hatt, C. & Buurman, P. Fossil redox-conditions in fl uence organic matter composition in loess paleosols. *Quat. Int.* 1–11

(2015) doi:10.1016/j.quaint.2015.11.057.

82. Nelson, P. N. & Baldock, J. A. Estimating the molecular composition of a diverse range of natural organic materials from solid-state C NMR and elemental analyses. *Biogeochemistry* **72**, 1–34 (2005).

83. Lorenz, K., Lal, R., Preston, C. M. & Nierop, K. G. J. Strengthening the soil organic carbon pool by increasing contributions from recalcitrant aliphatic bio (macro) molecules. *Geoderma* **142**, 1–10 (2007).

84. Dartnell, L. R. *et al.* Destruction of Raman biosignatures by ionising radiation and the implications for life detection on Mars. *Anal Bioanal Chem* **403**, 131–144 (2012).

85. Mojzsis, S. J., Abramov, O. & Kereszturi, Á. Exogenous carbonaceous matter in ancient martian sediments. in *American Geophysical Union, Fall Meeting 2015* (2015).

86. Liivamägi, S. *et al.* Paleosols on the Ediacaran basalts of the East European Craton: a unique record of paleoweathering with minimum diagenetic overprint. *Precambrian Res.* (2018) doi:10.1016/j.precamres.2018.07.020.

87. Nabhan, S., Wiedenbeck, M., Milke, R. & Heubeck, C. Biogenic overgrowth on detrital pyrite in ca. 3.2 Ga Archean paleosols. *Geology* **44**, 763–766 (2016).

88. Watanabe, Y., Martin, J. E. . & Ohmoto, H. *Geochemical evidence for terrestrial ecosystems 2.6 billion years ago*. *Nature* vol. 408 (2000).

89. Miltner, A. & Bombach, P. SOM genesis : microbial biomass as a significant source. *Biogeochemistry]* 41–55 (2012) doi:10.1007/s10533-011-9658-z.

90. Kremer, B., Kaźmierczak, J. & Środoń, J. Cyanobacterial-algal crusts from Late Ediacaran paleosols of the East European Craton. *Precambrian Res.* (2017) doi:10.1016/j.precamres.2017.12.018.

91. Cockell, C. S., Kelly, L. C. & Marteinsson, V. Actinobacteria-An Ancient Phylum Active in Volcanic Rock Weathering. *Geomicrobiol. J.* **30**, 706–720 (2013).

92. Retallack, G. J., Krinsley, D. H., Fischer, R., Razink, J. J. & Langworthy, K. A. Archean coastal-plain paleosols and life on land. *Gondwana Res.* **40**, 1–20 (2016).

93. Retallack, G. J., Krull, E. S., Thackray, G. D. & Parkinson, D. Problematic urn-shaped fossils from a Paleoproterozoic (2 . 2 Ga) paleosol in South Africa. *Precambrian Res.* **235**, 71–87 (2013).

94. Loron, C. *et al.* Early fungi from the Proterozoic era in Arctic Canada. *Nature* (2019) doi:10.1038/s41586-019-1217-0.

95. Mohanty, S. P. & Nanda, S. Geoscience Frontiers Geochemistry of a paleosol horizon at the base of the Sausar Group , central India : Implications on atmospheric conditions at the Archean-Paleoproterozoic boundary. *Geosci. Front.* (2015) doi:10.1016/j.gsf.2015.10.002.

96. Pandit, M. K., Wall, H. De & Chauhan, N. K. Paleosol at the Archean – Proterozoic contact in NW India revisited : Evidence for oxidizing conditions during paleo-weathering ? *J. Earth Syst. Sci.* **117**, 201–209 (2008).

97. Retallack, G. J. & Mao, X. Paleoproterozoic (ca . 1 . 9 Ga) megascopic life on land in Western Australia. *Palaeogeogr. Palaeoclimatol. Palaeoecol.* **532**, 109266 (2019).

98. Zeng, Q., Dong, H., Zhao, L. & Huang, Q. Preservation of organic matter in nontronite against iron redox cycling. *Am. Mineral.* **101**, 120–133 (2016).

99. Chen, C., Barcellos, D., Richter, D. D., Schroeder, P. A. & Thompson, A. Redoximorphic Bt horizons of the Calhoun CZO soils exhibit depth-dependent iron-oxide crystallinity. *J. Soils Sediments* (2018).

100. Gainey, S. R. *et al.* Clay mineral formation under oxidized conditions and implications for

paleoenvironments and organic preservation on Mars. *Nat. Commun.* **8**, 1–7 (2017).

101. Blattmann, T. M. *et al.* Mineralogical control on the fate of continentally derived organic matter in the ocean. *Science (80-.).* **745**, 742–745 (2019).

102. Kleber, M., Mikutta, R., Torn, M. . & Jahn, R. Poorly crystalline mineral phases protect organic matter in acid subsoil horizons. *Eur. J. Soil Sci.* 717–725 (2005) doi:10.1111/j.1365-2389.2005.00706.x.

103. Hazen, R. M. & Sverjensky, D. A. Mineral Surfaces, Geochemical Complexities, and the Origins of Life. *CSH Perspect.* **2**, 1–22 (2010).

104. Wattel-Koekkoek, E., Buurman, P., Van der Plicht, J., Wattel, E. & van Breeman, N. Mean residence time of soil organic matter associated with kaolinite and smectite. *Eur. J. Soil Sci.* **54**, 269–278 (2003).

105. Joshi, P. C., Dubey, K., Aldersley, M. F. & Sausville, M. Clay catalyzed RNA synthesis under Martian conditions : Application for Mars return samples. *Biochem. Biophys. Res. Commun.* **462**, 99–104 (2015).

106. Moni, C., Rumpel, C., Virto, I. & Chenu, C. Relative importance of sorption versus aggregation for organic matter storage in subsoil horizons of two. *Eur. J. Soil Sci.* **61**, 958–969 (2010).

107. Eigenbrode, J. L. *et al.* Organic matter preserved in 3-billion-year-old mudstones at Gale crater, Mars. *Science (80-.).* **360**, 1096–1101 (2018).

108. Horgan, B., Christensen, P. & Iii, J. F. B. Searching for pedogenic phyllosilicates in ancient martian soils. *AGU Fall Meet.* 1999 (2011).

109. White, P. D. & Schiebout, J. Paleogene paleosols and changes in pedogenesis during the initial Eocene thermal maximum : Big Bend National Park , Texas , USA C24r. *GSA Bull.*

1347–1361 (2008) doi:10.1130/B25987.1.

110. Staff, S. S. Keys to Soil Taxonomy. *United States Dep. Agric.* **12**, (2014).

111. Retallack, G. J. *Miocene paleosols and ape habitats of Pakistan and Kenya*. *Oxford Press* vol. 126 (1993).

112. Keil, R. G. & Mayer, L. M. *Mineral Matrices and Organic Matter*. *Organic Geochemistry* vol. 12 (Elsevier Ltd., 2014).

113. Goudge, T. A., Mustard, J. F., Head, J. W., Fassett, C. I. & Sandra, M. Assessing the Mineralogy of the Watershed and Fan Deposits of the Jezero Crater Paleolake System , Mars. *J. Geophys. Res. – Planets* (2015) doi:10.1002/2014JE004782.

114. Quantin, C. *et al.* Oxia Planum, the Landing Site for Exomars 2018. *47th Lunar Planet. Sci. Conf.* 2863 (2016).

115. Hedges, J. I. & Oades, J. M. Comparative organic geochemistries of soils and marine sediments. *Org. Geochem.* **27**, (1997).

116. Rampe, E. . *et al.* Amorphous phases on the surface of Mars. *Eighth Int. Conf. Mars* 1–2 (2014).

117. Morrisa, R. V. *et al.* Silicic volcanism on Mars evidenced by tridymite in high-SiO2 sedimentary rock at Gale crater. *Proc. Natl. Acad. Sci. U. S. A.* **113**, 7071–7076 (2016).

118. Smith, R. J., Rampe, E. B., Horgan, B. H. N. & Dehouck, E. Deriving Amorphous Component Abundance and Composition of Rocks and Sediments on Earth and Mars. *J. Geophys. Res. Planets* **123**, 2485–2505 (2018).

119. Pizarro, C., Escudey, M. & Fabris, J. D. Influence of Organic Matter on the Iron Oxide Mineralogy of Volcanic Soils. *Hyperfine Interact.* **148**, 53–59 (2003).

120. Schneider, M. P. W. *et al.* Sorptive stabilization of organic matter by amorphous Al

hydroxide. *Geochim. Cosmochim. Acta* **74**, 1606–1619 (2010).

121. Guggenberger, G. & Kaiser, K. Dissolved organic matter in soil : challenging the paradigm of sorptive preservation. *Geoderma* **113**, 293–310 (2003).

122. Huang, Y. T. *et al.* A new method to extract and purify DNA from allophanic soils and paleosols, and potential for paleoenvironmental reconstruction and other applications. *Geoderma* **274**, 114–125 (2016).

123. Rampe, E. B. *et al.* Mineralogy of an ancient lacustrine mudstone succession from the Murray formation , Gale crater , Mars. *Earth Planet. Sci. Lett.* **471**, 172–185 (2017).

124. Smith, R. ., Horgan, B., Rampe, E. & Dehouck, E. The Composition of Amorphous Phases in Soils and Sediments on Earth and Mars. *49th Lunar Planet. Sci. Conf. 2018* 14–15 (2018).

125. Baumgartner, R. J. *et al.* Nano − porous pyrite and organic matter in 3 . 5-billion-year-old stromatolites record primordial life. *Geology* 1–5 (2019) doi:10.1130/G46365.1/4834382/g46365.pdf.

126. Matthewman, R., Cotton, L. J., Martins, Z. & Sephton, M. A. Organic geochemistry of late Jurassic paleosols (Dirt Beds) of Dorset , UK. *Mar. Pet. Geol.* **37**, 41–52 (2012).

127. Benison, K. C. & Karmanocky, F. J. Could microorganisms be preserved in Mars gypsum? Insights from terrestrial examples. *Geology* **42**, 615–617 (2014).

128. François, P. *et al.* Magnesium sulfate as a key mineral for the detection of organic molecules on Mars using pyrolysis. *J. Geophys. Res. – Planets* 61–74 (2015) doi:10.1002/2015JE004884.Received.

129. Werne, J. . *et al.* Timing of early diagenetic sulfurization of organic matter : A precursor-product relationship in Holocene sediments of the anoxic Cariaco Basin , Venezuela.

Geochim. Cosmochim. Acta **64**, 1741–1751 (2000).

130. Raven, M. R. *et al.* Organic carbon burial during OAE2 driven by changes in the locus of organic matter sulfurization. *Nat. Commun.* **9**,.

131. Dubiel, R. & Hasiotis, S. T. Deposystems, Paleosols, and Climatic Variability in a Continental System: The Upper Triassic Chinle Formation, Colorado Plateau, USA. *Soc. Sediment. Geol. Spec. Publ.* **97**, 393–421 (2011).

132. Noe Dobrea, E. Z. *et al.* Characterizing the mechanisms for the preservation of organics at the Painted Desert: Lessons for MSL, Exo-Mars, and Mars 2020. *47th Lunar Planet. Sci. Conf.* Abstract #2796 (2016).

133. Sugitani, K., Kranendonk, M. J. Van, Oehler, D. Z., House, C. H. & Walter, M. R. Archean coastal-plain paleosols and life on land: Comment. *Gondwana Res.* (2016) doi:10.1016/j.gr.2016.12.002.

134. Sugitani, K., Mimura, K., Suzuki, K., Nagamine, K. & Sugisaki, R. Stratigraphy and sedimentary petrology of an Archean v olcanic Á sedimentary succession at Mt . Goldsworthy in the Pilbara Block , Western Australia : implications of e v aporite (nahcolite) and barite deposition. *Precambrian Res.* **120**, (2003).

135. Schopf, J. W. *et al.* An anaerobic ~3400 Ma shallow-water microbial consortium: Presumptive evidence of Earth's Paleoarchean anoxic atmosphere. *Precambrian Res.* **299**, 309–318 (2017).

136. Sugitani, K., Gray, K., Nagaoka, T. & Mimura, K. Three-Dimensional Morphological and Textural Complexity of Archean Putative Microfossils from the Northeastern Pilbara. *Astrobiology* **9**, (2009).

137. Maclean, L. . *et al.* A high-resolution chemical and structural study of framboidal pyrite

formed within a low-temperature bacterial biofilm. *Geobiology* 471–480 (2008) doi:10.1111/j.1472-4669.2008.00174.x.

138. Sawlowicz, Z., Arnstutz, P. G. C. & Love, L. G. Pyrite framboids and their development : a new conceptual mechanism. *Geol Rundsch* 148–156 (1993).

CHAPTER III.
MINERALOGY AND DIAGENESIS OF MARS-ANALOG PALEOSOLS FROM EASTERN OREGON, USA

Published as A. P. Broz, J. Clark, B. Sutter, D. W. Ming, V. Tu, B. Horgan, L. C. R. Silva, Mineralogy and diagenesis of Mars-analog paleosols from eastern Oregon, USA. *Icarus*. **380**, 114965 (2022).

1. Introduction

Today the surface of Mars is frigid, wind-deflated and barren, but there is extensive geological evidence for transient warm and wet habitable surface conditions in the Noachian (4.1–3.7 Ga) period of early Mars [1–4]. Orbital sensing of the Martian surface has revealed clay mineral deposits in thousands of locations, wherever Noachian-age terrains are not obscured by dust, sand, or overlying strata [5–8]. These ancient deposits are rich in smectite clay minerals and other hydrated phases, suggesting formation in subsurface and surface environments from the weathering of mafic rocks and sediments with liquid water.

While some phyllosilicates on Mars are associated with lacustrine deposition in surface environments (e.g., [9]) many phyllosilicate detections occur in regionally widespread deposits, inconsistent with deposition in basin settings. Two hypotheses to explain the formation, occurrence and distribution of these regionally widespread phyllosilicates on Mars are: 1) subsurface hydrothermal activity, diagenesis and/or authigenesis [10–14] and, 2) surface pedogenic alteration (e.g., subaerial chemical weathering) [2,6,14,15]. In some locations, trioctahedral smectites exhibiting lateral variations in Al and Fe/Mg smectites intermixed with chlorite, serpentinite, talc and zeolite are consistent with formation in hydrothermal subsurface environments, diagenesis, and/ or authigenesis during sediment emplacement [13,16,17]. However, dioctahedral smectites often outcrop as extensive vertical profiles of Fe/Mg smectites overlain by Al smectites, suggesting subaerial formation in surface environments, consistent with pedogenesis (soil formation) or large-scale leaching of sediments [14].

Paleosols are ancient, buried soils that are lithified into sedimentary rocks. On Earth, paleosols are a geological record of the atmospheric composition, climate, topography and organisms present before soil burial [18]. Paleosols are created by removal from their soil-forming factors, sometimes because of change in those factors, but most often by rapid burial. The

deposition of volcanic ash, flood basalts, sedimentation from flooding, landslides, and tsunami deposits all rapidly bury surface environments. Sequences of paleosols form when soils are periodically buried, for example by repeated volcanic eruptions which emplace tephra or lava onto soil surfaces, followed by successive pedogenic weathering of emplaced tephra or lava, and then subsequent burial by another eruption. Flooding by rivers also buries paleosols within alluvial sequences, and dune migration buries paleosols within eolian sequences. On Earth, sequences of paleosols formed by periodic burial can record weathering, paleoclimate and diagenetic alteration over 10^8 year timescales [19,20].

Paleosols are unique sedimentary rocks because before burial they witnessed the interaction between the atmosphere and a planetary surface [21]. The mineralogy of paleosols stores a record of this interaction, so the types and properties of minerals in paleosols can be used to help understand the nature of weathering and diagenesis on Mars [22,23]. The objective of this study was to examine the mineralogy and diagenetic alterations of Mars-analog paleosols from eastern Oregon, USA using analytical techniques similar to those onboard current and future missions to Mars.

1.1 Paleosols at John Day Fossil Beds National Monument

The John Day Fossil Beds National Monument in eastern Oregon, USA, is a Mars-analog site known for similarities in mineralogy and stratigraphy to clay-bearing sedimentary rocks on Mars. Here, Eocene and Oligocene (42-28 Ma) sedimentary rocks are a well-preserved sequence of andesitic to rhyodacitic paleosols [15,24–26]. The ~400-meter-thick sequence is host to over 500 individual clay mineral-rich (30-95 wt. %) paleosols spanning 15 Myr through the climatic cooling of the Eocene-Oligocene boundary (Figure 1). A record of dramatic climate change is preserved in the mineralogy of paleosols from the Eocene/Oligocene-age Clarno and John Day Formations, transitioning from high kaolinite and oxide abundances at the bottom (warm and wet Eocene), to high smectite abundances (drying out late Eocene), and then poorly crystalline phases at the stratigraphic top of the section (cool and dry Oligocene) [24,25].

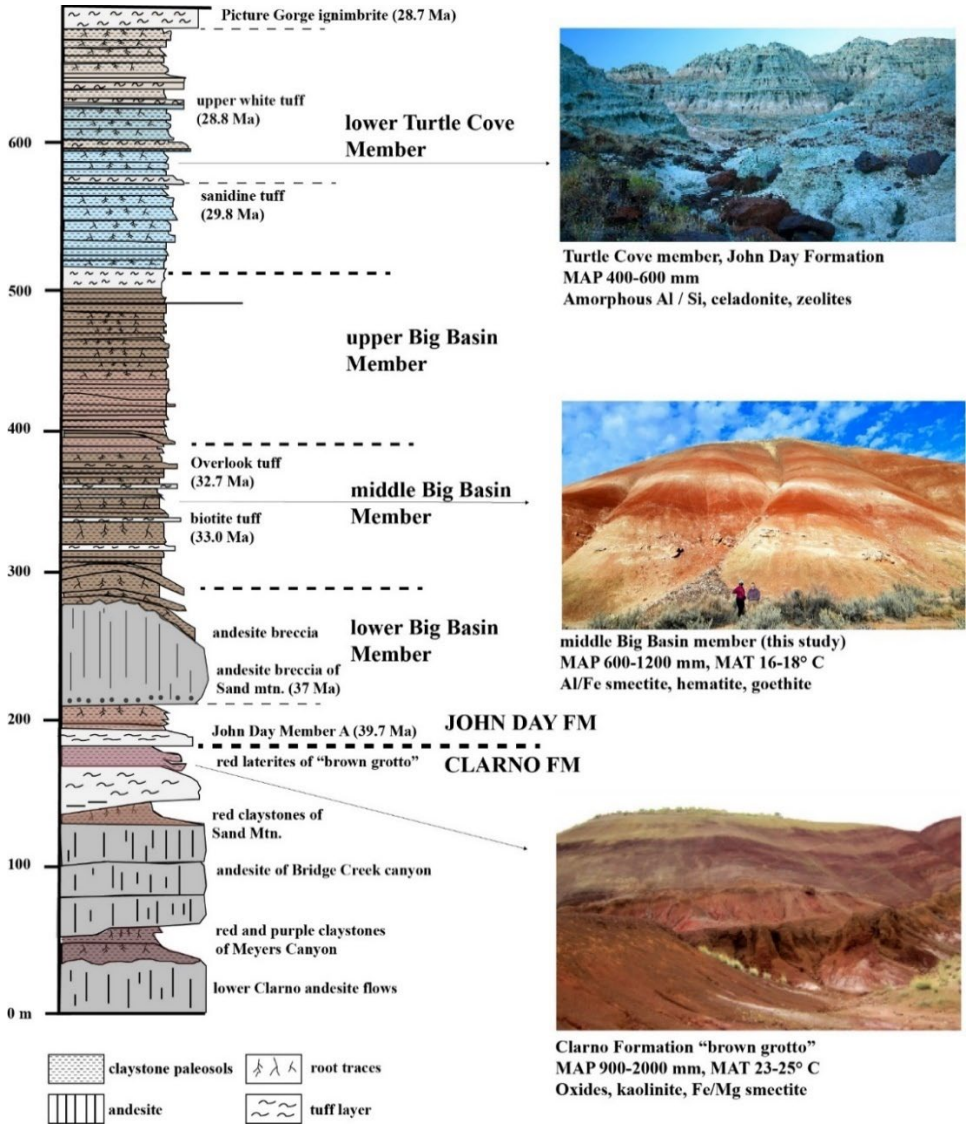

Figure 1. A sequence of Eocene through Oligocene (43-28 Ma) volcaniclastic paleosols in the Clarno and John Day Formations, John Day Fossil Beds National Monument (redrawn from [24]. Mean annual precipitation (MAP) and mean annual temperature (MAT) estimates are from [27].

Stratigraphically lowest in the section are deeply weathered red and purple lateritic paleosols (Oxisols and Ultisols in US Taxonomy [28]) within the uppermost Clarno and lowermost John Day Formations in the Painted Hills (~42 Ma). These paleosols formed under a warm and wet climate of an estimated 900-2000 mm mean annual precipitation (MAP) and mean annual temperature (MAT) of 23-25° C [25] (Figure 2). This unit of the section generally resembles the

basal Fe/Mg clay unit at Mawrth Vallis [20]. The Clarno paleosols have accumulations of oxides, kaolinite and Fe/Mg smectites and are erosionally truncated and abruptly overlain by less deeply weathered Al/Fe smectite-rich paleosols (Inceptisols and Alfisols) of the middle Big Basin Member of the John Day Formation (~33 Ma, samples from this location examined in this study). This truncation surface is correlated with the international Eocene-Oligocene boundary [25]. Big Basin member soils appear to have formed under a markedly cooler (MAT 16-18° C) and drier (MAP 600-1200 mm) climate relative to the early Eocene [27]. Stratigraphically above, in the Turtle Cove paleosols, another erosional truncation marks the base of the late Oligocene (~28 Ma) lower Turtle Cove Member of the John Day Formation which has minimally weathered calcareous paleosols (Aridisols and Andisols) containing abundant celadonite, calcite and amorphous colloids (imogolite, ferrihydrite and allophane) which indicate an even drier (MAP 400-600 mm) climate during the late Oligocene [29].

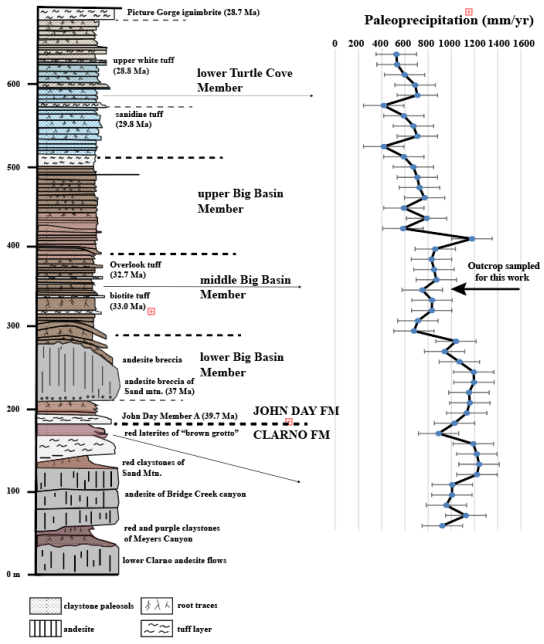

Figure 2. Declining precipitation through the Eocene/Oligocene boundary inferred from the mineralogy of paleosols from the Clarno and John Day Formations. The stratigraphic level of paleosols analyzed in this work is indicated (black arrow). Paleoprecipitation estimates are derived from an equation relating molecular weathering ratios (Bases/alumina [CaO + MgO + Na_2O + K_2O / Al_2O_3] to mean annual precipitation from a database of modern U.S soils (r=0.79, standard error = 179 mm) [27].

The Turtle Cove Member (late Oligocene) is composed of light brown and green colored Andisol (volcanic soils) and Aridisol (desert soils) paleosols that overlie the upper Big Basin member of the John Day Formation. The Turtle Cove Member has increased amounts of amorphous phases and calcite as well as the blue to green-colored clay mineral celadonite. Celadonite in the Turtle Cove paleosols is thought to form from the diagenetic Ostwald ripening of a poorly crystalline smectite and/ or other amorphous phases [25]. Although spectral signatures of celadonite and/or glauconite have been noted in the Mawrth Vallis region [30], it is currently unclear if celadonite is a component of putative Martian paleosols. In any case, the Turtle Cove paleosols have a dramatic reduction in smectite content and near absence of kaolin-group clays relative to the Clarno Formation paleosols at the base of the section [15,25]. Similarly, the accumulation of amorphous / nanocrystalline phases is observed at the stratigraphic top of the Noachian-age section at Mawrth Vallis [31] which is consistent with a drier, colder climate that was not sufficient to weather volcanic ash into more crystalline phases.

Stratigraphically above the Turtle Cove Member paleosols, approximately 300 vertical meters of flood basalts from the Columbia River Group cap the entire sequence. Based on these mineralogical transitions, the Eocene-age paleosols at the base of the section have accumulations of kaolinite and oxides that reflect a subtropical and humid climate, late Eocene/ early Oligocene paleosols in the middle of the section have Al/Fe smectites associated with a more arid climate, and paleosols with accumulations of nanophase aluminosilicates and amorphous phases higher in the stratigraphy indicate stepwise and cooling and drying during the late Oligocene [25]. Thus, sequences of paleosols at John Day are similar in mineralogy and stratigraphy to dioctahedral clay mineral sequences at Mawrth Vallis[15,32] and record a stepwise cooling and drying similar to proposed climates of early Mars.

Comparisons to putative Martian paleosols

Remote sensing of the Martian surface has revealed Noachian-age (4.1-3.7 Ga) layered sedimentary rocks rich in dioctahedral clay minerals that appear to be distributed globally across the surface of Mars [6,7,14]. These rocks are generally characterized by strong spectral signatures of Al clays overlying Fe/Mg clays over hundreds of vertical meters of stratigraphy. One hypothesis for their formation is from pedogenic weathering of mafic sediments like volcanic ash during intermittent warm periods early in Mars' history [6,14,22,33]. These materials are detected mantling

topographic highs including the summits and flanks of volcanoes, consistent with formation in surface environments via pedogenic weathering [4]. Many of the clearest examples of putative paleosols in Noachian-age terrains are observed in crater rims and generally resemble the stratigraphy and mineralogy of the John Day paleosols [15,32].

The rim of Muara Crater at Mawrth Vallis is host to a 150 – 200 m thick Fe/Mg smectite unit (topped by sulfate deposits in some areas) overlain by a 50 m thick Al-phyllosilicate or opal unit which transitions upward into poorly crystalline aluminosilicates or nanophase materials [34,35]. The entire section is then capped by an igneous deposit which appears to be composed of lava and/or basaltic sand [14], similar to the stratigraphy of the John Day Formation paleosols which are capped by approximately 300 meters of flood basalts. The layering of dioctahedral Al clay minerals and Fe/Mg clay minerals over hundreds of vertical meters suggests a subaerial formation environment for the clay minerals [14,22], and therefore congruent pedogenic alteration of basaltic parent material under warm and wet conditions is one hypothesis to explain the exceptional thickness of the Mawrth Vallis clay sequence [6,15,36,37].

The thickness of the Mawrth Vallis compositional stratigraphy (~150 -200 m) exceed the thickness of terrestrial weathering profiles (typically much less than 100 m thick) as well as having minor lateral and vertical diversity beyond the overall Fe/Mg smectite – Al-Si phase stratigraphy [15] which is also consistent with a pedogenic origin. Lateral and vertical diversity of clay minerals is not found in deep weathering profiles (e.g., saprolite mantles) but is common in paleosols, which have diversity in composition and color at ~1-meter scales. At Mawrth Vallis, there also appears to be relict bedding of dark-toned sands throughout the deposit, which suggests the coarse-sized fraction of the parent material may be preserved in certain layers as less-weathered bottom layers (C and R horizons) of paleosols. This relict bedding would presumably be destroyed if the entire deposit was a weathering profile [15]. Thus, dioctahedral phyllosilicate layers at Mawrth Vallis may be a paleosol sequence forming under a semi-arid climate, overlain by a thinner leaching profile and capped by a relatively unaltered igneous deposit [20,38]. This stratigraphy is consistent with climate hypotheses for early Mars, including a Noachian hyperarid frigid paleoclimate alternating with warmer and wetter conditions [14,23]. An alternative hypothesis is that the 150 meter-thick deposit resulted from sediment deposition and then extensive vertical leaching by liquid water during post-depositional diagenesis, but such

deep leaching profiles rarely exceed 100 m in thickness [15]. In contrast, the upper limit on terrestrial paleosol sequence thickness is ~ 9 km as observed in the Neogene Siwalik Group of India and Pakistan [18].

A similar pedogenic-like stratigraphy of dioctahedral Al clays overlying Fe/Mg clays has been detected in hundreds of locations across the surface of Mars which suggests widespread surface weathering was not limited to the Mawrth Vallis region [6,7]. Since many of layered clay mineral sequences on Mars resemble terrestrial paleosols [39], a detailed mineralogical analysis of paleosols from Earth can help with identification and interpretation of putative Martian paleosols. In this work, we sampled three consecutive paleosol profiles from the middle of the John Day Formation paleosol sequence (Figure 2) for a detailed examination of mineralogy and diagenetic alterations.

2. Methods

2.1 Sample collection

The paleosols examined in this study were collected from the Middle Big Basin Member of the John Day Formation (Figure 2) near the Painted Hills Unit of the John Day Fossil Beds National Monument in eastern Oregon, USA. Samples from three individual paleosols in vertical succession were collected approximately 7 km SW of the entrance to the Painted Hills unit of the John Day Formation (44.631105, -120.213107), in the Middle Big Basin Member of the John Day Formation, approximately 6 m above the local Eocene-Oligocene boundary (Figure 2). Samples were chosen from this site because it contained a sequence of three successive paleosols at a general topographic position (e.g., badland toeslope) that may be accessible for *in-situ* analysis on Mars, and because $^{40}Ar/^{39}Ar$ dating of volcanic tuffs above and below the sampling location allowed for a constrained age of 33.0 +/- 0.10 to 32.7 +/- 0.03 Ma (Biotite Tuff and Overlook Tuff, respectively) [24].

Samples were collected by trenching to ~30 cm into the paleosol outcrop and collecting samples down a vertical transect spanning three distinct paleosol profiles. Large, ~0.2 kg lithified chunks were removed from the brick-like paleosol surface for mineralogical analyses. Samples were collected down the vertical transect (parallel with the hillslope) at approximately 10 cm

intervals, similar to sampling the horizons of a modern soil profile. The Munsell color and qualitative calcareousness of samples were described during collection **(Figure 3**).

The three paleosols sampled were a red Alfisol ("Luca" pedotype from Retallack et al. (2000) [25], a tan Entisol ("Kskus" pedotype), and a brown Inceptisol ("Ticam" pedotype). In modern soil taxonomy, Alfisols are moderately weathered soils typically forming in semi-arid to humid climates under broadleaf temperate forests and are characterized by a clay-enriched subsurface horizon (layer) as well as accumulations of Al and Fe, lending the "Alf" of Alfisol. Entisols are minimally developed soils which are characterized by a lack of pedogenic horizon development and are generally minimally altered from their parent material. Inceptisols are "new soils" and typically have only weak development of horizons produced by top-down pedogenic weathering[28].

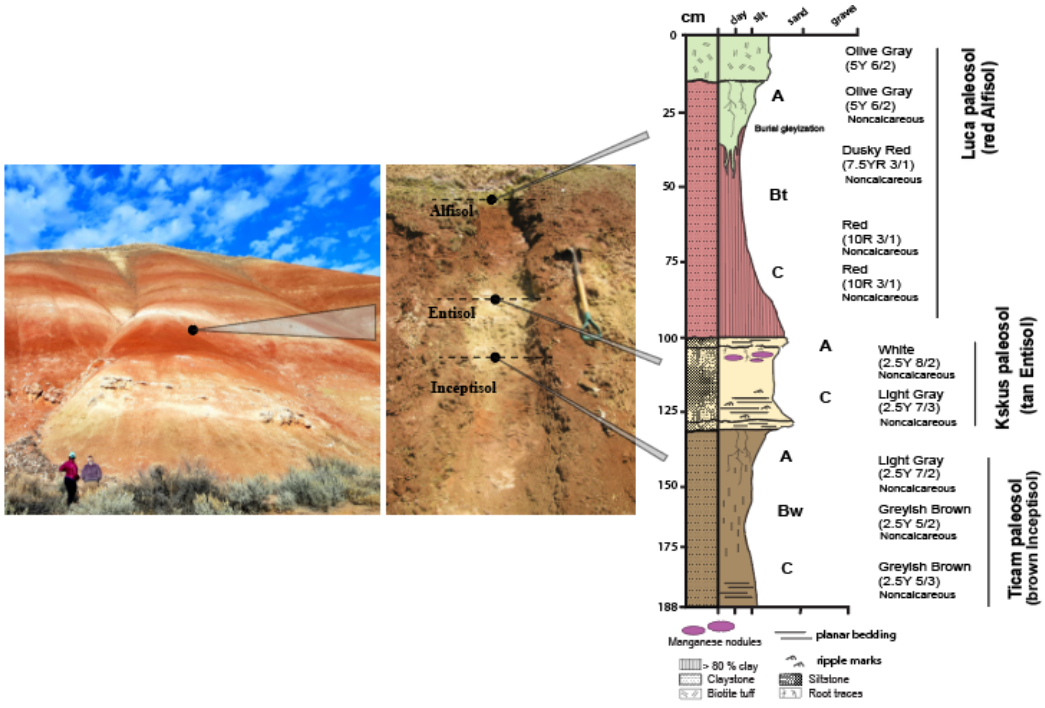

Figure 3. Morphology of three successive paleosols examined in this work. Paleosols are from the early Oligocene (33 Ma) middle Big Basin Member of the John Day Formation in eastern Oregon, USA showing lithology, grain size, horizon designations, and Munsell color. The upper paleosol (red with drab green top) is a moderately weathered red Alfisol (Hapludalf in US Taxonomy [28]) with a clay-enriched subsurface (Bt) horizon; stratigraphically below is a

minimally weathered and weakly developed Entisol with minimal pedogenic horizon development and persistent relict bedding in the subsurface (C) horizon (Fluvent in US Taxonomy, tan color); the lowest soil (brown color) is an Inceptisol with slight enrichment of clay into a weakly-developed subsurface (Bw) horizon (Andic Eutrochrept in US Taxonomy).

2.4 Visible-near infrared spectroscopy

Orbital and *in-situ* visible-near infrared (VNIR) spectroscopic techniques are used by current and future missions to Mars and are a useful tool for identifying minerals across the global Martian surface [5,40,41]. *In-situ* visible-near infrared (VNIR) spectroscopy was performed to identify clay minerals, zeolites and oxides in bulk paleosol samples using a portable ASD QualitySpec Trek spectrometer (Analytik, Cambridge, UK). Reflectance features from 0.35 – 2.5 μm were measured on bulk lithified samples at ambient (25 °C) temperature at the Condon Paleontology Center at the John Day Fossil Beds National Monument, and samples were not ground or sieved before analysis. Dioctahedral clay mineralogy was inferred from cation-OH combination bands in the 2.2 – 2.5 um region [42]. Band centers between 2.12 – 2.21 microns indicated the presence of Al-smectite. Fe/Mg clays and carbonates were identified from absorption bands between 2.27 and 2.36 microns while oxides were identified from bands between 0.75 – 1.03 microns. Absorption bands from zeolites are noted across the 2.1-2.5-micron range which overlap with Si-OH and/or metal-OH absorption bands in phyllosilicates. Zeolites were identified by the presence of absorption bands at 1.9, 1.4 and ~1.75 microns. Spectra were not gathered from the thinnest and least developed paleosol (Entisol), but all three paleosol types were subject to X-ray diffraction and evolved gas analysis, discussed below. \

2.5 X-ray diffraction of paleosol samples

The *Curiosity* rover employs X-ray diffraction (XRD) for identification of crystalline minerals in rocks, sediments and soils on Mars [43,44]. Thus, quantitative X-ray diffraction was used to identify crystalline minerals and estimate their abundances in bulk paleosol samples from the three consecutive profiles. Samples were first powdered and homogenized to < 45 μm grain size, then unoriented paleosol samples were mounted on aluminum holders and measured using a PANalytical X'pert Pro MPD XRD at NASA Johnson Space Center. XRD patterns were

collected using an X'celerator detector and Co Kα X-ray source, with a Fe filter to reduce Kβ peak intensities. Samples were analyzed under the following conditions: 45 kV, 40 mA, ½° antiscatter slit, ¼° fixed divergence slit, and a beam knife to reduce low-angle scattering. Samples were measured from 4° to 80° 2θ with a 0.02° step size at 100s/step. Mineral identification was accomplished using HighScore and Jade MDI software by comparing XRD patterns to International Center for Diffraction Data (ICDD) database patterns, and with Crystallography Open Database (COD) patterns.

2.6 Thermal and evolved gas analysis (EGA) of paleosol samples

The purpose of this work was to use analytical conditions similar to the Sample Analysis at Mars evolved gas analysis (SAM-EGA) instrument onboard the *Curiosity* rover to characterize the mineralogy of hydrated phases in samples, specifically by examining evolutions of H_2O and SO_2 from bulk paleosol samples during heating. Since thermal techniques such as evolved gas analysis will fly onboard future missions to Mars (e.g. ExoMars 2022 Rosalind Franklin rover [45]), a detailed characterization of terrestrial paleosol mineralogy can aid with interpretations of Noachian-age layered sedimentary rocks on Mars.

A Setaram Labsys Evo differential scanning calorimeter (DSC) / thermal gravimeter (TG) connected to a Pfeiffer Omnistar quadrupole mass spectrometer (QMS) was configured to operate similarly to the SAM evolved gas analyzer. The SAM instrument does not have TG/DSC capabilities, but these components permit a better understanding of phase transitions and chemical reactions in laboratory experiments. Approximately 50 mg ± 3 mg of ground paleosol sample were placed in an Al_2O_3 sample crucible which was ashed at 500° C to remove organic contaminants before use. The sample crucible and an identical empty reference crucible were placed in the furnace and then the system was purged twice with helium gas and then set to a pressure of 30 mbar. Helium was chosen as a carrier gas because it is inert and because it used as a carrier gas in the SAM instrument. The crucibles were heated from approximately 35 °C to 1000 °C at a heating rate of 35°C/min and at a flow rate of 10 sccm. Volatiles ranging from mass/charge (m/z) 1 - 100 were measured. All analyses were performed in duplicate.

Evolved water abundances were determined using a Netzsch TG/DSC coupled to a Pfeiffer QMS. An Al_2O_3 sample crucible and an identical reference crucible were placed in the furnace. The instrument was purged twice with ultra-high purity O_2 and set to a pressure of 1000 mbar

prior to sample analyses to remove any contamination in the system. Oxygen was chosen as a carrier gas because it encourages complete combustion of all organic and inorganic carbon in samples. The crucibles were heated from approximately 35 °C to 1000 °C at a heating rate of 35°C/min and at a flow rate of 19 ml O_2/min. A series of three blanks were analyzed before and after each group (n=10) of samples. A calibration curve for CO_2 was created by analyzing a calcite standard (Iceland sparry calcite 40 µM) at eight sample masses ranging from 0.01 – 4 mg. This calibration curve was used to calculate the amount of CO_2 evolved from each sample, and these values were converted to weight percent and subtracted from the thermogravimetric data to estimate mass loss from water evolutions. Since there were no major overlapping gases with evolved water, mass loss from low amounts (< 0.1 wt. %) of organic and inorganic carbon were the only significant sources of mass loss aside from water loss from hydrated phases (~3-5 wt. %), so the remaining mass loss after accounting for CO_2 evolutions was attributed to evolved H_2O, thus allowing for estimates of evolved water abundances from the thermogravimetric data. All analyses were performed in duplicate.

2.7 Bulk geochemistry and grain size

Oriented paleosol samples from the Condon Fossil Center at the John Day Fossil Beds National Monument (NPS permit # JODA-2019-SCI-0007) were used for a variety of lab analyses by point-counting (500 points) using a Swift automated stage and Hacker counting box fitted to a Leitz Orthoplan Pol research microscope. Relative percent of sand, silt and clay was determined by point counting and accuracy of point counting was determined to be ± 2 wt. % for common constituents. Bulk density was determined by the clod method [18] first by determining raw weight, then weight of clods coated in paraffin of known density (0.86g cm^{-3}) in and out of chilled (6°C) water (1.00 g cm^{-3}). Major element chemistry of paleosols was determined by X-ray fluorescence, atomic absorbance, and X-ray diffraction at Washington State University, Pullman. All data are included as supplementary data.

3. Results and Discussion

3.1 Chemical weathering trends

Trends in molecular weathering ratios across the three paleosol types were attributed to differences in chemical weathering intensity and duration. All profiles showed evidence of hydrolysis of volcaniclastic sediments from increases in alumina/silica and alumina/bases toward the top of profiles (Figure 4). Clay mineral content derived from point counting of thin sections ranged from 75.0 to 95.4 ± 2 wt. % and was greatest in the subsurface (Bt) horizon of the Alfisol and lowest in the surface (A) horizon of the Entisol. Generally low ranges of calcification ($CaO + MgO/Al_2O_3$) were noted in all three profiles and suggested minimal or absent accumulation of $CaCO_3$ which is characteristic of subtropical to temperate soils receiving annual rainfall of 600-1200 mm[27]. Pedogenic $CaCO_3$ typically accumulates in arid to semi-arid soils where annual evapotranspiration exceeds precipitation[46] and thus significant $CaCO_3$ accumulation was unlikely for paleosols from the Big Basin Member of the John Day Formation. There were negligible trends in alumina/silica ratios, but declining trends in Na_2O/K_2O suggest slight salinization in the uppermost paleosol (Alfisol), although this trend terminated in the surface (A) horizon of the Inceptisol. Salinization, a rough measure of the original salt content of paleosols, is defined by the molar ratio of Na_2O to K_2O and results from the deposition and/or precipitation of salts in the original soil. Minimal salinization may have caused the slight increase in this ratio at the surface of the Alfisol, but salinization was likely not severe because there was a lack of domed columnar peds and salt crystals that are characteristic of salt-affected soils and paleosols [18,47]. Lack of carbonate and generally deep weathering inferred from high smectite content is consistent with acidic pH, but low alumina/bases ratio, smectite mineralogy and residual feldspar clasts indicate moderate base saturation across all profiles. High oxidation of iron ($FeO/Fe_2O_3 = 0$) and deeply penetrating root traces indicate soil formation in well-drained settings, though the surface (A) horizon of the Alfisol showed slight gleyization ($FeO/Fe_2O_3 > 0$) most likely from the onset of chemically reducing conditions shortly after burial. This has been attributed to a diagenetic phenomenon known as burial gleization (discussed in detail in Section 3.5) that typically affects the organic matter-rich surface horizons of rapidly buried paleosols.

The chemical index of alteration (CIA) ranged from 72.1 to 80.8 and generally decreased with depth across the Alfisol and Inceptisol (Figure 4). The highest values (80.8) were in the subsurface clay (Bt) horizon of the Alfisol and lowest (72.1) in the C-horizon of the lowermost Inceptisol. The CIA in clayey paleosols is generally highest in subsurface

horizons due to illuvial accumulation of clay minerals during top-down hydrolytic weathering and therefore these horizons are thought to be the most reliable for paleoclimate estimations [27]. In contrast, the unweathered, lowermost C and R horizons of paleosols (e.g., saprolite) reflect the characteristics of the soil parent material rather than alteration from weathering, and thus CIA is lower in these horizons. The thinnest and least developed paleosol (Entisol) preserves a parent material of redeposited tuffaceous clayey siltstone that was minimally altered by soil formation, inferred from relict bedding in the C-horizon. The high clay content of this paleosol (~75 wt. %) was most likely inherited from preexisting soils by sheet erosion or flooding. It is unlikely that the Entisol was developed for long enough to develop characteristics indicative of paleoclimate, and therefore estimations of CIA are unreliable and not shown.

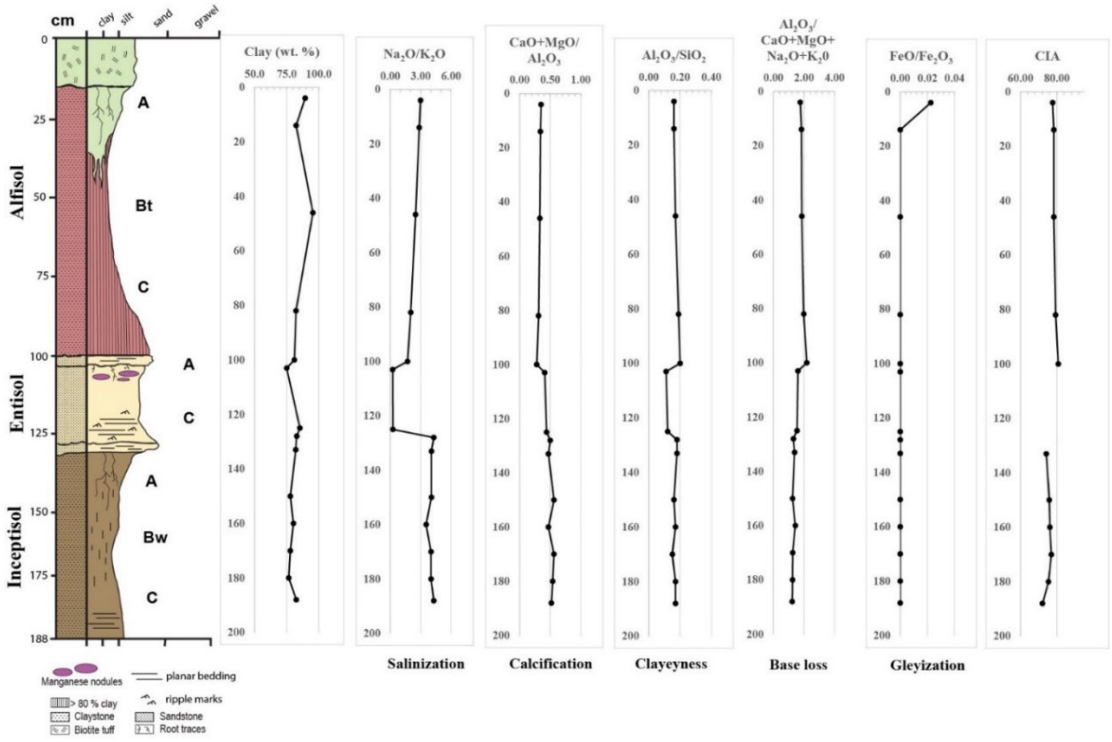

Figure 4. Chemical weathering trends as a function of depth across three paleosol profiles from the Oligocene (33 Ma) Big Basin Member of the John Day Formation. CIA = Chemical index of alteration, not shown for the weakly developed Entisol (middle profile).

3.2 Visible/ near infrared spectroscopy of paleosols

The mineralogy of paleosols observed with VNIR spectroscopy was dominated by dioctahedral phyllosilicates and occasionally zeolites and hematite. All paleosol samples had strong spectral signatures of 2:1 Al/Fe dioctahedral smectites (Figure 5) and distinct changes in mineralogy were observed within and between paleosol profiles. Spectral absorption bands were consistent with mixtures of Al-montmorillonite and Fe-nontronite, and/or Fe substitution in montmorillonite. There were no apparent reflectance features characteristic of trioctahedral smectites such as saponite [48] or 1:1 smectites such as kaolin group clays [42].

At the stratigraphically highest location, the near-surface horizon of the Alfisol, characterized by a drab green color, showed strong spectral signatures of Al-smectite with an asymmetric doublet feature centered at 2.22 with shoulders at 2.21 and 2.25 μm, and a strong water band at 1.92 μm (Figures 5 and 6). Band depths of the 1.9 and 2.2 μm absorption bands were variable across all samples **(Table S1).** Al smectites such as montmorillonite have a characteristic band at 2.21 μm, but the position of this band varies with Al-Fe-Mg abundance, where substitution of Fe for Al can cause additional bands at 2.23-2.25 μm [42]. A broad absorption band beginning near 2.4 μm was consistent with zeolites such as clinoptilolite. Zeolites are likely also be responsible for the strong hydration overtone bands at 0.98, 1.19, 1.45, 1.78, and 1.95 μm, of which usually only the 1.4 and 1.9 μm bands are visible in most other hydrated minerals. Diagenetic zeolitization of a poorly crystalline smectite or volcanic glass is thought to have led to the formation of clinoptilolite in paleosols from the John Day Formation [25]. At shorter wavelengths, the sample showed a shoulder at 0.5 μm and a strong band at 0.65 μm due to Fe^{3+} in smectite, as well as a broad weak absorption near 1.1 μm likely due to $Fe^{2+/3+}$ in smectite[40].

Stratigraphically lower, the subsurface (Bt) horizon of the Alfisol had much weaker signatures of an Al smectite with minor amounts of Fe-smectite. (Figure 5). Below this sample, the Alfisol C-horizon had a broad absorption band at 0.9 μm attributed to hematite, as well as weak absorption bands of Al smectite similar to the Bt-horizon. The 0.65 and 0.95 μm bands were absent in these samples which was consistent with an absence of Fe-smectite. Hematite in the C-horizon of the Alfisol may have formed from burial dehydration of ferric (oxy)hydroxides (e.g., goethite) which is a common diagenetic alteration in paleosols [18]. Bulk geochemistry of the Alfisol samples indicated lower Fe_2O_3 in the surface horizons of samples relative to subsurface horizons (Table 1) which is consistent with VNIR detections of hematite in subsurface horizons.

All samples of the brown colored Inceptisol had spectral signatures of a mixed Al/Fe smectite, with a clear band centered at 2.21 µm, a shoulder at 2.23 µm, and a weak band at 2.29 µm, and no detection of hematite. The light brown Munsell color of this sample (2.5Y 5/2) was markedly different than the brick-red (10R 7/1) color of the overlying Alfisol and suggests hematite abundances were much lower or absent in the Inceptisol. Sharp 0.65 and 0.95 µm Fe smectite absorption bands throughout the profile were consistent with accumulations of nontronite and/or Fe montmorillonite. Like the overlying Alfisol, band depths of the 1.9 and 2.21 µm absorption bands were also variable across all samples in the Inceptisol profile **(Table S1).**

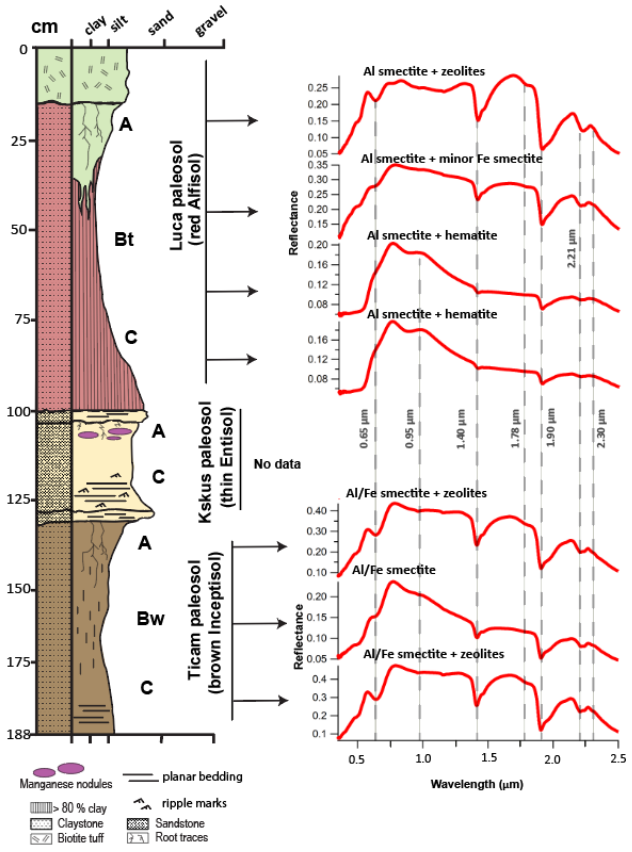

Figure 5. Visible/near infrared reflectance (VNIR) spectra of two paleosols (Alfisol and Inceptisol) from the early Oligocene (33 Ma) middle Big Basin Member of the John Day Formation in eastern Oregon, USA.

The spectral "doublet" feature with bands near 2.21 and 2.23-2.25 µm was observed in all samples and was attributed to OH stretching and bending combination vibrations in phyllosilicates (Figure 6). Doublet-type spectra typically represent mixtures of various hydrated minerals including kaolinite, Al-smectites and sulfate minerals [31,49], and previous work has shown that Fe^{2+}/Fe^{3+} smectites exhibit bands in this region [48]. A doublet feature near 2.21 and 2.23-2.25 µm may be a unique spectroscopic feature of pedogenic smectites that results from isomorphous substitution in the tetrahedral layer of 2:1 phyllosilicates during subaerial weathering. Previous work on smectite-rich mafic soils and paleosols show similar doublet features between 2.2 and 2.3 µm that are absent in standard clays [42,50]. The position and shape of the bands is highly variable, which may result from the isomorphic substitution of large amounts of Fe for Al which presumably distorts the crystal structure of clay minerals formed in mafic soils. These doublet features noted in paleosol samples here are similar to doublet features previously observed in paleosols from the John Day Formation [50]. Thus, the doublet features here are consistent with a pedogenic origin for Fe/Al smectites as has been previously suggested [50], though it should be noted that the phyllosilicate doublet feature has not been observed in silicic soils or other phyllosilicate-rich rocks [38,51], so absence of the feature is not necessary evidence against a pedogenic origin for clay minerals.

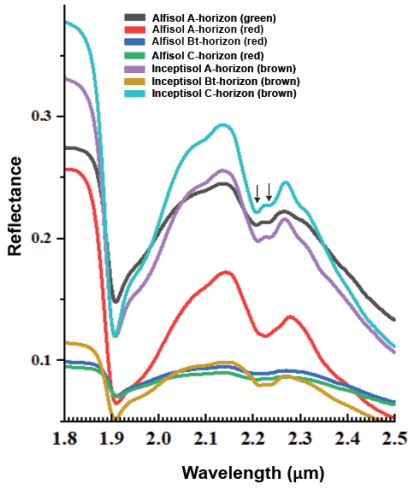

Figure 6. Near-infrared spectra from surface and subsurface horizons of two paleosols (Alfisol and Inceptisol) from the early Oligocene (33 Ma) middle Big Basin Member of the John Day Formation. Spectral doublet feature between 2.2 and 2.23-2.25 µm is indicated with black arrows.

3.3 X-ray diffraction of paleosols

XRD diffractograms showed abundant (> 70 wt. %) strongly crystalline clay minerals and low amounts (< 5 wt. %) of x-ray amorphous phases across all samples (Figure 7, Table 2). Major phases identified in all samples (> 5 wt. %) were montmorillonite (Al smectite) and nontronite (Fe smectite) while minor phases (< 5 wt. %.) identified from patterns in all samples were clinoptilolite, cristobalite, Opal-CT, quartz, andesine, orthoclase, gypsum and jarosite. Notably, the zeolite mineral clinoptilolite ($Na_{.66}Ca_{.86}K_{.64}Mg_{.26}Si_{18}O_{49.42}H_{26.4}$) was identified from patterns in all paleosol samples, which likely formed from Ostwald ripening of volcanic glass or other poorly ordered phases including smectite during Miocene-age burial recrystallization [25].

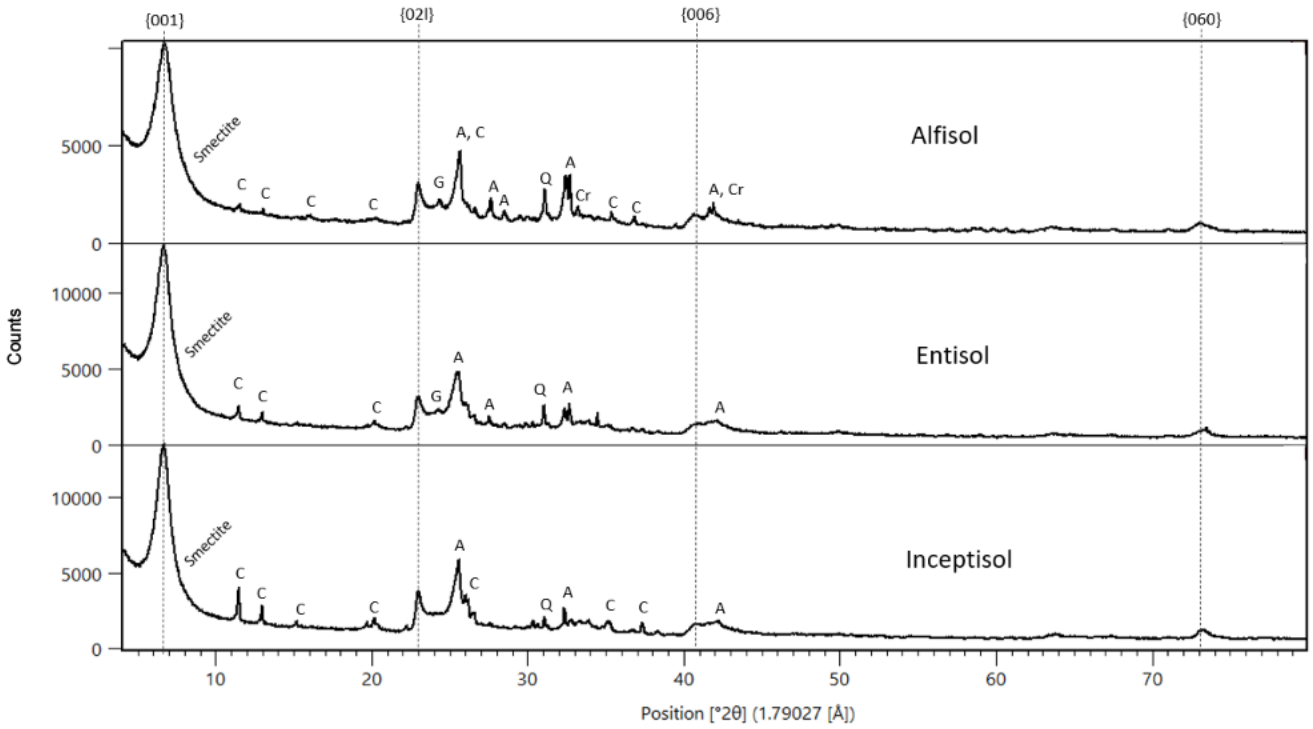

Figure 7. X-ray diffraction patterns from the near surface (A-horizon) of three paleosol types from the early Oligocene (33 Ma) middle Big Basin Member of the John Day Formation in eastern Oregon, USA. S=Smectite; G=Gypsum; A=Andesine; C=Clinoptilolite; Cr=Cristobalite; Q=Quartz. Highlighted are the 001 and 02l smectite peaks; difference in 02l band position corresponds to a difference in octahedral occupancy.

Beginning with the stratigraphically highest sample (Alfisol 4 cm), major phases identified from patterns were montmorillonite and nontronite while minor phases identified were andesine, Opal-CT and cristobalite, with lesser abundances of clinoptilolite, quartz, gypsum, jarosite, and anatase (Figure 7). Stratigraphically below this sample, the Alfisol A-horizon at 14 cm showed a similar mineral assemblage with the addition of albite as a minor phase (Table 2). A deeper sample of the Alfisol at 46 cm (Bt horizon) had montmorillonite and nontronite as major phases and albite, cristobalite, opal-CT, clinoptilolite, hematite, quartz and anatase as minor phases. Directly below, the pattern from Entisol A-horizon at 7 cm was consistent with montmorillonite and nontronite as major phases and cristobalite, anatase, clinoptilolite, labradorite, and orthoclase as minor phases (Figure 7). Stratigraphically below this sample, the pattern for the near-surface (A) horizon of the Inceptisol (3 cm) identified montmorillonite, nontronite and Opal-CT as major phases and clinoptilolite, cristobalite, andesine, orthoclase, quartz, and gypsum as minor phases. The pattern from the stratigraphically lowest sample, the Inceptisol Bw-horizon at 21 cm, showed the same major phases as the A-horizon (3 cm) sample, but with the additions of hematite, ilmenite ($FeTiO_3$) and anatase along with clinoptilolite, cristobalite, quartz and andesine as minor phases.

The abundance of crystalline clay minerals and lack of x-ray amorphous materials across all samples is consistent with formation from surface weathering of the andesitic to rhyolitic tuff / ash parent material under a temperate climate (MAT of ~10° C and MAP of 600-1200 mm) over 10-100 Kyr of soil formation [25]. This agrees with other estimates of MAT > 12° C and MAP of > 1000 mm from geochemical climofunctions applied to the subsurface horizons of paleosols from the middle Big Basin Member (~33.7 Ma) of the John Day Formation [27]. This amount of surface weathering over tens to hundreds of thousands of years transformed most volcanic glass to smectite via hydrolytic weathering, leaving only a small x-ray amorphous component (e.g., unweathered volcanic glass and/or poorly ordered phases) which presumably was diagenetically altered via zeolitization to clinoptilolite. There were no XRD detections of illite, which suggests minimal or absent potash metasomatism despite burial by an estimated ~2 km of overburden[52].

Table 2. Summary of major and minor phases detected with x-ray diffraction. Major phases (> 5 wt. % are noted with an X while minor phases (< 5 wt. %) are noted with an asterisk.

	Alfisol (4 cm)	Alfisol (14 cm)	Alfisol (46 cm)	Entisol (3 cm)	Entisol (7 cm)	Inceptisol (3 cm)	Inceptisol (7 cm)
Montmorillonite	X	X	X	X	X	X	X
Nontronite	X	X	X	X	X	X	X
Saponite			*				
Andesite		X				*	*
Clinoptililite		*		*	*	*	*
Cristobalite	*	*	*	*	*	*	*
Opal-CT	*	*	*	X	X	X	X
Quartz	*	*	*	*	*	*	*
Anatase	*	*	*	*	*	*	*
Albite		X	X	*	*		
Orthoclase					*	*	*
Hematite			*				*
Gypsum	*		*	*	*	*	*
Jarosite	*						
Others/Amorphous				*	*	*	*

3.4 Evolved Gas Analysis

3.5.1 H_2O evolutions

All samples evolved H_2O (m/z 18) during evolved gas analyses which was attributed to the release of adsorbed water, interlayer water, and water from dehydroxylation in the octahedral layer of a dioctahedral clay mineral (Figure 8). Low temperature (< 450 °C) and high temperature (>450 °C) evolutions of water from paleosol samples co-occurred with an endotherm in the heat flow data (dotted line, Figure 8) resulting from endothermic dehydration and dehydroxylation reactions, respectively. Evolved water abundances ranged from 3.24 ± 0.47 wt. % to 5.03 ± 0.12 wt. % across all samples (n = 20) and trends in water abundances were

apparent across the three paleosols. The Alfisol evolved the lowest amount of water observed with 3.24 ± 0.47 in the subsurface (Bt) horizon whereas the Entisol averaged 5.03 ± 12 wt. % which the highest amount of evolved water observed in the experiment. The Inceptisol ranged from 4.32 ± 0.03 wt. % to 4.81 ± 0.13 wt. % and showed a trend of decreasing abundance with depth. Despite significant differences in evolved water abundances between profiles, each profile generally showed a decrease in evolved water abundance with depth. Though many factors control the abundance and persistence of hydrated phases in paleosols, trends in evolved water abundances could have resulted from lateral and vertical diversity in mineralogy within each of the paleosol profiles.

Water evolutions at temperatures less than 300 °C were consistent with adsorbed water on mineral surfaces [53]. Evolutions of H_2O between 100 °C and 300 °C can result from the release of interlayer H_2O from smectite and other 2:1 clay minerals (McAdam et al., 2020) or from dehydroxylation and/or dehydration of poorly crystalline, nanophase or amorphous aluminosilicates such as allophane and imogolite [55]. Nanophase oxides/oxyhydroxides including ferrihydrite can evolve adsorbed H_2O at temperatures ranges below ~450 °C due to their high specific surface areas [56] and could have contributed to water evolutions below 200 °C. Other sources of minor H_2O evolutions near 300 °C could be from oxyhydroxides such as goethite which dehydroxylate at temperatures ranging from 280-320 °C [57].

Differences in evolved H_2O peaks < 450 °C across the three paleosols examined here may have resulted from differences in abundance and composition of x-ray amorphous components. Though amorphous phase composition was not examined in this work, a previous study identified basaltic glass (5.6 wt. %), allophanes (7.9 wt. %) and ferrihydrite (0.6 wt. %) as the dominant amorphous phases in paleosols from the Oligocene (~28 Ma) Turtle Cove member of the John Day Formation (Smith et al., 2018) which are stratigraphically higher than paleosols examined here (Figure 1). Turtle Cove paleosols have mineralogical and paleobotanical evidence of a cool and dry climate of an estimated MAP of 400–600 mm (Figure 2) and thus minor alteration of volcanic ash and tuff [27]. A SAM-EGA analog analysis of a Turtle Cove paleosol was performed by Smith et al. (2018) [55] who noted a water release peak at ~290 °C which was attributed to the abundance (> ~40 wt. %) of amorphous materials in the sample, unlike the low amount (< 5 wt. %) of x-ray amorphous phases found in smectitic paleosols in the middle Big Basin member of the John Day Formation. Paleosols from the Big Basin Member formed under a

much warmer (MAT 16-18° C) and wetter (MAP 600-1200 mm) climate than those from the Turtle Cove Member and was sufficient to transform amorphous and nanocrystalline phases to Al/Fe smectites. In the present study there were no sharp water release peaks at ~290 °C (Figure 8), possibly because samples are composed primarily of strongly crystalline clay minerals rather than amorphous colloids, especially the Alfisol with up to 95 wt. % clay minerals (Figure 3). However, a minor 300 °C endotherm in all samples is consistent with small amounts of amorphous phases, which were also detected with XRD as minor phases in the Entisol and Inceptisol (Table 2). In contrast to the moderately weathered Alfisol, the Entisol and Inceptisol were only minimally weathered before burial, inferred from morphological features such as absence of clay illuviation and persistence of relict bedding in subsurface horizons (Figure 3). As such, differences in the duration of weathering before burial can explain the persistence of amorphous phases in the Entisol and Inceptisol and absence of amorphous phases in the Alfisol.

Overall, the preservation of metastable amorphous phases over geological time scales is uncommon in sedimentary rocks; however, recent work has shown that large amounts (> 40 wt. %) of amorphous colloids have persisted for millions of years in lithified and diagenetically altered volcaniclastic paleosols from the Oligocene (~28 Ma) Turtle Cove Member of the John Day Formation [19]. Thus, detections of minor amounts of amorphous phases (< 5 wt. %) with both EGA and XRD suggest metastable amorphous and/or nanocrystalline phases may have also persisted for ~33 Ma in paleosols from the middle Big Basin Member of the John Day Formation.

Evolutions of H_2O above 450° C are consistent with the dehydroxylation of the octahedral layer of a 2:1 phyllosilicate [54,58], and there was a ~200° C difference in H_2O peak release temperature between the three paleosols. The Alfisol with ~95 wt. % smectite evolved H_2O with peaks centered at ~500° C, while the Entisol (~75 wt. % smectite) and the Inceptisol (~78 wt. % smectite) evolved H_2O with peaks centered at ~ 700 °C. Differences in clay mineralogy between the soils may be responsible for shifting the peaks and shoulders of the high-temperature (> 450° C) evolutions. The considerable difference in peak H_2O release temperature between the red Alfisol (~500° C) and the other soils (~700° C, Figure 8) could have resulted from differences in the occupation of the octahedral sheet of a 2:1 phyllosilicate [53] which leads to differences in the high temperature H_2O peak release temperature during SAM-EGA [59,60]. Clay minerals with Fe in the octahedral layer (e.g., nontronite or Fe-montmorillonite)

dehydroxylate at a lower temperature (~500° C) relative to smectite with Al in the octahedral layer (e.g., Al-montmorillonite, 700° C) [60], though mixed illite-smectite mineralogy also show peak H_2O release at 698° C. The Alfisol (~500° C peak H_2O release) exhibited strong VNIR signatures of an Al-smectite with minor Fe-smectite and hematite. The brown Inceptisol (~700° C peak H_2O release) had strong VNIR signatures of an Al/Fe smectite and lacked hematite (Table 2, Figure 5). Differences in clay mineralogy across the samples likely caused the large difference (~200° C) of peak water release temperatures from smectite dehydroxylation. Together these results show that EGA in conjunction with XRD and VNIR spectroscopy are suitable techniques to constrain smectite mineralogy in paleosols.

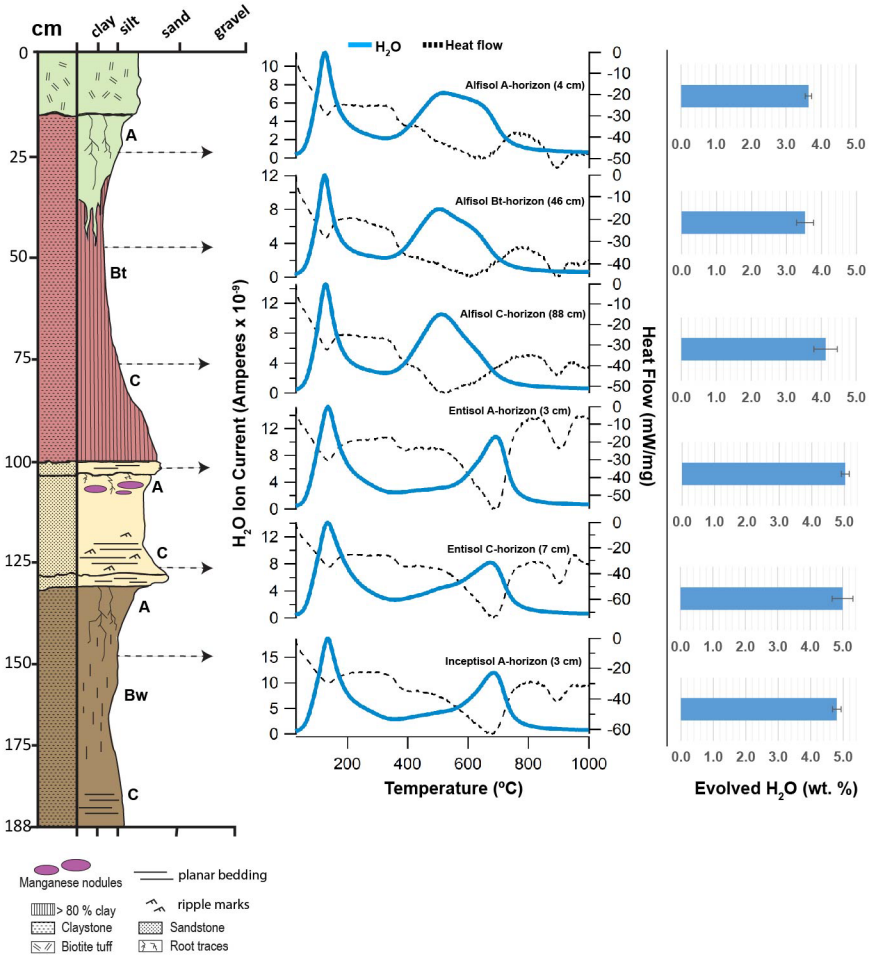

Figure 8. Evolutions of H_2O from early Oligocene (33 Ma) paleosols from the John Day Fossil Beds National Monument, Oregon. Blue trace is H_2O (m/z 18), and dashed trace is heat flow from differential scanning calorimetry (DSC).

3.5.2 SO_2 evolutions

All samples evolved minor amounts of SO_2 primarily above 450° C (Figure 9). Minor SO_2 peaks below 400° C were observed in the Bt-horizon of the Alfisol and the A-horizon of the Entisol (Figure 9) which most likely resulted from instrument background sources. A distinct SO_2 peak at 400° C in the A-horizon of the Entisol is consistent with the presence of minor amounts of sulfides such as pyrite and/or pyrrhotite which thermally decompose at temperatures above 400° C under SAM-EGA analog conditions [61]. Oxidative sulfite decomposition directly to SO_2 could have resulted from trace amounts of oxygen in the instrument furnace even after successive purges with helium and are the likely source of the broad 400° C SO_2 peak noted in the Entisol.

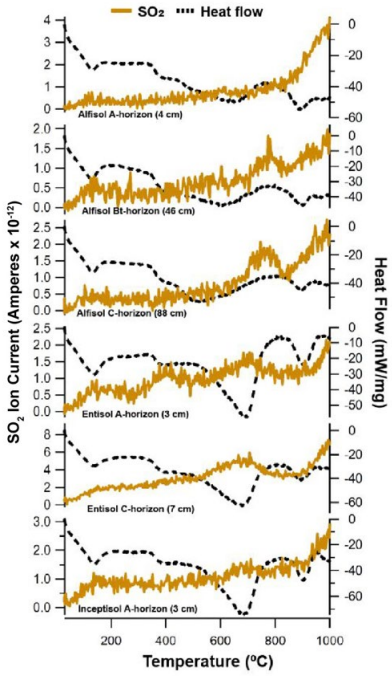

Figure 9. Evolutions of SO_2 from early Oligocene (33 Ma) paleosols from the John Day Fossil Beds National Monument, Oregon. Yellow trace is SO_2 (m/z 64), and dashed trace is heat flow from differential scanning calorimetry (DSC).

Evolutions of SO_2 above 500° C are consistent with the thermal decomposition of Ca and Fe sulfates ranging from crystalline (gypsum and jarosite) to amorphous and/or adsorbed sulfate [56,61]. Also possible are contributions from organo-sulfur compounds and/or S phase inclusions in volcanic glass. Crystalline sulfate species including jarosite and gypsum have peak SO_2 release

temperatures near 900° C and 1200° C, respectively [57]. Thus, jarosite and gypsum most likely account for the evolutions of SO_2 above 600° C and both were confirmed as minor phases with XRD (**Table 2**). Samples from the Bt and C horizons of the Alfisol had a broad SO_2 release with a peak at ~790° C which was absent in the Entisol and Inceptisol. At higher temperatures, all soils showed a major release of SO_2 beginning at 900° C which co-occurred with an endotherm, both of which are consistent with the thermal decomposition of crystalline sulfates [58,62]. Since the samples were only heated to ~1000° C for this work, the maximum peak height of this release cannot be ascertained.

The presence of sulfate minerals is uncommon in smectite-rich soils such as those examined here. Sulfate minerals such as gypsum and jarosite tend to form at low pH and low water:rock ratios whereas pedogenic smectites such as montmorillonite typically form at circumneutral pH and increased water:rock ratios. Both gypsum and jarosite are unlikely to be original minerals in the paleosols, but more likely formed in the current weathering zone. One possibility for the origin of sulfate minerals in these paleosols is leaching from the modern soils forming atop paleosols (e.g., the weathered paleosol surface). These modern soils that mantle paleosol outcrops have visibly accumulated pedogenic gypsum into a thin (~1 cm) subsurface gypsic (By) horizon, allowing for their classification as Gypsids (gypsum-rich desert soils) in US Soil Taxonomy[28]. The modern soils are subject to an estimated MAT of 33° C and MAP of 290 mm which is significantly warmer and drier than the estimated conditions during the formation of John Day Formation paleosols (MAT 16–18° C and MAP of 600–1,200 mm). Sulfate minerals observed with XRD and EGA could have accumulated over time in the underlying paleosols and therefore it is likely that the modern Gypsic soils forming atop paleosol outcrops are the source of sulfate minerals observed here.

3.5 Diagenetic Alteration

Diagenetic alterations, or alterations after burial, are common in paleosols. By definition, soils are an early diagenetic alteration because water-rock interactions during pedogenesis alters the physical and chemical properties of sediments. After burial, however, soils are subject to additional early and late diagenetic alterations ranging from minor (e.g., decomposition of organic matter) to severe (e.g., metamorphic alteration). Four types of alteration after burial that have affected paleosols examined in this work are 1) Drab olive-green surface horizons

attributed to burial gleization; 2) brick-red color from burial-induced dehydration of ferric hydroxide minerals; 3) zeolitization of volcanic glass and/or poorly crystalline phases; and 4) significant mechanical compaction.

Burial gleization, also known as gley overprinting [63], has been envisaged as the chemical reduction of iron oxides and hydroxides by anaerobic bacteria in the near-surface horizons of paleosols and is thought to occur shortly after soil burial[64,65]. Burial gleization is an early diagenetic process in paleosols which involves the reduction of Fe^{3+} to Fe^{2+} in clays, oxides and other minerals after rapid burial, and promotes anaerobic decay of organic matter[18], even in soils that originally formed under oxidizing conditions before burial. Typical burial gleization is closed system alteration, without depletion of total iron, and is usually limited to the surface (A) horizons where organic matter is most concentrated. The surface (A) horizon of the uppermost paleosol (Alfisol) examined in this work showed classic evidence of burial gleization with drab-colored mottles and tubular features predominantly in the A-horizon with minor radiation downward into the subsurface (Bt) horizon (Figure 3) as well as accumulations of Fe^{2+} exclusively in the A-horizon (Table 1). Spectroscopic techniques such as VNIR employed here can readily identify burial gleization by observing absorbance features attributed to Fe^{2+} in the surface horizons of paleosols. This was presumably the cause of the broad 1.1-micron Fe^{2+} band in the surface of the Alfisol, and the shoulders at 2.23-2.25 microns noted in the gleyed surface horizon of the Alfisol (Figures 5 and 6).

Burial gleization can be distinguished from other original redoximorphic features such as groundwater alteration because it is limited to the surface (A) horizon unlike the gleyed subsurface (Bg) horizons of seasonally or perennially waterlogged soils, and because the mineralogy and morphology of this soil provide evidence of well-drained and oxidizing conditions during soil formation. Morphological evidence of burial gleization in paleosols is a drab greenish-gray color exclusively in near-surface horizons directly below the burial contact[65]. Geochemical evidence of burial gleization can include depletions of Fe^{3+} coupled with increases in Fe^{2+} and the formation of siderite and pyrite. Most soils accumulate organic matter in near-surface horizons, which after burial and the onset of anoxic conditions is generally the horizon most affected by burial gleyization. Though the timing of burial gleization remains poorly constrained, reduction haloes around buried organic matter such as roots can form in tens to hundreds of years after burial[66]**.** In the Alfisol, burial gleyization can be distinguished from

groundwater alteration because it is limited to the surface horizon directly below the white biotite-bearing tuff layer which buried the uppermost soil (Figure 3). The original color of the surface horizon of the Alfisol was most likely brown and darkened by accumulation of organic matter. Burial gleization thus indicates the surface horizon of the Alfisol may be enriched in organic matter relative to unaffected subsurface horizons (Bt and C horizons), but burial degradation of organic carbon over geological time scales has likely reduced the original organic carbon content by up to two orders of magnitude [67].

Directly below the drab surface horizon, the remainder of the Alfisol profile was brick-red in color (Figure 3, Munsell 10R 3/1) which most likely resulted from dehydration of iron oxyhydroxides [68]. This phenomenon, also known as "burial reddening", is one of the most common types of diagenetic alteration in the fossil record of soils on Earth [18,64]. Diagenetic dehydration of oxyhydroxides such as goethite and ferrihydrite forms strongly crystalline hematite which leads to reddening of soils that are originally brown or yellow in color; however, there is little information about the specific temperatures and pressures at which dehydration reactions occur [68]. Such a deep red color is unlikely to be the original color of the Alfisol because comparable modern Alfisols with smectite mineralogy are brown to yellow in color [27]. Brown and yellow weakly to moderately developed Eocene paleosols from Antarctica also have deep red hues attributed to burial dehydration of ferrihydrite and goethite [68]. Some of the kaolinitic and lateritic paleosols in the Clarno and lower John Day Formations show evidence of deep weathering comparable to modern tropical soils that are red in color; however, soils that are not so deeply weathered such as the Alfisol examined here also have a brick-red color which is consistent with burial reddening. Other factors which cause reddening of paleosols include heating by lava flows [69] which can also cause iron oxyhydroxides to dehydrate to hematite and maghemite, but the effects of reddening are typically limited to the near-surface horizons due to the thermal insulation properties of soils [70]. Another possibility is that the protolith of the soil was red in color, but relict bedding and volcanic shards in the subsurface (C) horizon (Figure 3) imply a tuffaceous parent material unlikely to be red in color.

The presence of clinoptilolite detected with XRD in all samples (Table 2) suggests zeolitization has pervasively altered paleosols from the John Day Formation. Though zeolites can form in alkaline volcanic soils [71], a diagenetic origin for clinoptilolite is likely because zeolites are commonly destroyed by hydrolysis during original soil formation, especially in the

case of the moderately weathered, smectite-rich Alfisol. There are two proposed mechanisms of zeolitization to the John Day Formation paleosols. First, the aqueous flushing model by Hay (1963) [72] proposed that volcanic glass in the lower John Day Formation was diagenetically altered to zeolites by open-system interactions with groundwater that added Ca and H_2O while removing Si, Na and K. Zeolitization may have occurred during early Miocene deep burial at depths of 380-1200 meters and temperatures of 27-55° C during deposition of the overlying Mascall and Rattlesnake Formations. Though the timing of zeolitization is well constrained, the mechanism of alteration by aqueous flushing is not likely because many silty tuff beds in the John Day Formation escaped zeolitization while the clay mineral-rich paleosols did not [25]. These permeable silty tuff beds would have presumably been channels for groundwater, but they include both zeolitized and non-zeolitized segments along strike, suggesting a more localized or patchy distribution of zeolitized facies. These observations are consistent with the hypothesis that some tuffs and paleosols were subject to zeolitization, while others were not.

Rather than zeolites forming from groundwater alteration, diagenesis may have been more localized and the formation of clinoptilolite may have instead resulted from burial-induced Ostwald ripening of amorphous colloids and/or volcanic glass [73,74]. The "burial ripening" model of Retallack (2000) [25] for zeolitization of paleosols is supported by observations of only small differences between abundances of alkali and alkali earths in paleosols most altered by zeolitization (the Turtle Cove Member paleosols) when compared with minimally altered tuffs. The stepwise increase in alkali and alkali earths in paleosols from the lower John Day Formation to the upper Turtle Cove Member most likely resulted from decreases in weathering intensity during climatic cooling and drying and is independently supported by soil morphological and paleobotanical evidence of cooling and drying[24,25]. Altogether these lines of evidence support the ripening model for zeolitization which led to localized formation of clinoptilotile from burial-induced Ostwald ripening of volcanic glass and/or amorphous colloids. The mechanism(s) of zeolitization are important for interpreting paleosols of the middle John Day Formation including those examined here because their chemical composition would be pervasively altered by the aqueous flushing model, whereas by the burial ripening model their original chemical composition would not have been significantly altered [25].

Paleosols from the lower John Day formation are buried by approximately 2 kilometers of overburden which has led to significant mechanical compaction. Burial of soil most often results

in compaction of void spaces, fossils and pore water. In clayey soils such as those examined here, compaction of originally loose soil peds creates a complex pattern of slickenslides with random orientation that resembles that slickenslides in modern smectitic soils with high shrink-swell capacity (Vertisols in US Taxonomy). Paleosols from the John Day Formation are geologically young enough to allow for comparisons with standard compaction curves for sedimentary rocks. Individual profiles from the middle Big Basin Member of the John Day Formation are covered by an additional 499 m of John Day formation, 305 m of Columbia River Basalt, up to 605 m of Mascall Formation, and 244 m of Rattlesnake Formation. From this overburden, compaction of paleosols can be estimated using the compaction curve of Sclater and Christie (1980)[75] and are compacted to an estimated ~70% of their original thickness, which would suggest an original thickness of about 1.3 m for the uppermost Alfisol profile, 0.4 m for the Entisol profile, and 1.3 m for the lowermost Inceptisol profile.

3.6 Implications for Mars

Paleosols at the John Day Fossil Beds National Monument have been proposed to be comparable with putative weathering profiles on Mars because of similarities in mineralogy, morphology and stratigraphy[15,20,32,67], and can therefore be used to help interpret the alteration history of sedimentary rocks on Mars. Specifically, work on terrestrial paleosols presented here has implications for a) interpreting orbital remote sensing data for the pedogenic/diagenetic history of sedimentary rocks on Mars, b) constraining climate and habitability from Martian weathering profiles, c) comparing with *in-situ* results from Mars weathering profiles, and d) biosignature preservation in paleosols.

Orbital VNIR spectroscopic observations can be compared with VNIR spectra from terrestrial paleosols to evaluate the pedogenic and diagenetic history of ancient sedimentary rocks on Mars. *In-situ* VNIR spectroscopy of multiple individual paleosol profiles in this work provides a reference frame for evaluating a pedogenic alteration hypothesis for ancient sedimentary rocks on Mars. Though pedogenic processes may have been ubiquitous across the surface of early Mars [6], it is currently unclear from orbital VNIR spectroscopy if weathering sequences formed from continuous pedogenic alteration (e.g., a single, massive leaching profile) [22,39], or if multiple episodes of alteration followed by burial occurred (e.g., repeated episodes of

volcanic ash deposition, subaerial weathering, and burial)[14]. The latter formation mechanism is characteristic of paleosol sequences that are composed of hundreds of individual paleosol profiles [18] such as the paleosol sequence observed here. At Marth Vallis, meter-scale relict bedding of the middle (α2) Al-smectite stratigraphic unit at Muara Crater [22] is consistent with the repeated alteration and burial hypothesis, though previous work has considered this unit part of a single, massive (~200 m-thick) weathering profile [22]. However, relict bedding of dark-toned layers in the α2 unit [35] would presumably be destroyed if the entire deposit was a single weathering profile, and stratigraphic changes in mineralogy and geochemistry could be due to changes in climate, weathering intensity and geochemistry rather than top-down leaching of acidic and reducing fluids through hundreds of vertical meters of stratigraphy. The orbital remote sensing resolution of CRISM (18 m/ pixel)[5] is much coarser compared to our *in-situ* observations (sub-meter scale), which perhaps makes sequences of individual paleosol profiles appear as "units" with similar mineralogy. Our observations of the Oregon paleosol sequence suggest that changes in climate (e.g. Eocene-Oligocene cooling and drying) led to changes in mineralogy. These are reflected in the tens of individual paleosol profiles composing the lowermost Fe/Mg smectite and oxide unit (Clarno Formation, **Figure 1**) that are overlain by hundreds of individual profiles with Al/Fe smectite mineralogy in the middle unit (Big Basin Member, John Day Formation) which are subsequently overlain by hundreds of profiles dominated by nanophase/amorphous Al and Si materials, hydrated silica, calcite and celadonite (Turtle Cover Member). Therefore, stratigraphic changes in mineralogy reflect a cycle of continuous soil formation and burial that occurred during ~15 million years of climactic cooling and drying [27]. However, other putative weathering sequences on Mars are more consistent with the continuous alteration and leaching hypothesis[39], and the rim of Muara Crater currently stands as the best example of a paleosol sequence on Mars. From an orbital scale, resolving the formation mechanism of weathering sequences is important for understanding the nature of pedogenic alteration of sediments on early Mars. Future comparisons of other paleosols from the ~500 individual profiles within the eastern Oregon paleosol sequence with orbital VNIR spectra from Muara Crater may provide addition information to constrain the mechanism of formation of the weathering sequence at Mawrth Vallis.

Future *in-situ* investigation of putative Mars weathering profiles can be compared to spectral and morphological features observed in this study to constrain the pedogenic and diagenetic history. Here, these features included strong VNIR absorbance bands characteristic of dioctahedral Al and Fe smectites; changes in clay mineralogy with depth, primarily observed in the 2.1-2.5 micron range; illuvial accumulation of clay minerals into subsurface (Bt) horizons; the formation of pedogenic structures such as peds and cutans [18]; destruction of sedimentary bedding; relict bedding in unweathered bottom layers (C horizons); and centimeter-scale changes in color and composition. These are all diagnostic features of terrestrial soils and should be considered permissive evidence of pedogenic alteration on Mars. Spectral features of diagenetic alterations included absorbances characteristic of zeolites and hematite that are indicative of zeolitization via Ostwald ripening of amorphous colloids and burial dehydration of iron (oxy)hydroxides, respectively. These and other forms of diagenesis are common in paleosols that formed from weathering of volcaniclastic sediments [18] and may also explain occurrences of zeolites [76] and hematite [39] detected from orbit in putative weathering sequences on Mars.

This study also provides a protocol for constraining climate and habitability from the geochemistry of weathering profiles on Mars. By using a suite of molecular weathering ratios and geochemical climofunctions (Figure 4), a reconstruction of the climate and nature of weathering can be inferred from weathering profiles on Mars. Molecular weathering ratios that have been well studied in terrestrial paleosols (e.g.,[27,77]) and could be useful for interpreting climate and habitability of weathering profiles on Mars. However, differences in the nature of weathering and diagenesis between Earth and Mars present challenges for making direct comparisons. Such differences include a presumably anoxic early Mars atmosphere that perhaps led to Fe^{2+} mobility during subaerial weathering [22], and the apparent absence of plate tectonics on the planet which has implications for the nature and severity of diagenesis of weathering profiles on Mars [78]. One additional consideration is application of the chemical index of alteration to weathering profiles on Mars that show evidence of acidic alteration. Weathering indices such as CIA may not accurately reflect acid sulfate weathering of mafic Fe/Mg rich sediments because weathering rates of mafic materials such as olivine proceeds more efficiently than feldspars, especially under acidic conditions. In addition, acidic conditions also affect the mobility of alkaline elements which may further confuse interpretations of weathering intensity through CIA [39]. Martian weathering profiles that were subject to alteration by fluids with

circumneutral pH are better candidates for application of molecular weathering ratios, weathering indices, and geochemical climofunctions presented here.

The mineralogy and diagenetic alteration of paleosols also has implications for biosignature preservation in Martian weathering profiles. Biosignatures in paleosols can include biomarkers, biominerals, macro and microstructures and textures, chemistry, and isotopes [32], and the rapid burial that characteristically entombs paleosols often creates favorable taphonomic environments for the preservation of biosignatures. However, the preservation of chemical and isotopic biosignatures often relies on the bulk abundance of organic matter preserved in a sample. Many factors contribute to the preservation and degradation of organic matter in terrestrial paleosols including redox state prior to burial, clay mineralogy, amorphous phase compositions and abundance, diagenetic alterations, and interactions with sulfur (e.g., sulfurization) [15,67]. Redox state provides a first-order control on the preservation of organic carbon in rapidly buried soils [67]; for example, soils forming under reducing conditions (e.g., wetlands) generally preserve higher abundances of organics relative to those forming in oxidized, well-drained conditions. Oxidized and Al-smectite rich paleosols such as those examined here are associated with longer organic carbon residence time relative to kaolin group clays [79], but well-drained, oxidizing conditions before burial are associated with severe losses of organic C after burial [18,67]. In addition, most types of diagenetic alterations commonly observed in terrestrial paleosols are associated with the degradation of organic matter. Illitization, zeolitization and celadonization are all thought to facilitate desorption of organic carbon held on mineral surfaces, interlayer spaces, and crystal edges, thus possibly contributing to the burial-induced degradation of organic matter[80,81]. In this work, illitization and celadonization of smectite was not observed, but zeolitization of amorphous colloids and/or poorly crystalline smectite may have liberated adsorbed or chemisorbed organic carbon[82] and likely contributed to the degradation of the bulk organic fraction. One the other hand, diagenetic features of paleosols such as burial gleization observed in this work (Table 1 and Figure 3) may indicate organic carbon enrichment and the preservation of chemical biosignatures in the surface horizons of paleosols. The drab green surface layer of the uppermost paleosol examined in this work showed an accumulation of Fe^{2+} attributed to diagenetic burial gleization via anaerobic microbial decay of organic matter. Previous investigations showed that this gleyed layer was enriched in organic

carbon relative to deeper layers in the paleosol [67], and thus burial gleization features most likely constitute a chemical biosignature in paleosols. If features resembling burial gleization are detected in weathering profiles on Mars, they should be considered a high-priority location for *in-situ* biosignature investigation.

Conclusions

The objective of this study was to analyze the mineralogy and diagenetic alterations of paleosols from eastern Oregon, USA using techniques similar to those utilized by current and future missions to Mars. Samples were gathered from three successive paleosol profiles in the early Oligocene (33 Ma) middle Big Basin Member of the John Day Formation that formed from pedogenic weathering of volcanic ash and tuff. Visible/near infrared spectroscopy, X-ray diffraction and evolved gas analysis confirmed dioctahedral smectite was the major phase in all samples, with most samples primarily containing a mixture of montmorillonite (Al smectite) and nontronite (Fe smectite). Minor phases detected with x-ray diffraction included Opal-CT, cristobalite, andesine and gypsum. All samples contained minor amounts of the zeolite mineral clinoptilolite which most likely formed from the diagenetic Ostwald ripening of amorphous or nanocrystalline phases such as allophane, imogolite and/ or poorly crystalline smectite. Across all samples only minor (< 5 wt. %) abundances of amorphous phases were observed; instead, most samples contained between 70-95 wt. % crystalline clay minerals.

The mineralogy and morphology of paleosols examined here is consistent with formation under well-drained, oxidizing conditions with moderate weathering rates. Geochemical climofunctions based on molecular weathering ratios applied to these paleosols indicate soil formation under mean annual precipitation of ~600 mm and mean annual temperature of approximately 10° C. Pedogenic weathering of volcanic ash under these climatic conditions was sufficient to transform volcanic glass and amorphous/nanocrystalline phases into strongly crystalline dioctahedral clay minerals.

Four types of alteration after burial that have affected paleosols examined in this work are 1) Drab green surface horizons due to burial gleization of organic matter; 2) brick-red color from burial-induced dehydration of ferric oxides and hydroxides; 3) zeolitization of volcanic glass and/or poorly crystalline phases; and 4) significant mechanical compaction. Burial

gleization, limited to the surface horizons of paleosols, was most likely an early diagenetic alteration that resulted from the chemical reduction of iron hydroxides and oxides by anaerobic bacteria consuming buried organic matter at or below the water table. The timing of burial dehydration of (oxy)hydroxides remains poorly constrained, but late diagenetic alterations such as zeolitization may have occurred during early Miocene burial at depths of 380 to 1200 meters and temperatures of 27-55° C during deposition of the overlying Mascall and Rattlesnake Formations. The current overburden of ~2 km has also resulted in the mechanical compaction of paleosol profiles to approximately 70% of their original thickness before burial. Despite significant overburden, absence of illite/chlorite and celadonite imply a lack of diagenetic K-metasomism and celadonization, respectively. The high clay mineral content (up to 95 wt. %) of paleosols from the middle Big Basin Member of the John Day Formation may have insulated profiles from diagenetic alterations which have pervasively altered stratigraphically higher and less clay mineral-rich (~40 wt. %) paleosols in the overlying Turtle Cove member of the John Day Formation.

On Mars, there are distinct stratigraphic changes in clay mineral and amorphous phase abundance in sedimentary rocks across the Mawrth Vallis region and these general stratigraphic trends are observed in the eastern Oregon paleosol sequence. Mineralogical changes across the compositional stratigraphy at Muara Crater, Mawrth Vallis are comparable to the up-section decline in crystalline clay minerals and subsequent increase in Al smectite, amorphous phases and hydrated silica through the Clarno and John Day Formations resulting from the aridification of eastern Oregon during the late Eocene and Oligocene. Strong spectral signatures of a nanophase aluminosilicate consistent with allophane and /or imogolite have been noted at the stratigraphically highest layers across the Mawrth Vallis region and are thought to represent a cool and dry climate where nanophase aluminosilicates resulted from minor alteration of volcanic ash[37], and these uppermost layers share mineralogical similarities with the Turtle Cove Member paleosols. In contrast, the lowermost layers at Mawrth Vallis have strong spectral signatures of crystalline Fe/Mg smectite and are perhaps more akin to deeply weathered paleosols from the Clarno and lower John Day Formations.

Pedogenic features observed in this work include dioctahedral smectite mineralogy, a clay mineral doublet feature observed with VNIR spectroscopy possibly resulting from isomorphous substitutions during pedogenic weathering, destruction of sedimentary bedding,

sub-meter scale differences in composition and color, and illuvial accumulation of clay minerals into subsurface horizons, all of which resulted from precipitation-driven pedogenic weathering of andesitic to rhyodacitic volcanic ash and tuff. Results from this work can help distinguish paleosols and weathering profiles from other types of sedimentary rocks in the geological record of Mars.

Additional Information

Acknowledgements

This work was performed on the ancestral homelands of the Umatilla indigenous people who were present before western settlement. Many thanks to Elizabeth Rampe and Paul Niles for the opportunity to work on this project and for providing research direction during a summer internship. Greg Retallack provided invaluable knowledge and guidance in support of this project. Barry Hughes and Megan Barrington assisted with fieldwork and entertained thoughtful discussion. Angela Olsen, Marshall Styczinski, Paul Regensberger and Joe Caggiano reviewed early versions of the manuscript. Funding from the Geological Society of America, The Clay Minerals Society, The Society of Sedimentary Geology, and the Central Oregon Geoscience Society aided in the completion of this project.

Author Contribution Statement

A.P.B designed the study, performed laboratory analyses and drafted the manuscript. B.H.H identified similarities between Mars and John Day paleosols, assisted with fieldwork and provided VNIR spectra of paleosols. J.V.C guided all thermal analyses and facilitated data interpretation. B.S, J.V.C and D.W.M contributed to data analysis and interpretation. V.T. performed x-ray diffraction and assisted with interpretation of mineralogy. L.C.R.S aided with comparisons of modern soils with paleosols and supervised the project. All authors contributed to the manuscript.

Author Disclosure Statement

No competing financial interests exist.

References

1. Bishop, J. . et al. Phyllosilicate Diversity and Past Aqueous Activity Revealed at Mawrth Vallis, Mars. *Sci. e* 830–834 (2008).
2. Bishop, J. L. *et al.* What the ancient phyllosilicates at Mawrth Vallis can tell us about possible habitability on early Mars. *Planet. Space Sci.* **86**, 130–149 (2013).
3. Scheller, E. L., Ehlmann, B. L., Hu, R., Adams, D. J. & Yung, Y. L. Long-term drying of Mars by sequestration of ocean-scale volumes of water in the crust. *Science (80-.).* **372**, 56–62 (2021).
4. Ye, B. & Michalski, J. R. Precipitation-Driven Pedogenic Weathering of Volcaniclastics on Early Mars. *Geophys. Res. Lett.* **48**, 1–10 (2021).
5. Murchie, S. *et al.* Compact Reconnaissance Imaging Spectrometer for Mars (CRISM) on Mars Reconnaissance Orbiter (MRO). *J. Geophys. Res.* **112**, 1–57 (2007).
6. Carter, J., Loizeau, D., Mangold, N., Poulet, F. & Bibring, J. Widespread surface weathering on early Mars : A case for a warmer and wetter climate. *Icarus* **248**, 373–382 (2015).
7. Loizeau, D. *et al.* Quantifying widespread aqueous surface weathering on Mars : The plateaus south of Coprates Chasma. *Icarus* **302**, 451–469 (2018).
8. Franklin, R. *et al.* Oxia Planum : The Landing Site for the ExoMars. *Astrobiology* **21**, 1–22 (2021).
9. Bristow, T. F. *et al.* Clay mineral diversity and abundance in sedimentary rocks of Gale crater , Mars. *Sci. Adv.* **4**, 1–9 (2018).
10. Ehlmann, B. L., Mustard, J. F. & Murchie, S. L. Geologic setting of serpentine deposits on Mars. *Geophys. Res. Lett.* **37**, 1–5 (2010).
11. Ehlmann, B. L. *et al.* Clay minerals in delta deposits and organic preservation potential on Mars. *Nature* **1**, 355–358 (2008).
12. Michalski, J. R. *et al.* Constraints on the crystal-chemistry of Fe / Mg-rich smectitic clays on Mars and links to global alteration trends. *Earth Planet. Sci. Lett.* **427**, 215–225 (2015).

13. Vaniman, D. T. *et al.* Mineralogy of a Mudstone at Yellowknife Bay , Gale Crater , Mars Mineralogical Analysis and Quantitative Mineralogy. *Science (80-.).* 1–14 (2014) doi:10.1126/science.1243480.

14. Bishop, J. L. *et al.* Surface clay formation during short-term warmer and wetter conditions on a largely cold ancient Mars. *Nat. Astron.* **2**, 206–213 (2018).

15. Horgan, B., Bishop, L., Christensen, P. R. & Bell, J. F. Potential ancient soils preserved at Mawrth Vallis from comparisons with Eastern Oregon paleosols: Implications for Early Martian Climate. *Third Conf. Early Mars* **7074**, 12–13 (2012).

16. Cannon, K. M., Stephen, W. & Mustard, J. . Primordial clays on Mars formed beneath a steam or supercritical atmosphere. *Nature* **552**, 88–91 (2017).

17. Ehlmann, B. L. *et al.* Subsurface water and clay mineral formation during the early history of Mars. *Nature* **479**, 53–60 (2011).

18. Retallack, G. J. *Soil of the Past*. (Wiley Blackwell, 2019).

19. Smith, R. . & Horgan, B. H. N. Nanoscale Variations in Natural Amorphous and Nanocrystalline Weathering Products in Mafic to Intermediate Volcanic Terrains on Earth : Implications for Amorphous Detections on Mars. *J. Geophys. Res. Planets* **126**, 1–30 (2021).

20. Horgan, B. Strategies for Searching for Biosignatures in Ancient Martian Sub-Aerial Surface Environments. *Biosignature Preserv. Detect. Mars Analog Environ.* 7463 (2016) doi:10.1089/ast.2016.1627.

21. Heard, A. W. *et al.* Anoxic continental surface weathering recorded by the 2.95 Ga Denny Dalton Paleosol (Pongola Supergroup, South Africa). *Geochim. Cosmochim. Acta* **295**, 1–23 (2021).

22. Liu, J. *et al.* Anoxic chemical weathering under a reducing greenhouse on early Mars. *Nat. as* (2021) doi:https://doi.org/10.1038/s41550-021-01303-5.

23. Retallack, G. J. Paleosols and paleoenvironments of early Mars. *Geology* **42**, 755–758 (2014).

24. Bestland, E. . Alluvial Terraces and Paleosols As Indicators Of Early Oligocene Climate

Change (John-Day Formation, Oregon). *J. Sediment. Res.* **67**, 840–855 (1997).

25. Retallack, G. J., Bestland, E. . & Fremd, T. . Eocene and Oligocene Paleosols of Central Oregon. *Geol. Soc. Am. Spec. Pap.* **344**, 1–192 (2000).

26. Smith, R. ., Horgan, B., Rampe, E. & Dehouck, E. The Composition of Amorphous Phases in Soils and Sediments on Earth and Mars. *49th Lunar Planet. Sci. Conf. 2018* 14–15 (2018).

27. Sheldon, N. D., Retallack, G. J. & Tanaka, S. Geochemical Climofunctions from North American Soils and Application to Paleosols across the Eocene - Oligocene Boundary in Oregon Geochemical Climofunctions from North American Soils and Application to Paleosols across the Eocene-Oligocene Boundary in Or. *J. Geol.* **110**, 687–696 (2015).

28. Staff, S. S. Keys to Soil Taxonomy. *United States Dep. Agric.* **12**, (2014).

29. Bestland, E. A. Fossil Andisols identified with mass-balance geochemistry (Oligocene John Day Formation, Oregon, U.S.A.). *J. Sediment. Res.* **72**, 673–686 (2002).

30. Milliken, R. ., Mustard, J. ., Ehlmann, B. L., Bishop, J. L. & Murchie, S. L. Interpreting and constraining the compositional and depositional environments of phyllosilicates on Mars. *Gr. Truth From Mars* **4036**, 7–8 (2008).

31. Bishop, J. L. *et al.* Multiple mineral horizons in layered outcrops at Mawrth Vallis, Mars, signify changing geochemical environments on early Mars. *Icarus* **341**, 113634 (2020).

32. Hays, L. E. *et al.* Biosignature Preservation and Detection in Mars Analog Environments. *Astrobiology* **17**, 363–400 (2017).

33. Deit, L. Le *et al.* Extensive surface pedogenic alteration of the Martian Noachian crust suggested by plateau phyllosilicates around Valles Marineris. *J. Geophys. Res.* **117**, 1–25 (2012).

34. Dobrea, E. Z. N. *et al.* Mineralogy and stratigraphy of phyllosilicate - bearing and dark mantling units in the greater Mawrth Vallis / west Arabia Terra area : Constraints on geological origin. *J. Geophys. Res.* **115**, 1–27 (2010).

35. Lowe, D. R. *et al.* Deposition of > 3 . 7 Ga clay-rich strata of the Mawrth Vallis Group, Mars, in lacustrine, alluvial, and aeolian environments. *GSA Bull.* 17–30 (2020).

36. Loizeau, D. *et al.* History of the clay-rich unit at Mawrth Vallis, Mars: High- resolution mapping of a candidate landing site. *J. Geophys. Res. Planets* 1820–1846 (2015) doi:10.1002/2015JE004894.Received.

37. Bishop, J. . *et al.* Mineralogy of layered outcrops at Mawrth Vallis and implications for early aqueous geochemistry on Mars. *47th Lunar Planet. Sci. Conf.* **2**, 2–3 (2016).

38. Horgan, B., Baker, L., Carter, J. & Chadwick, O. Where is the climate signature in the mineral record of early Mars? *Fourth Conf. Early Mars 2017* **3077**, 2014–2015 (2017).

39. J. C. Liu, J. R. Michalski, M.-F. Z. Intense subaerial weathering of eolian sediments in Gale crater, Mars. *Sci. Adv.* **In review**, (2021).

40. Barrington, M. . *et al.* Mastcam-Z Analog Spectral Imager. *51st Lunar Planet. Sci. Conf.* **1595**, 51–52 (2020).

41. Horgan, B. *et al.* New constraints from CRISM and MASTCAM spectra on the mineralogy and origin of Mt. Sharp geologic units, Gale Crater, Mars. *48th Lunar Planet. Sci. Conf.* **3021**, 2–3 (2017).

42. Bishop, J. L., Lane, M. D., Dyar, M. D. & Brown, A. J. Reflectance and emission spectroscopy study of four groups of phyllosilicates: smectites, kaolinite-serpentines, chlorites and micas. *Clay Miner.* **43**, 35–54 (2008).

43. Rampe, E. B. *et al.* Mineralogy and geochemistry of sedimentary rocks and eolian sediments in Gale crater, Mars: A review after six Earth years of exploration with Curiosity. *Geochemistry* **80**, (2020).

44. Morris, R. V. *et al.* Silicic volcanism on Mars evidenced by tridymite in high-SiO2 sedimentary rock at Gale crater. *Proc. Natl. Acad. Sci. U. S. A.* **113**, 7071–7076 (2016).

45. Goesmann, F. *et al.* The Mars Organic Molecule Analyzer (MOMA) Instrument: Characterization of Organic Material in Martian Sediments. *Astrobiology* **17**, 655–685 (2017).

46. Breecker, D. O., Sharp, Z. D. & McFadden, L. D. Seasonal bias in the formation and stable isotopic composition of pedogenic carbonate in modern soils from central New Mexico, USA. *Bull. Geol. Soc. Am.* **121**, 630–640 (2009).

47. Retallack, G. J. *et al.* Late Pleistocene mammoth trackway from Fossil Lake , Oregon. *Paleogeography, Paleoclimatology, Paleoecol.* (2018) doi:10.1016/j.palaeo.2018.01.037.

48. Chemtob, S. M., Nickerson, R. D., Morris, R. V., Agresti, D. G. & Catalano, J. G. Synthesis and structural characterization of ferrous trioctahedral smectites: Implications for clay mineral genesis and detectability on Mars. *J. Geophys. Res. E Planets* **120**, 1119–1140 (2015).

49. Danielson, J. . *et al.* Characterization of outcrops containing 'doublet' spectra at Mawrth Vallis, Mars. *Lunar Planet. Sci. Conf.* **2019**, 1–179 (2019).

50. Horgan, B., Christensen, P. & Iii, J. F. B. Searching for pedogenic phyllosilicates in ancient martian soils. *AGU Fall Meet.* 1999 (2011).

51. Horgan, B. *et al.* The effects of climate , environment , and diagenesis on the spectral properties of volcanic soils. in *GSA Annual Meeting, Cordilleran Section* 1–24 (2017).

52. Novoselov, A. A., Roberto, C. & Filho, D. S. Potassium metasomatism of Precambrian paleosols. *Precambrian Res.* **262**, 67–83 (2015).

53. Earnest, C. M. Thermal analysis of selected illite and smectite clay minerals. Part II. Smectite clay minerals. in *Thermal Analysis in the Geosciences* (eds. Smykatz-Kloss, W. & Warne, S. S. J.) 288–312 (Springer Berlin Heidelberg, 1991).

54. Mcadam, A. ., Sutter, B., Archer, P. ., Franz, H. . & Eigenbrode, J. . The chemistry and mineralogy of the Glen Torridon clay-bearing unit from Mars Science Laboratory Sample Analysis at Mars. *51st Lunar Planet. Sci. Conf.* **2243**, 60–74 (2020).

55. Smith, R. J., Rampe, E. B., Horgan, B. H. N. & Dehouck, E. Deriving Amorphous Component Abundance and Composition of Rocks and Sediments on Earth and Mars. *J. Geophys. Res. Planets* **123**, 2485–2505 (2018).

56. Sutter, B. *et al.* Evolved gas analyses of sedimentary rocks and eolian sediment in Gale Crater, Mars: Results of the Curiosity rover's sample analysis at Mars instrument from Yellowknife Bay to the Namib Dune. *J. Geophys. Res. Planets* 2574–2609 (2017) doi:10.1002/2016JE005225.

57. Sutter, B., Laurer, H. ., Golden, D. ., Ming, D. . & Boynton, W. . PHOENIX LANDER'S THERMAL EVOLVED GAS ANALYZER: DIFFERENTIAL SCANNING

CALORIMETER AND MASS SPECTROMETER DATABASE DEVELOPMENT. in *35th Lunar and Planetary Science Conference* vol. 21 1–3 (2008).

58. Ming, D. W. *et al.* Volatile and Organic Compositions of Sedimentary Rocks in Yellowknife Bay , Gale Crater , Mars. *Sci. Express* 1–15 (2014) doi:10.1126/science.1245267.

59. Hogancamp, J. V *et al.* Identification of phyllosilicates in mudstone samples using water releases detected by the Sample Analysis at Mars (SAM) instrument in Gale Crater, Mars. *Lunar Planet. Sci. XLVIII* 1620 (2017) doi:10.1126/science.1243480.

60. Mcadam, A. . *et al.* Constraints on Gale Crater mudstone from MSL SAM evolved water. in *Lunar and Planetary Science XLVIII* 7–8 (2017). doi:10.1126/science.1245267.

61. Mcadam, A. . *et al.* Sulfur-bearing phases detected by evolved gas analysis of the Rocknest aeolian deposit, Gale Crater, Mars. *J. Geophys. Res. Planets* **119**, 6121–6139 (2014).

62. François, P. *et al.* Magnesium sulfate as a key mineral for the detection of organic molecules on Mars using pyrolysis. *J. Geophys. Res. – Planets* 61–74 (2015) doi:10.1002/2015JE004884.Received.

63. Driese, S. G. & Ober, E. G. Paleopedologic and paleohydrologic records of precipitation seasonality from early Pennsylvanian 'Underclay' paleosols, U.S.A. *J. Sediment. Res.* **75**, 997–1010 (2005).

64. Retallack, G. J. Untangling the effects of burial alteration and ancient soil formation. *Annu. Rev. Earth Planet. Sci.* 183–206 (1991).

65. PiPujol, M. D. & Buurman, P. The distinction between ground-water gley and surface-water gley phenomena in Tertiary paleosols of the Ebro basin, NE Spain. *Palaeogeogr. Palaeoclimatol. Palaeoecol.* **110**, 103–113 (1994).

66. Allen, J. R. L. Time scales of colour change in late Flandrian intertidal muddy sediments of the Severn Estuary. *Proc. Geol. Assoc.* **97**, 23–28 (1986).

67. Broz, A. P. Organic Matter Preservation in Ancient Soils of Earth and Mars. *Life* **10**, (2020).

68. Spinola, D. N. *et al.* Diagenetic reddening of Early Eocene paleosols on King George Island, Antarctica. *Geoderma* **315**, 149–159 (2018).

69. Sheldon, N. D. Pedogenesis and geochemical alteration of the Pacific Gorge subgroup Columbia River basalt, Oregon. *Bull. Geol. Soc. Am.* **115**, 1377–1387 (2003).

70. Solleiro-Rebolledo, E. *et al.* Paleosols beneath a lava flow in the southern basin of Mexico: The effect of heat on the paleopedological record. *Catena* **137**, 622–634 (2016).

71. Ming, D. W. & Mumpton, F. . Zeolites in Soils. in *Minerals in Soil Environments* vol. 18 873–911 (1989).

72. Hay, R. . Stratigraphy and zeolitic diagenesis of the John Day formation of Oregon. **42**, 199–252 (1963).

73. Steefel, C. I. & Van Cappellen, P. A new kinetic approach to modeling water-rock interaction: The role of nucleation, precursors, and Ostwald ripening. *Geochim. Cosmochim. Acta* **54**, 2657–2677 (1990).

74. Chadwick, O. A. & Chorover, J. The chemistry of pedogenic thresholds. *Geoderma* **100**, 321–353 (2001).

75. Sclater, J. G. & Christie, P. Continental Stretching: An explanation of the Post-Mid-Cretaceous subsidence of the Central North Sea Basin. *J. Geophys. Res.* **85**, 3711–3739 (1980).

76. Bishop, J. L. & Rampe, E. B. Evidence for a changing Martian climate from the mineralogy at Mawrth Vallis. *Earth Planet. Sci. Lett.* **448**, 42–48 (2016).

77. Liivamägi, S. *et al.* Paleosols on the Ediacaran basalts of the East European Craton: a unique record of paleoweathering with minimum diagenetic overprint. *Precambrian Res.* (2018) doi:10.1016/j.precamres.2018.07.020.

78. Tosca, N. J. & Knoll, A. H. Juvenile chemical sediments and the long term persistence of water at the surface of Mars. *Earth Planet. Sci. Lett.* **286**, 379–386 (2009).

79. Wattel-Koekkoek, E., Buurman, P., Van der Plicht, J., Wattel, E. & van Breeman, N. Mean residence time of soil organic matter associated with kaolinite and smectite. *Eur. J. Soil Sci.* **54**, 269–278 (2003).

80. Li, Y., Cai, J., Song, M., Ji, J. & Bao, Y. Influence of organic matter on smectite illitization : A comparison between red and dark mudstones from the Dongying Depression , China. *Am. Mineral.* **101**, 134–145 (2016).

81. Elliott, W. C. & Matisoff, G. Evaluation of kinetic models for the smectite to illite transformation. *Clays Clay Miner.* **44**, 77–87 (1996).

82. Kaiser, K. & Guggenberger, G. The role of DOM sorption to mineral surfaces in the preservation of organic matter in soils. *Org. Geochem.* **31**, 711–725 (2000).

CHAPTER IV.
DETECTION OF ORGANIC CARBON IN MARS-ANALOG PALEOSOLS WITH THERMAL AND EVOLVED GAS ANALYSIS

Published as A. P. Broz, J. Clark, B. Sutter, D. W. Ming, B. Horgan, P. Douglas, A. Jr, L. C. R. Silva, Detection of organic carbon in Mars-analog paleosols with thermal and evolved gas analysis. *J. Geophys. Res. Planets* (2022), doi:https://doi.org/10.1029/2022JE007340.

Introduction

Paleosols are ancient, buried soils that are often lithified into sedimentary rocks. Terrestrial paleosols are a geological record of the atmospheric composition, climate, topography and organisms present before soil burial (Retallack, 2019). On Mars, paleosols, also known as weathering profiles, may have formed in sediments such as basaltic sand or volcanic ash that were subject to subaerial weathering by surface waters (Retallack, 2014; Amundson, 2018; Liu et al., 2021b; Ye and Michalski, 2021) and were subsequently buried and preserved in the geological record. Orbital remote sensing of the global martian surface has detected dioctahedral clay minerals within Noachian (4.1-3.7 Ga) layered sedimentary rocks, which are consistent with precipitation-driven pedogenic weathering of mafic sediments (Carter et al., 2015; Bishop et al., 2018b; Loizeau et al., 2018). Noachian sedimentary rocks with spectral signatures of subaerial weathering have been detected in thousands of locations across the surface of Mars (Bishop et al., 2018b). One hypothesis is that these deposits are paleosols (Carter et al., 2015), which are the common products of pedogenic alteration followed by burial. Mounting evidence of global-scale aqueous alteration of the Martian surface during the Noachian (Carter et al., 2015; Liu et al., 2021a) suggests that pedogenesis could have been a critical process early in the planet's history. As such, paleosols have been recently named a high priority location for biosignature investigation (Bishop et al., 2018a) and Mars Sample Return (Beaty et al., 2019), but the biosignature preservation potential of paleosols with Mars-like mineralogy remains poorly constrained (Horgan, 2016).

On Earth, soils are highly habitable environments. Modern soils are teeming with microbial biomass, often averaging 10^{10}–10^{11} bacterial cells and 10^3 and 10^4 species per gram of soil (Raynaud and Nunan, 2014). Modern soils also contain more organic carbon than global vegetation and the atmosphere combined (Lehmann and Kleber, 2015; Dynarski et al., 2020). Similarly, Earth's oldest soils also appear to have been highly habitable environments. Many

Precambrian (> 541 Ma) paleosols contain organic carbon and other chemical biosignatures that are thought to be remnants of surface biomass (Matthewman et al., 2012; Kremer et al., 2017; Liivamägi et al., 2018; Broz, 2020). Furthermore, Archean (> 2 Ga) paleosols contain filamentous organic carbon and organo-mineral complexes possibly derived from cyanobacterial mats on the soil surface (Rye and Holland, 2000; Watanabe et al., 2000).

However, many terrestrial paleosols preserve only trace amounts of organic carbon, especially compared to modern soils, marine shales, and lacustrine rocks (Retallack, 2019). Organic carbon losses during diagenesis can reduce the organic carbon content of paleosols by up to two orders of magnitude relative to their modern soil counterparts (Broz, 2020). Severe losses of organic carbon are most common in paleosols that originally formed under oxidizing, well-drained conditions (Retallack and Mao, 2019). In general, oxidized paleosols typically contain only low amounts (< 0.1 wt. %) of organic carbon (Broz, 2020). Diagenetic losses of organic carbon in oxidized terrestrial paleosols poses major challenges for detection of chemical and isotopic biosignatures preserved within the organic matter fraction. However, this is not the case for all paleosols. Those that originally formed under reducing conditions, such as Permian (~250 Ma) Histosols (poorly drained organic soils), preserve organic carbon with abundances > 25 wt. % (Retallack and Krull, 1999), implying that redox state before burial may provide a first-order control on the preservation of organic carbon in ancient soils (Krull and Retallack, 2000).

An additional concern for the study of terrestrial paleosol organic matter is that diagenetic alterations ranging from groundwater alteration to precipitation-driven leaching of dissolved organic carbon can result in the addition of exogenous (e.g., allochthonous) organic molecules, so caution is necessary for interpreting whether the organic fraction has indeed been "preserved" over geological time scales. In other words, terrestrial paleosols can be contaminated by organic molecules that were not original to the soil, thereby complicating efforts to interpret their biosignature preservation potential.

One way to constrain the biosignature preservation potential of putative paleosols on Mars is to examine the organic fraction of paleosols from Earth that share compositional and morphological similarities to layered sedimentary rocks on Mars. Examination of oxidized paleosols with Mars-like mineralogy can help determine if low amounts of organic molecules within natural pedogenic mineral matrices can be detected with Mars flight-analog instruments.

Furthermore, cosmogenic nuclide dating of these analog paleosols can also identify potential diagenetic additions of organic carbon.

This study builds on and combines previous results from an established Mars-analog paleosol sequence (Broz et al., 2021, 2022). The focus here is to determine if organic molecules in oxidized paleosols are detectable with Mars flight-analog instrumentation, and to determine if there have been post-depositional additions of modern organic carbon to ancient samples. The objectives of this study were a) to determine whether organic carbon in ~33-million-year-old Mars-analog paleosols can be detected with thermal and evolved gas analysis, and b) constrain the age of organic carbon using radiocarbon (^{14}C) dating.

1.1 Paleosols at John Day Fossil Beds National Monument in eastern Oregon, USA

Eocene and Oligocene (42 to 28 Ma) sedimentary rocks at John Day Fossil Beds National Monument in eastern Oregon are a thick sequence of volcaniclastic paleosols, which altogether spans over 400 meters of vertical stratigraphy (Bestland, 1997; Retallack et al., 2000; Horgan et al., 2012; Smith et al., 2018a). The paleosol sequence contains over 500 clay-rich (30-95 wt. %) paleosols formed over ~15 Myr through the Eocene-Oligocene boundary (Figure 1) (Retallack et al., 2000; Horgan et al., 2018). Each of the individual profiles formed from pedogenic alteration of andesitic to rhyodacitic volcanic ash and/or tuff, followed by rapid burial via emplacement of an additional layer of tephra onto the soil surface. This process of soil formation and burial repeated for nearly 15 million years, and as such, the paleosol sequence provides a unique record of Cenozoic climate change in eastern Oregon (Fremd, 1996). Changes in mineralogy throughout the paleosol sequence reflect the Eocene-Oligocene cooling and drying of the climate (Bestland, 2002; Retallack et al., 2004).

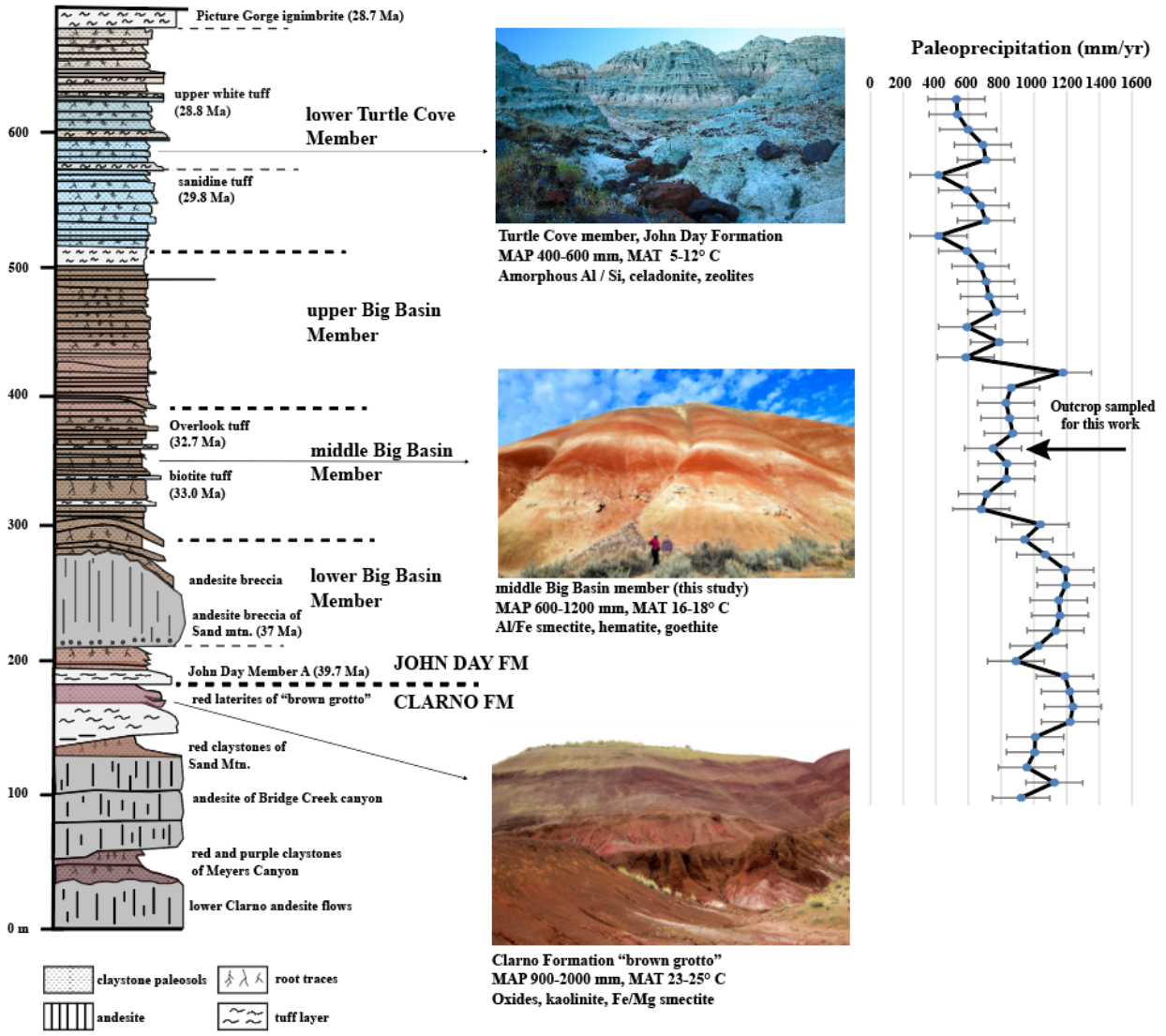

Figure 1. A sequence of Eocene and Oligocene (42-28 Ma) volcaniclastic paleosols in the Clarno and John Day Formations, John Day Fossil Beds National Monument (after Bestland (1997) **and** Sheldon et al. (2002)**.** Decreasing rainfall in Oregon through the Eocene/Oligocene boundary is inferred from the geochemistry of paleosols within the Clarno and John Day Formations. Paleoprecipitation estimates are derived from Sheldon et al. (2002) who used an equation relating molecular weathering ratios (Bases/alumina [$CaO + MgO + Na_2O + K_2O$ / Al_2O_3] to mean annual precipitation (MAP), which were gathered from a database of modern soils (r=0.79, standard error = 179 mm). The approximate stratigraphic location of samples analyzed in this study are indicated with a black arrow (right panel).

The Eocene (42-39 Ma) Clarno Formation represents the lowest and oldest unit of the Oregon paleosol sequence. The basal Clarno Formation is characterized by andesite flows interspaced with severely weathered paleosols with accumulations of kaolinite, Fe/Mg smectite and oxides (Oxisols and Ultisols in US soil taxonomy), which indicate tropical weathering

conditions in the middle to late Eocene (Retallack et al., 2000). A particularly striking exposure of the late Eocene Clarno Formation at the "Brown Grotto" area of the Painted Hills is characterized by thick (~2-6 meter), repeated profiles of deeply weathered lateritic paleosols (**Figure 1,** bottom) that are similar to modern soils from Southern Mexico and Central America in climates that are subtropical and humid (Retallack et al., 2000). Stratigraphically above the Clarno Formation, the early Oligocene (~33 Ma) Big Basin Member of the John Day Formation is characterized by less intensely weathered paleosols (Alfisols and Inceptisols) that are rich in Al and Fe smectites such as nontronite and montmorillonite (Figure 1, middle). This middle unit represents a dramatic cooling and drying of the climate through the Eocene-Oligocene boundary. Overlying this unit of the paleosol sequence is the mid-late Oligocene (~28 Ma) Turtle Cove Member of the John Day Formation (Figure 1, top). The brown, green and celadon-colored paleosols of this unit are minimally weathered Aridisols (desert soils) and Andisols (amorphous-rich volcanic soils). Paleosols in this unit are characterized by accumulations of amorphous and nanocrystalline materials (e.g., allophane and imogolite), pedogenic calcite, and diagenetic celadonite (Horgan et al., 2012). There is a dramatic reduction in smectite content and absence of kaolinite, which is consistent with weathering under a semi-arid to arid climate regime (Bestland, 2002). Finally, the entire paleosol sequence is capped by approximately 300 vertical meters of flood basalts from the Miocene (~16 Ma) Columbia River Basalt Group. Based on these mineralogical transitions, the Eocene paleosols with accumulations of kaolinite and oxides appear to reflect a subtropical and humid climate, while accumulations of nanophase aluminosilicates and amorphous phases in overlying paleosols indicate stepwise and cooling and drying during the late Oligocene (Retallack et al., 2000).

1.2 Pedogenic weathering on early Mars and comparisons to terrestrial paleosols

From a global perspective, orbital remote sensing from Observatoire pour la Minéralogie, l'Eau, les Glaces, et l'Activité (OMEGA) and the Compact Reconnaissance Spectrometer at Mars (CRISM) instrument onboard the Mars Reconnaissance Orbiter provide the most compelling evidence of extensive pedogenic-like alteration across the surface of Mars. Potential weathering sequences have been detected in hundreds of locations across Noachian terrains, wherever these ancient rocks are not obscured by dust, sand, or overlying strata (Carter et al., 2015; Loizeau et al., 2018). OMEGA and CRISM have collectively gathered visible and near-infrared (VNIR)

reflectance spectra of sedimentary deposits at Mawrth Vallis, Oxia Planum, Nili Fossae and other altered Noachian terrains. (Horgan et al., 2012, 2018; Hays et al., 2017; Smith et al., 2018b; Poulet et al., 2020). Spectral refinements for CRISM images (e.g., Viviano-Beck et al., 2014) now allow for identification of smaller-scale hydrated mineral deposits at Mawrth Vallis that facilitate a detailed reconstruction of possible geochemical environments on early Mars (Bishop et al., 2020). Some of these deposits, such as layered outcrops at Mawrth Vallis, have spectral and stratigraphic similarities to terrestrial paleosol sequences (Horgan et al., 2012; Broz et al., 2022).

Terrestrial paleosols: Mineralogy and diagenesis

The present study focuses on three paleosol profiles from the early Oligocene (33 Ma) Big Basin Member of the John Day Formation (Figure 1, middle). A detailed analysis of mineralogy and diagenetic alteration of these samples was previously performed (Broz et al., 2022). X-ray diffraction, evolved gas analysis and visible-near-infrared spectroscopy revealed high abundances (> 80 wt. %) of montmorillonite and nontronite with lesser amounts of hematite, zeolites, gypsum, and hydrated silica (Tables S4-S6). Diagenetic alterations previously observed in these samples included a) "burial gleization" of near-surface horizons, which is attributed to microbial reduction of Fe^{3+} in near-surface horizons of paleosols resulting from anaerobic decay of organic matter; b) dehydration of ferrous oxyhydroxides (goethite) to form fine-grained hematite; c) zeolitization to form clinoptilolite, possibly resulting from diagenetic recrystallization of a poorly crystalline smectite; and d) significant mechanical compaction to approximately 70% of the original soil thickness (Retallack et al., 2000).

Previously, there was no effort to examine the organic component of these paleosols, and the resulting influence of diagenesis on the organic fraction is poorly understood. Examination of terrestrial paleosols with Mars flight-analog instruments such as evolved gas analysis allows for a detailed characterization of the organic fraction (discussed below). This can help ascertain if diagenesis has resulted in significant losses of organic carbon and determine if organic carbon that remains is detectable with analytical techniques relevant to Mars exploration.

1.3 Sample Analysis at Mars (SAM) instrument onboard *Curiosity* Mars Rover

The overall goal of the SAM instrument is to assess the potential for past habitability by characterizing the martian chemical and isotopic composition of the atmosphere and volatile-bearing surface materials (Mahaffy et al., 2012). The SAM instrument is integral in providing an understanding of organic materials and phases undetectable by CheMin (e.g., amorphous phases, low abundance phases). SAM heats scooped or drilled rock samples from ~30 – 870° C at 35° C min^{-1}. Evolved gases produced from the thermal decomposition of volatile-bearing phases are analyzed by a quadrupole mass spectrometer (QMS), gas chromatograph columns for GCMS, or a tunable laser spectrometer (TLS) (Mahaffy et al., 2012). In evolved gas analysis (SAM-EGA) mode, SAM detects bulk gas evolution, whereas in gas chromatography-mass spectroscopy (SAM-GCMS) mode, SAM performs molecular separation and identification of organic molecules (Mahaffy et al., 2012; Eigenbrode et al., 2018). This study focused on SAM-EGA, so SAM-GCMS will not be further discussed. A comprehensive discussion on how organic molecules are detected with SAM- GCMS mode can be found in Mahaffy et al. (2012) and Freissinet et al. (2015).

Evolved gases and their release temperatures detected by SAM-EGA provide constraints on the mineralogy and organic content of samples in Gale Crater (Archer et al., 2014; Ming et al., 2014; Freissinet et al., 2015; Eigenbrode et al., 2018). The thermal decomposition of solid samples during SAM-EGA occurs during ramped heating, which releases volatile gases including CO_2, CO, hydrocarbons, and organic fragments (i.e., CH_2, CH_3, C_2H_2 and others) that are detected by the QMS. The intensity (relative abundance) of volatile release is plotted as a function of the release temperature, generating a time and temperature series of data for each volatile gas release. The volatile release peak temperature during sample decomposition depends on the thermodynamics of the reaction and can be used to constrain the composition of minerals and organic carbon in the sample (Archer et al., 2014), as well as to identify possible associations between minerals and organics (McAdam et al., 2020b).

Additional future missions to Mars will also employ EGA-like analysis to search for organic molecules. The Mars Organic Molecule Analyzer (MOMA) onboard European Space Agency's ExoMars 2022 *Rosalind Franklin* rover will use pyrolysis gas chromatography-mass spectrometry (GCMS) and laser desorption spectroscopy to search for biosignatures on Mars. The *Rosalind Franklin* rover will land at Noachian (3.9 Ga) Oxia Planum, which appears to be a westward extension of the lower parts of the stratigraphy observed at Mawrth Vallis (Ivanov et

al., 2020; Loizeau et al., 2020). Like Mawrth Vallis, strong and ubiquitous spectral signatures of dioctahedral Al-rich clay minerals overlying Fe/ Mg clay minerals suggests Oxia Planum may host remnants of a thick (~200 m) deep weathering profile or paleosol sequence that the rover could encounter during its primary mission.

1.4 Previous detections of organic carbon on Mars with SAM-EGA

Organic carbon has been detected in sedimentary rocks at Gale Crater with the SAM instrument using both QMS and GCMS (Ming et al., 2014; Rampe et al., 2014; Freissinet et al., 2015; Szopa et al., 2020). CO_2 and CO releases from oxidation of martian carbon sources have been identified by SAM, as well as small contributions from instrument background. Abundances of reduced carbon were very low (< 1 wt. %) and restricted to three samples (Cumberland [CB], Confidence Hills [CH], and Mojave [MJ]). However, high-temperature (> 600° C) CO releases were consistent with indigenous oxidized martian organics. Additionally, chlorinated hydrocarbons (chlorobenzene [*m/z* 112], ~30 pmol) in the Cumberland drill sample and organo-sulfur compounds including thiophenes and thiols (~90 nmol) in the Mojave and Confidence Hills drill samples were identified in a ~3.5 Ga mudstone, but the sources of these organic molecules was not constrained (Freissinet et al., 2015; Eigenbrode et al., 2018). Observation of dichlorobenzene and trichloromethylpropane in the CB sample at Yellowknife Bay could have been produced by chemical reactions between organic molecules and oxychlorines occurring in the SAM ovens. These chlorinated hydrocarbons could have been derived from organic carbon, either from an indigenous martian source and/or from meteoritic infall (Fornaro et al., 2018; Szopa et al., 2020). Though organic carbon has been detected by SAM in numerous sedimentary rocks at Gale Crater, the source(s) of the organic molecules are not yet fully understood. Recent work has suggested that organic salts such as Ca/Mg oxalates and/or Ca/Mg acetates may be present in abundances of 1-2 wt. % in modern eolian sediments (Rocknest sample) as well as in ancient sedimentary rocks at Gale Crater (JK and CB samples) (Lewis et al., 2021). The accumulation of organic salts in eolian deposits suggests that they may be a component of regional or global dust on Mars (Lewis et al., 2021).

2. Methods

2.1 Sample collection

The paleosols examined in this study were collected from the Painted Hills Unit of the John Day Fossil Beds National Monument in eastern Oregon, USA. A previous study (Broz et al., 2022) determined the mineralogy and diagenetic alteration of the same set of samples examined in the present study. Samples from three individual paleosols in vertical succession were described and sampled approximately 7 km SW of the entrance to the Painted Hills unit (Lat: 44.631105, Long: -120.213107), in the Middle Big Basin Member of the John Day Formation, approximately 6 m above the local Eocene-Oligocene boundary (Figure 1, middle). Samples were chosen from this location because they were previously examined for mineralogy and diagenesis, and because $^{40}Ar/^{39}Ar$ dating of volcanic tuffs at this stratigraphic level in the section allow for a constrained age of 33.0 +/- 0.10 to 32.7 +/- 0.03 Ma (Biotite Tuff and Overlook Tuff, respectively) (Bestland, 1997).

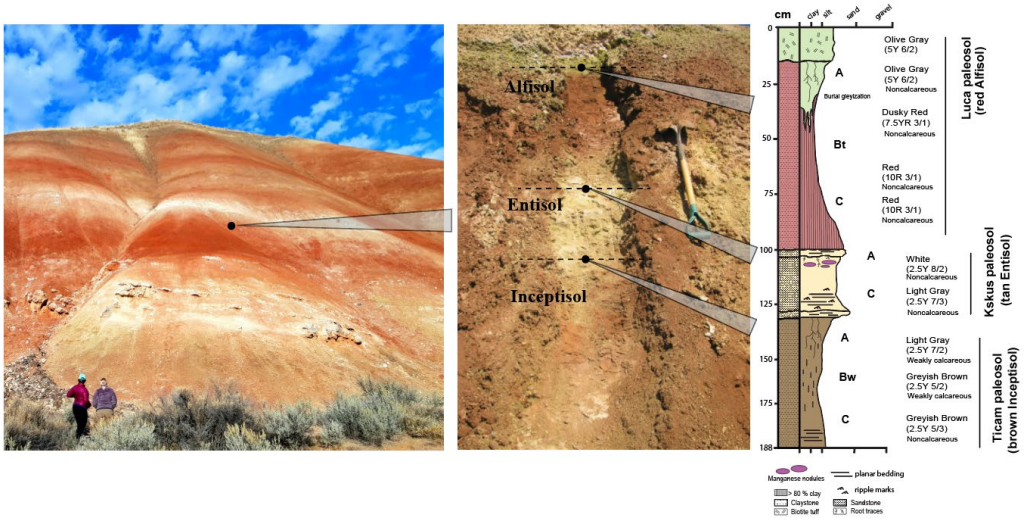

Figure 2. Field appearance and morphology of three paleosols in section from the early Oligocene (33 Ma) middle Big Basin Member of the John Day Formation in eastern Oregon, USA. The right panel shows lithology, grain size, horizon designations, and Munsell color of each profile. The uppermost profile (red with drab green top) is a moderately weathered red Alfisol (Hapludalf in USDA Taxonomy); stratigraphically below is a minimally weathered and weakly developed Entisol (Fluvent; tan color); the lowest soil (brown color) is an Inceptisol (Andic Eutrochrept, brown color).

To minimize contamination from modern organic carbon during sampling, all loose surface soil and saprolite was removed until the lithified, brick-like, unweathered paleosol surface was exposed. Below the saprolite of the thin (~30 cm) modern soil, all three paleosols were lithified claystone. Before collection, all sampling and storage materials were ashed at 550° C to remove organic contaminants. Sample collection for evolved gas analysis (EGA) began by trenching with a rock hammer to a ~30 cm depth into (perpendicular to) the lithified paleosol sequence. A set of samples were gathered down a vertical transect at approximately 10 cm intervals, similar to sampling the horizons of a modern soil. Large (~1 kg) lithified blocks of claystone were broken out of the outcrop and placed into aluminum foil to ensure subsampling for thermal analysis had sufficient volume to expose fresh sample surface (e.g., no weathered surfaces were selected for analysis). Small (5-8 g) subsamples were acquired from the inside of bulk lithified samples with steel chisels. These subsamples were then ground to < 0.02 mm using an agate mortar and pestle and stored in glass vials prior to thermal analysis and radiocarbon dating. No vegetation was present within ~30 m of the sampled paleosol sequence (Figure 2), likely because the "popcorn" weathering of the smectite-rich modern soil appears to inhibit plant germination and growth. The Munsell color and qualitative calcareousness of samples were described during collection. The three paleosols sampled were a red Alfisol ("Luca" pedotype from (Retallack et al., 2000), a tan Entisol ("Kskus" pedotype), and a brown Inceptisol ("Ticam" pedotype, Figure 2).

2.2 Radiocarbon dating of organic carbon in paleosols

The purpose of radiocarbon (^{14}C) dating was to constrain the age of organic carbon in paleosol samples. Specifically, radiocarbon dating was used to determine if the organic carbon fraction of paleosols was entirely endogenous (e.g., autochthonous, deposited during soil formation) and had been preserved for millions of years, or if there had been additions of exogenous (allochthonous) organic carbon to paleosols in the last ~45,000 years (a typical method-level detection limit for radiocarbon dating techniques).

For radiocarbon analysis, samples were gathered by trenching at a horizontal angle into the outcrop, whereas sampling for EGA was performed vertically (down section) once the surface soil had been removed from the outcrop (Figure 2). In other words, EGA samples were collected down section (e.g., vertical depth in the section) whereas radiocarbon samples were

obtained by trenching further into the outcrop (e.g., horizontal depth into the outcrop) at the vertical intervals where EGA samples were collected. The purpose of this sampling difference was to help determine if the horizontal sampling depth into the outcrop was related to the amount of radiocarbon accumulation in the brick-like paleosol samples collected within ~0.5 meters of the modern weathering zone.

A radiocarbon age of organic carbon was obtained from four samples, two from the exposed surface and near-surface horizons (A and Bt horizons) of the stratigraphically highest soil (Alfisol) and two from the surface and near-surface horizons of the stratigraphically lowest profile (Inceptisol). All samples for radiocarbon dating were acid-washed to remove inorganic carbonates. Ground paleosol samples (~5 g) were treated with approximately 20 mL of 0.1 M HCl at room temperature for 1 hour, then washed three times with ~30 ml of deionized water and dried at 60° C for 24 hr. Radiocarbon dating of acid-washed paleosol samples was performed at the W.M. Keck Carbon Cycle Accelerator Mass Spectrometer at the University of California, Irvine. Additional TOC determination of these samples was performed at UC Irvine and are reported in Table 1. The accuracy and precision (1 σ) of this analysis on modern carbon ($\Delta^{14}C$ >0‰) was better than 9‰. Laboratory blanks yielded a $\Delta^{14}C$ value of -996.2 ‰.

Quantifying additions of modern carbon to bulk paleosol samples

Calibrated radiocarbon dates, taken at face value, may represent a mixture of radiocarbon-free Oligocene carbon and some amount of modern organic carbon. To test the hypothesis that paleosols contained modern organic carbon, we used a two-endmember mixing model to estimate the relative proportion of modern carbon in bulk paleosol samples. Based on the distinct isotopic composition of modern organic carbon and radiocarbon-free Oligocene carbon, a two-endmember mixing model (Sickman et al., 2010; Silva et al., 2013) was used to quantify the relative proportions of modern and ancient carbon as distinct sources of the paleosol organic carbon pool (Zech et al., 2017). We used the following equation to partition modern organic carbon sources ($D^{14}C$ = 0 ‰) from radiocarbon-dead Oligocene organic carbon ($D^{14}C$ ~ -999‰):

$$\mathbf{C_{modern} = C_t(D^{14}C_{bulk} - D^{14}C_{Oligocene})/(D^{14}C_{Modern} - D^{14}C_{Oligocene})} \quad \mathbf{(1)}$$

Where C_t is the total amount of organic carbon (TOC) measured in bulk samples, $D^{14}C_{bulk}$ is the measured $D^{14}C$ value of bulk samples, $D^{14}C_{Modern}$ is a typical value for a modern organic carbon endmember ($D^{14}C$ = 0 ‰), $D^{14}C_{Oligocene}$ is a typical $D^{14}C$ value for a radiocarbon-free organic carbon endmember ($D^{14}C$ = -999‰), and C_{modern} is the modelled fraction of modern organic carbon in bulk samples. Errors were propagated to estimate uncertainty associated with modelled values. The sources of uncertainty considered in the model were a) the uncertainty of the measured TOC values and b) uncertainty of the measured $D^{14}C$ values, both from analysis of duplicate samples.

2.3 Thermal and evolved gas analysis of paleosol samples

The purpose of this work was to use SAM-EGA-like conditions to characterize bulk gas evolution and to measure the abundance of organic and inorganic carbon in Mars-analog paleosol samples. A Setaram Labsys Evo differential scanning calorimeter (DSC) / thermal gravimeter (TG) connected to a Pfeiffer Omnistar QMS was configured to operate similarly to the SAM evolved gas analyzer. The SAM instrument lacks TG/DSC capabilities, but in laboratory settings on Earth, these methods allow for a more thorough understanding of the chemical rections and phase transitions in analog samples. For SAM-EGA like analysis, approximately 50 mg ± 3 mg of ground paleosol sample (previously stored in glass vials ashed at 550° C to minimize organic contamination) were placed in an Al_2O_3 sample crucible (also previously ashed at 550° C). The sample crucible and an identical (empty) reference crucible were placed in the furnace. The instrument was purged twice with helium gas and set to a pressure of 3 kPa. Helium was chosen as a carrier gas because it is inert and because it used as a carrier gas in the SAM instrument. The crucibles were heated from approximately 35 °C to 1000 °C at a heating rate of 35°C/min and at a flow rate of 10 cm^3/s. Volatiles ranging from mass/charge (*m/z*) 1 - 100 were measured. All analyses were performed in duplicate.

Total organic carbon (TOC) content was determined using a Netzsch TG/DSC coupled to a Pfeiffer QMS using a modified method of Fernández et al., (2012). An Al_2O_3 sample crucible and an identical reference crucible were placed in the furnace. The instrument was purged twice with ultra-high purity O_2 and set to a pressure of 1000 mbar prior to sample analyses as a way to mitigate contamination of the system. Oxygen was chosen as a carrier gas because it encourages complete combustion of all reduced carbon in samples. The crucibles containing samples were

heated from approximately 35 °C to 1000 °C at a heating rate of 35°C/min and at a flow rate of 19 ml O_2/min. A series of three blanks were analyzed before and after each group (n=10) of samples. A calibration curve for CO_2 was created by analyzing a calcite standard (Iceland sparry calcite 40μM) at eight sample masses ranging from 0.01 – 4 mg (Table S1). This calibration curve was used to calculate the amount of CO_2 evolved from each sample, and these values were used to calculate total carbon in each sample (Table S2). Errors ranged from 0.01 – 0.003 wt. % carbon. All evolved gas plots were background-corrected to account for possible atmospheric contamination.

Thermal techniques including TG-DSC-EGA allow for quantitative estimates of organic and inorganic carbon without sample pretreatment, in part due to the large differences in thermodynamics and peak CO_2 release temperatures. By contrast, TOC determinations via elemental analysis involve an acid pretreatment step to remove carbonates. Paleosol samples were not acid-pretreated for thermal and evolved gas analyses because some organic carbon can be oxidized during acid-washing (e.g., Apesteguia et al., 2018). In the present study, carbon was considered organic between 150-550° C and inorganic from ~700-900° C. Total organic carbon was quantified by deconvolving CO_2 peaks if a carbonate-C peak was present. This was done by determining the relative percentage of peak area from inorganic carbon-evolved CO_2 (~700-900° C) then subtracting this value from total carbon-evolved CO_2 peak area to solve for TOC. However, it is possible that mineral-associated organic carbon could be co-eluting with inorganic mineral CO_2, and thus our TOC estimates may be missing a portion of mineral-associated organic carbon. This is a function of the EGA method, which has limitations for detection of mineral-associated organic carbon in natural samples.

3. Results/Discussion

3.1 Radiocarbon dating of paleosol organic carbon

Radiocarbon dating of four samples from two different paleosol profiles showed raw $D^{14}C$ values ranging from -539.1‰ ± 1.3‰ to -836.7‰ ± 3.4‰ and calibrated ages between 6,265 ± 25 years BP and 14,560 ± 170 years BP (Table 1). The fraction of modern carbon (FM) ranged from 0.469 ± 0.039 to 0.1633 ± 0.034 (Table 1) and was highest in the surface horizon of the Alfisol and lowest in the subsurface horizon, suggesting this paleosol contained a mixture of

ancient and modern organic carbon. These samples all showed a distinct signature of exogenous organic carbon because the samples were not radiocarbon dead (^{14}C-free). Two hypotheses to explain the radiocarbon dates are A) additions of modern organic carbon to bulk samples (e.g., a $D^{14}C \sim 0‰$ modern carbon pool mixing with an ancient, radiocarbon-free pool) or B) a Holocene (6-14 Ka) productivity event introduced carbon into the paleosols (e.g., the carbon is indeed tens of thousands of years old). One possible source of modern organic carbon may derive from precipitation-driven leaching of dissolved organic carbon from modern biota living in the current weathering zone above the paleosol outcrop. As such, it is possible that small amounts of exogenous modern organic carbon from the weathered zone above paleosol outcrops have mixed with larger amounts of ^{14}C-free organic carbon endogenous to paleosols. In this way, a radiocarbon date of ~6-14 Ka BP could represent a mixing of modern organic carbon and ~33 Ma organic carbon. This hypothesis is supported by the erosion rate for the site, which was previously determined to be approximately 4.94 ± 0.05 mm/yr. (Sweeney et al., 2015). Using this erosion rate, the 20 cm-thick soils that formed on top of the paleosol outcrops are only about 40 years old and could have leached modern organics into the underlying paleosols during this time.

Table 1. Radiocarbon dates and application of a two-endmember isotopic mixing model to measured $D^{14}C$ values from four bulk paleosol samples. Depth (cm) represents the horizontal depth into the outcrop from where samples were gathered. TOC, total organic carbon; FM, fraction of modern.

Sample ID	Depth (cm)	TOC (%)	TOC ±	FM	$D^{14}C$	±	^{14}C age (years BP)	±	Modern carbon (%)	±
Alfisol	32	0.015	0.001	0.163	-836.7	3.4	**14560**	170	0.487	0.066
Alfisol	14	0.010	0.001	0.461	-539.1	3.9	**6220**	70	3.141	0.105
Inceptisol	20	0.031	0.001	0.459	-541.5	1.3	**6265**	25	0.916	0.032
Inceptisol	22	0.018	0.001	0.437	-563.3	1.8	**6655**	35	0.872	0.056

Application of a two-endmember isotopic mixing model to raw $D^{14}C$ values (Equation 1) for estimation of modern organic carbon abundances in bulk paleosol samples is shown in Table 1. The modelled abundances of modern carbon ranged from 0.487 ± 0.066 % and 3.141 ± 0.105 % of the total organic carbon in each sample. These results support the hypothesis that the measured $D^{14}C$ values represent the mixing of small amounts of modern organic carbon with larger amounts of presumably radiocarbon-free Oligocene carbon. There was also a significant power law relationship between the modeled organic carbon abundance and the horizontal depth into the profile from where the sample was collected (**$y = 21.518x^{-0.418}$, $R^2 = 0.9194$**, **Figure S1).** Modelled abundances of modern carbon in samples from shallower horizontal depths in the outcrop were significantly ($P < 0.053$) greater compared to samples from deeper depths (Figure S1), which was consistent with precipitation-driven leaching of modern organic carbon into paleosol outcrops. Due to the limited sample size (n=4), additional efforts are needed to determine if this relationship exists across larger samples sizes and within deeper transects (e.g., > 100 cm). In summary, additions of exogenous carbon were most likely modern (last 40 years), rather than from the Holocene (6-14 Ka). However, results from this work alone cannot definitively exclude the possibility of a Holocene productivity event which could have led to leaching of carbon into ancient samples during that time. These results demonstrate that a radiocarbon approach can be a useful technique for constraining the age and sources of organic carbon in ancient pedogenic samples.

3.2 Thermal and Evolved Gas Analysis

3.2.1 CO_2 and CO evolutions

When subject to thermal and evolved gas analysis, all samples evolved CO_2 at temperatures ranging from ~150 – 800° C and had two to three distinctive CO_2 peaks (Figure 3). In several of the samples, a broad low temperature ~200 - 500° C peak was followed by a well-resolved (e.g., sharp) high-temperature peak at ~650-750° C. Four of the six samples also showed a well-resolved CO_2 peak at 600° C which was consistent with the decomposition of inorganic carbon. In general, CO_2 evolved at 150-500° C is primarily from organic carbon decomposition (Sutter et al., 2017; Apesteguia et al., 2018) but also possible are contributions are from CO_2 inclusions in minerals or amorphous phases. The organic C contributing to evolved

CO_2 is most likely from simple organic compounds (~350° C) or refractory macromolecular organic compounds (300-600° C) (Eigenbrode et al., 2018). Table 2 shows the calculated organic carbon content of EGA samples.

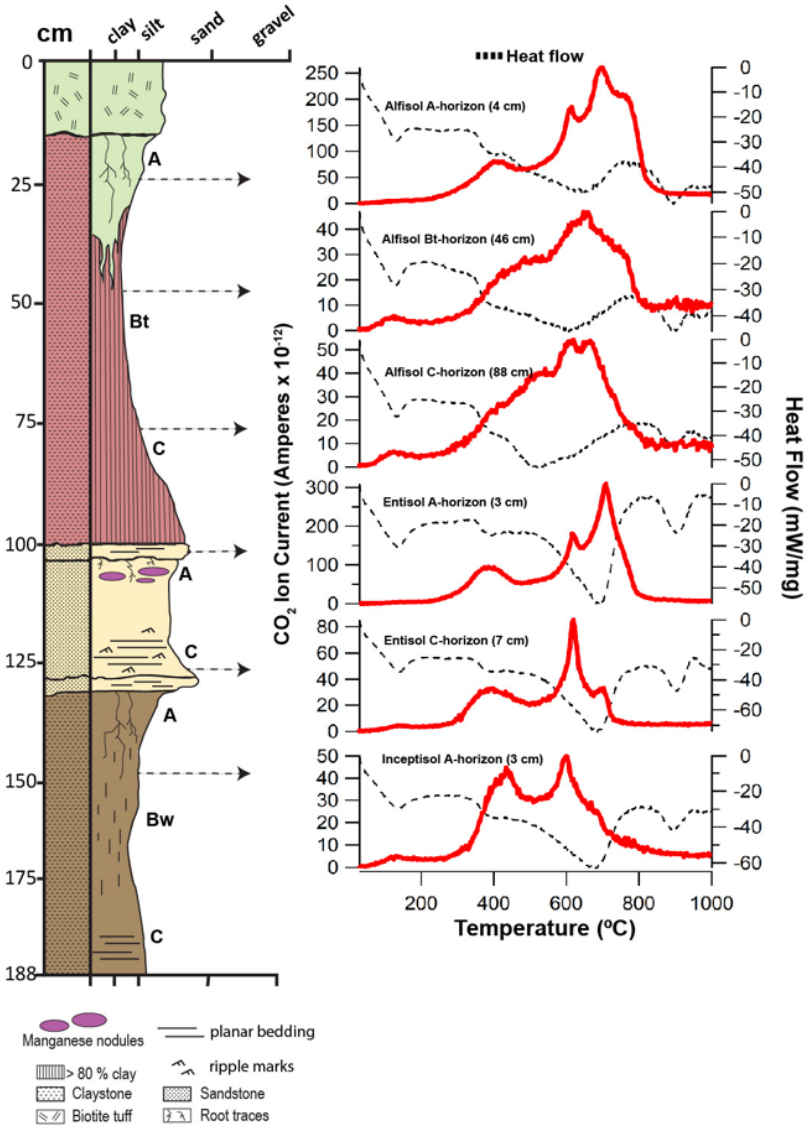

Figure 3. Evolutions of CO_2 (red traces) and heat flow (dashed traces) from early Oligocene (33 Ma) Al/Fe smectite-rich paleosols from the John Day Fossil Beds National Monument, Oregon. Red trace is CO_2 (*m/z* 44) and dashed trace is heat flow from differential scanning calorimetry (DSC). Helium was used as a carrier gas for all analyses.

Table 2. Total organic carbon (TOC) and total inorganic carbon (TIC) of paleosols examined in this study. Depth (cm) represents the vertical depth of each paleosol profile within the measured stratigraphic section

Paleosol	Horizon ᵠ	Depth (cm)	Total C (wt. %)	TOC (wt. %)†	±σ TOC §	TIC (wt. %)
Alfisol	A	4	0.073	0.031	0.0062	0.042
Alfisol	A	14	0.094	0.026	0.0097	0.068
Alfisol	Bt_1	46	0.021	0.018	0.0016	0.003
Alfisol	Bt_2	63	0.067	ND ʊ	-	0.067
Alfisol	C	88	0.033	0.002	0.007	0.031
Entisol	A	100	0.046	0.021	0.0068	0.024
Entisol	C	120	0.036	0.013	0.0037	0.024
Inceptisol	A	125	0.024	0.018	0.007	0.006
Inceptisol	Bw_1	131	0.027	0.008	0.0013	0.019
Inceptisol	Bw_2	160	0.020	0.011	0.0023	0.010
Inceptisol	C	175	0.026	0.001	0.0013	0.026

ᵠ Horizons follow USDA Soil Survey Staff (2014) major horizon designations
† Determined by thermal analysis (TG-DSC-EGA) without acid pre-treatment of samples; average of two duplicates.
ʊ ND = No detection; below limit of quantification
§ Standard error for TOC determination from duplicate analysis

The endothermic thermal decomposition of Ca carbonate was a probable source of CO_2 release from approximately 550 – 800° C (Figure 3) (Cannon et al., 2012; Sutter et al., 2012). High temperature (> 650° C) CO_2 evolutions generally exceeded the low temperature (150-550° C) CO_2 evolutions in peak area across all samples. Total inorganic carbon (TIC) values varied from 0.006 to 0.068 wt. % (Table 2) and the ratio of inorganic carbon to total carbon ranged from 0.14 to 1, consistent with variable mixtures of Ca carbonate and organic carbon in each sample. There are well-defined Ca carbonate endotherms in the heat flow data from the Entisol and Inceptisol, but this trend was not so well-defined in the Alfisol (Figure 3) and there also appears to be "doublet" high-temperature CO_2 peaks for the Entisol, suggesting a combination of Ca-carbonate and perhaps dolomite or ankerite, though these phases were not previously observed with XRD (Table S3 and Figure S2). DSC-EGA analysis of modern soils containing

various amounts of calcite have a similar sharp endothermic CO_2 peak release temperature at ~700° C that was attributed to the thermal decomposition of Ca carbonate (Apesteguia et al., 2018). An additional ~900° C endotherm observed in all samples was unrelated to carbonate decomposition and instead was attributed to thermal decomposition of sulfate minerals such as jarosite, which was previously detected in trace amounts with x-ray diffraction (Tables S3 and S4). Interestingly, Ca carbonate was not previously identified from x-ray diffraction patterns (Table S3 and Figure S2), and thus it is likely that these samples contain inorganic carbon below detection limit of XRD (~1 wt. %), but not SAM-EGA (0.01 wt. %). This agrees with estimated abundances of TIC, which were below 1 wt. % (Table 1) and demonstrates the ability of SAM-EGA-like analyses to detect trace amounts of inorganic carbon in complex pedogenic mineral matrices.

Other sources of high temperature CO_2 release could have result from the decarboxylation of organic compounds in refractory or thermally mature organic matter that occur over a broad range of temperatures (150 - 800° C). Previous investigation showed no coalification of organic matter or development of secondary porosity in any paleosols from the Painted Hills, which were buried by an estimated 1.5 - 2 km of overburden (Retallack et al., 2000; Horgan, 2016), suggesting paleosol samples here contain refractory but not thermally mature organic compounds, and are thus expected to have organic carbon evolution temperatures below 550° C.

All samples evolved CO with a peak release temperature of ~350° C (Figure 4). Evolution of CO was consistent with incomplete combustion of organics and/ or the presence of oxygen-bearing organics (Sutter et al., 2017). We did not observe clear co-evolutions of CO and CO_2 because the peak release temperature for CO was ~50° C lower than for CO_2 (Figure 4), but there was a distinct overlap in the peak release temperature (e.g., they have overlapping elution times, but they are not coeluting) suggesting that a portion of the CO could have been released from incomplete combustion of organic carbon. The co-occurrence of CO and CO_2 was not observed at high (~700 °C) temperatures (Figure 4) because the thermal decomposition of Ca carbonate does not produce CO. Thus, evolved CO detections near 400° C were consistent with the decomposition of organic compounds.

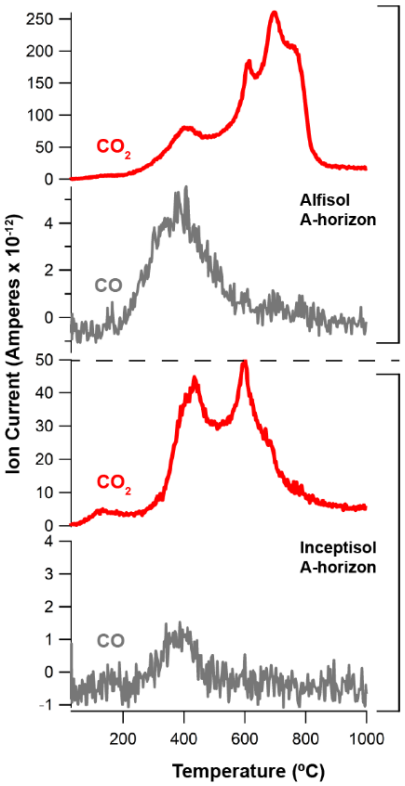

Figure 4. CO_2 (red trace) and CO (*m/z* 28) (grey trace) evolutions from the surface horizons of paleosols at the John Day Fossil Beds National Monument, Oregon. Top panel is surface (4 cm) horizon of the Alfisol; bottom panel is surface (3 cm) horizon of the Inceptisol.

3.2.2 *m/z* 30 evolutions

A *m/z* 30 peak was identified in all samples (Fig 5) and was consistent with either the oxidation of formic acid or the oxidation of nitrogen-bearing organics (e.g., the *m/z* 30 peak is nitrous oxide [NO]). In the sample with the greatest amount of organic carbon (Alfisol A-horizon), evolutions of *m/z* 30 start at ~300° C and show a peak release temperature of ~ 400° C as well as a small shoulder at ~ 600° C (Figure 5). Organic fragments observed in this sample included CH_2 (*m/z* 14), CH_3 (*m/z* 15), and C_2H_2 (*m/z* 26) (Figure 6). Evolutions of *m/z* 30 were simultaneous with evolutions of these organic fragments at ~400° C, suggesting the oxidation of a nitrogen-bearing organic compound could have been a significant contributor to evolved NO (*m/z* 30) (Navarro-González et al., 2009). On the other hand, formic acid (HCOOH), a simple carboxylic acid, also has a fragment at *m/z* 30. Thus, the oxidation of formic acid could also explain the peak observed at *m/z* 30, primarily because a *m/z* 29 peak was observed that tracked with *m/z* 30 (Figure S5). By contrast, co-elutions of *m/z* 30 and 31 would be indicative of NO,

but instead, *m/z* 30 and 31 did not track with one another in most samples (Figure S5), potentially suggesting formic acid as a contributor to the *m/z* 30 peak.

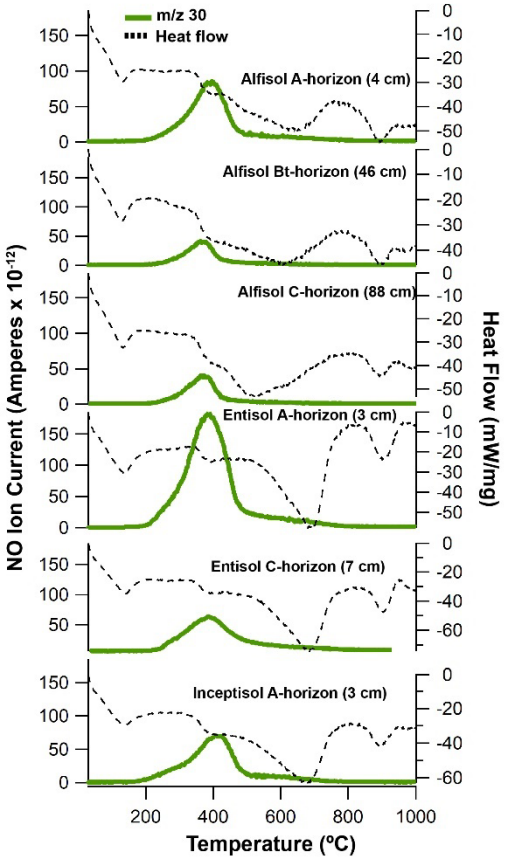

Figure 5. Evolutions of *m/z* 30 from paleosols at the John Day Fossil Beds National Monument, Oregon. Green trace is *m/z* 30 and dashed trace is heat flow from differential scanning calorimetry (DSC).

The thermal decomposition of nitrates can also release NO, though at elevated temperatures (> 500° C) relative to nitrogenated organics (Stern et al., 2015), and therefore the NO release temperate can constrain the origin of NO. For example Alkali (Na, K) and alkaline earth (Mg, Ca) metal nitrates decompose to NO at temperatures > 560° C (Stern et al., 2015). In laboratory experiments under SAM-like conditions, $Fe(NO_3)_3$ begins to decompose to NO at < 200° C and exhibits two distinct releases of NO at ~300 and ~450° C, which has been attributed to dehydration and hydrolysis of $Fe(NO_3)_3$ hydrates, respectively (Stern et al., 2015). Instead, NO release in paleosol samples begins at ~250° C and exhibited a single peak at ~400° C across all samples (Figure 5), unlike the dual high-temperature NO peaks from decomposition of $Fe(NO_3)_3$

hydrates. The simultaneous evolution of NO, CO_2, and organic fragments in paleosol samples analyzed here (Figure 6) are an additional line of evidence suggesting NO releases could have resulted from oxidation and/or decarboxylation of nitrogen-bearing organic compounds. We also observed evolutions of small nitrogen-bearing organics (HCN, m/z 27, 26) that co-occurred with evolutions of *m/z* 30 in several samples, including the surface horizon of the Alfisol (Figure S6).

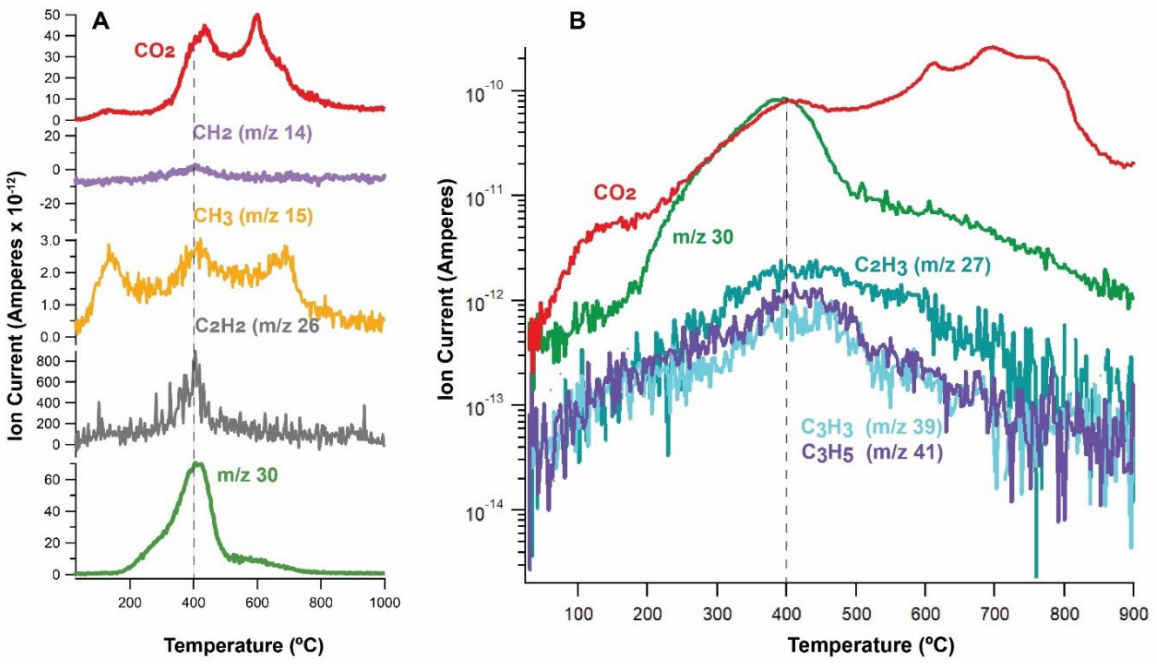

Figure 6. Simultaneous evolutions of CO_2, *m/z* 30 and organic fragments in paleosol surface horizons. (A) Evolutions of CO_2, *m/z* 30, and organic fragments (*m/z* 14, 15, 26) from the surface horizon of the Inceptisol (3 cm). **(B)** Semi-log scale plot of CO_2, *m/z* 30 and additional organic fragments (*m/z* 27, 39, 41) from the surface horizon (4 cm) of the Alfisol

One possible source of nitrogen-bearing organic carbon compounds is pyrogenic carbon (char) in paleosol samples that formed as a result of wildfires across the original soil landscape (Kurth et al., 2006). Nitrogen-bearing organic compounds such as nitriles, pyridine and pyrrole-derive compounds have been observed with pyrolysis GC/MS in modern fire-affected soils (De la Rosa et al., 2008). These modern soils were observed to have a sharp ~550° C peak release temperature of NO (*m/z* 30) during TG-DSC-EGA, suggesting that pyrogenic carbon may be one source of NO evolutions from soils. Although it is impossible to determine the original inputs of nitrogen-bearing organics in paleosols, nitrogen may have been incorporated into increasingly stable organic matter as a consequence of forest fires, and may persist in paleosols today as char. Previous authors have reported the occurrence of preserved char in paleosols of late Permian

(Miller et al., 1996) and late Jurassic age (Matthewman et al., 2012), so it is possible that nitrogen-bearing char may be responsible for the overlapping 400° C *m/z* 30 and and CO_2 peaks observed in this study. In summary, the *m/z* 30 peak at 400° C observed in all samples is most likely from the oxidation of organic matter, but whether it resulted from nitrogen-bearing pyrogenic carbon or carboxylic acids (e.g., formic acid) remains unclear.

3.3 Possible mechanisms of organic carbon preservation in paleosols

There are many competing factors that control the preservation and degradation of organic carbon in terrestrial environments. Possible mechanisms of organic carbon preservation include the formation of organo-mineral complexes, and/or the formation of microaggregates that may have increased the biochemical stability of organic molecules, as observed in modern soils (Plante et al., 2011) and Quaternary paleosols (Marin-Spiotta et al., 2014). Smectite clay minerals in particular preserve organic molecules due to their high specific surface area, negatively charged interlayers, and cations that inhibit water flow, thus making them favorable locations for the preservation of organic carbon over millions or possibly billions of years (Bishop et al., 2013; Noe Dobrea et al., 2016; Szopa et al., 2020). Paleosols examined here contained between ~70-90 wt. % smectite, primarily as mixtures of montmorillonite and nontronite (Tables S3 and S5), so it is possible that organic compounds could have been associated with clay minerals.

We observed evolutions of volatile gases from clay-rich paleosols that may have resulted from the preservation of organic carbon over geological time scales, as well as possible contributions from small amounts of modern organic carbon detected with radiocarbon analysis. The fragmentation of organic molecules during pyrolysis EGA provides limited constraints on the types of molecules present, but it can help determine if there are any associations between minerals and organic molecules. These associations can include physical occlusion, chemisorption and/or adsorption to mineral surfaces, or intercalation in clay minerals (Kleber et al., 2005, 2021; Schmidt et al., 2011; François et al., 2015). A strong correlation between the peak release temperature of organic fragments and the release of H_2O or other volatiles would suggest that organic matter could have been associated with minerals.

In all samples, there were no apparent co-occurring evolutions of organic fragments, CO_2, and water releases from clay dehydroxylation (Figure 7). The Al-smectite in the surface

horizon of the Alfisol began dehydroxylation near 400° C. Figure 7 shows the peak release temperature of organics and CO_2 was ~100° C lower relative to peak H_2O release from Al-smectite dehydroxylation. This sample had the highest TOC (~0.03 wt. %), FM of ~0.46 (Table 1), and a phyllosilicate content of ~85 wt. % (Table S3). Interestingly, samples from other depths had higher temperatures of clay dehydroxylation due to differences in clay mineralogy (e.g., Fe vs. Al in the octahedral sheet) and/or abundance. This was observed in the Entisol and Alfisol (Figures S3 and S4), but these samples were depleted in organic carbon relative to the Al smectite-rich surface horizon of the Alfisol (Table 1). Though our EGA results do not provide evidence that phyllosilicates and organics were strongly associated with one another, it is possible that the high clay mineral abundances provided other means of organic preservation, including physical occlusion, the formation of organic-mineral aggregates, or other weaker types of sorption to phyllosilicate surfaces, such as outer-sphere complexation (Guggenberger and Kaiser, 2003; Schmidt et al., 2011).

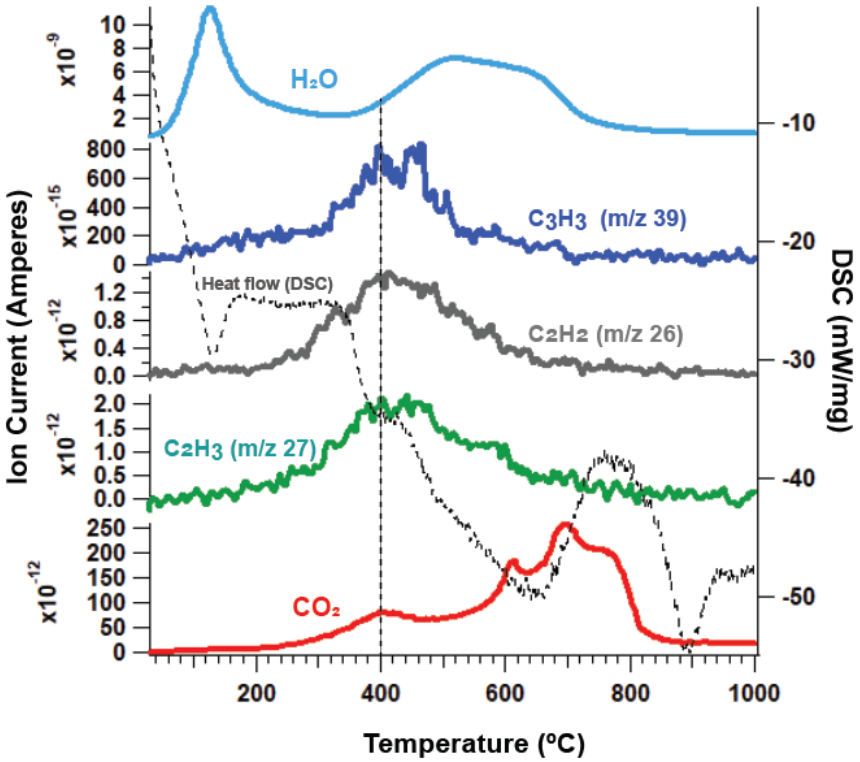

Figure 7. Evolutions of CO_2, organic fragments, and H_2O from the surface horizon of the Alfisol (4 cm). Dashed trace is heat flow from differential scanning calorimetry (DSC).

Interactions with sulfur can also aid in the preservation of organic molecules in soils and sediments over geological time scales (Matthewman et al., 2012; François et al., 2015; Eigenbrode et al., 2018; Alekseeva et al., 2019). The incorporation of organic C into the crystal lattice of sulfate minerals can increase thermodynamic stability and therefore increase the temperature of organic carbon decomposition during EGA (François et al., 2015). Minor detections of jarosite and gypsum in XRD patterns (< 5 wt. %) were observed, and these minerals could have also contributed to the preservation of organics (Tables S5 and S6). Minor SO_2 evolutions at ~800° C across all samples (Figure S3) were consistent with the decomposition of sulfate minerals. A single sample (Entisol 7 cm) had a low-temperature SO_2 peak that co-occurred with the CO_2 release at ~400° C (Figure 8).

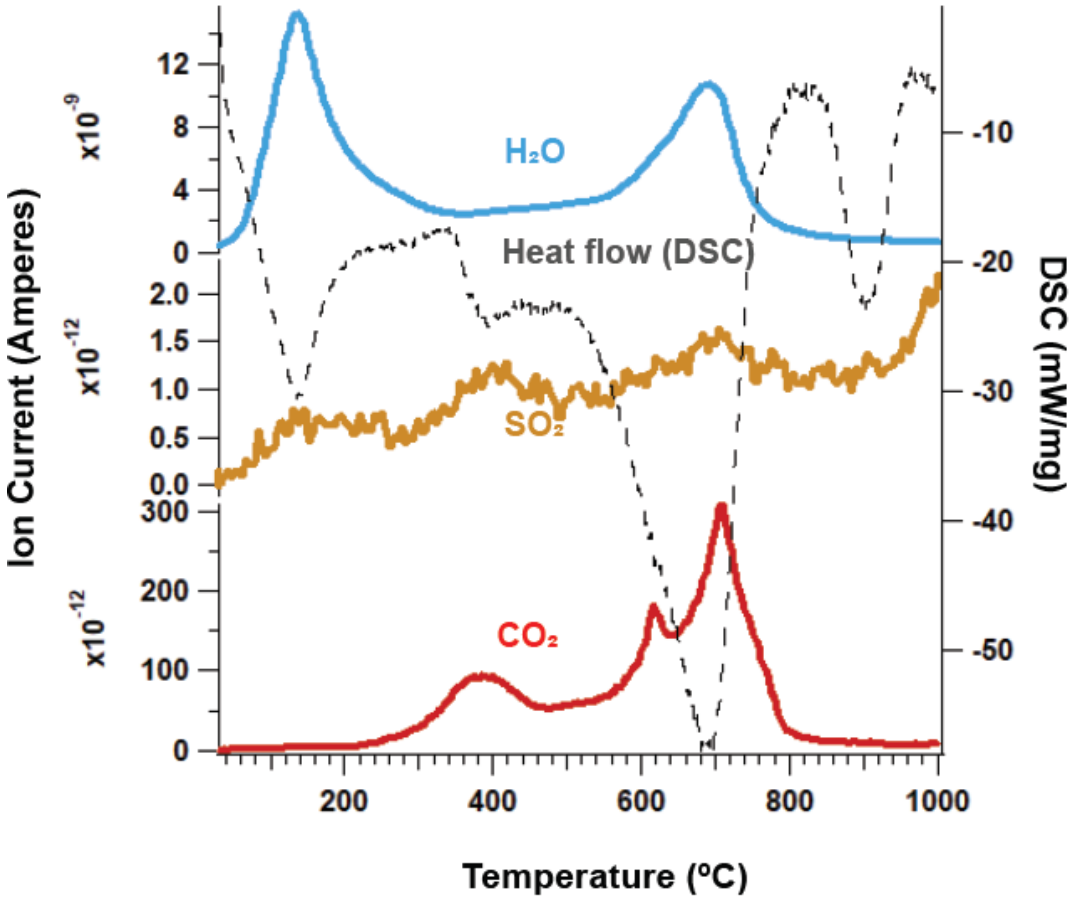

Figure 8. Evolutions of H_2O (blue trace), SO_2 (yellow trace), CO_2 (red trace), and heat flow (dashed trace) from the surface horizon of the Entisol (3 cm). DSC – differential scanning calorimetry (heat flow), H_2O – *m/z* 18, SO_2 – *m/z* 64, CO_2 – *m/z* 44.

Trace amounts of Mg sulfates in the Alfisol could account for minor SO_2 releases > 700° C including the ~790° C SO_2 peaks (François et al., 2015; Mcdam et al., 2020a). At higher temperatures, all soils showed a major release of SO_2 beginning at 900° C that co-occurred with an endotherm, both of which are consistent with the thermal decomposition of crystalline sulfates (Ming et al., 2014; François et al., 2015). Since the samples were only heated to ~1000° C for this work, the maximum peak height of this release cannot be ascertained. Peak SO_2 release temperatures generally did not co-occur with low-temperature (~400° C) CO_2 evolutions across the rest of the samples (Figure S3), so it is unlikely that sulfate minerals played a significant role in organic preservation in samples examined here. However, it has been hypothesized that sulfate minerals were most likely diagenetic and not original to the paleosols, but instead were inherited from the modern weathering zone (Broz et al., 2022). Thus, if modern sulfate minerals were associated with small amounts of modern organic carbon, the sulfate minerals could have been a source of radiocarbon in samples with co-occurring SO_2 and CO_2 evolutions.

3.4 Enrichment of organic carbon in surface layers of paleosols

The near-surface horizons of all paleosols examined here had greater amounts of total organic carbon (TOC) relative to deeper horizons (Figure 9, Table 1). The highest amounts of CO_2 released from decomposition of organic carbon (150-500° C) were in the near surface (A) horizons of all three paleosol types while subsurface layers of paleosols generally had lower quantities of evolved CO_2 from organic carbon (Figure 3, Table 1). The A horizon of the Alfisol had TOC of 0.031 ± 0.006 wt. % and progressively decreased to 0.002 ± 0.007 wt. % in the C horizon.

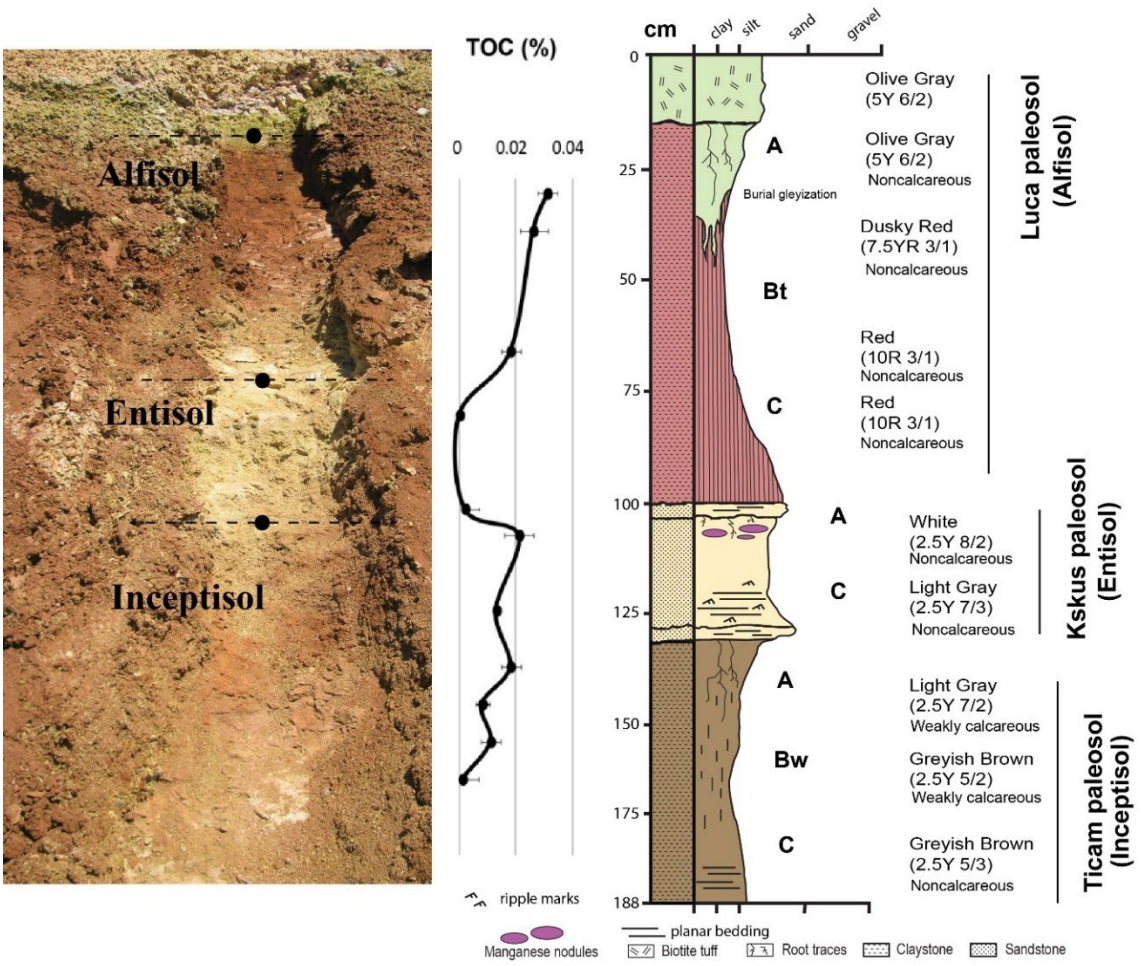

Figure 9. Trends of organic carbon enrichment in the near-surface horizons of three paleosols from the early Oligocene (33 Ma) middle Big Basin Member of the John Day Formation in eastern Oregon, USA**.** The surface (A) horizons of all three profiles had significantly ($P > 0.05$) higher total organic carbon (TOC) content relative to subsurface horizons (Bt, Bw and C horizons, respectively). Average TOC content of samples (n=2) was determined by thermal and evolved gas analysis (with oxygen as a carrier gas).

Samples from the A-horizon of the Alfisol had been affected by burial gleization (Broz et al., 2022). Burial gleization is a product of early diagenesis of paleosols that involves the reduction of Fe^{3+} to Fe^{2+} by anaerobic microbes as a result of rapid burial (PiPujol and Buurman, 1994; Retallack, 2019). This phenomenon is also thought to promote anaerobic decay of organic matter (Retallack, 2019), even in soils that originally formed under oxidizing conditions before burial. Burial gleization is envisaged as closed system alteration (e.g., without depletion of total iron) and is in most cases limited to the near-surface horizons of paleosols where organic matter is most concentrated (typically A and B horizons). The surface horizon of the Alfisol examined

in this work had distinct evidence of burial gleization which included drab-colored mottles and tubular features predominantly in the A-horizon, which impinged downward into the subsurface (Bt) horizon at several locations within the profile (Figure 9). The emplacement of a biotite-bearing tuff on the paleosurface of the Alfisol may have led to gleization of the A-horizon after burial. Similar trends of near-surface TOC enrichment were noted in the Entisol and Alfisol (Table 1), but these samples lacked chemical ($FeO/Fe_2O_3 > 0$) and morphological evidence (drab green color) of burial gleization (Tables S5 and S6). Previous work on terrestrial paleosols has shown positive and significant correlations between Fe^{2+} content and TOC (Broz, 2020). This supports the interpretation that burial gleization, which increases Fe^{2+} in bulk samples, may have been associated with the preservation of organic carbon in the surface horizon of the Alfisol.

Organic carbon from organisms living in surface horizons of soils may have been preserved upon rapid burial of the paleosurface, and therefore the trend of organic enrichment may represent the preservation of endogenous organic carbon. However, major losses of endogenous organic carbon from burial decomposition of organic matter are common in paleosols that originally formed under oxidizing conditions such as those examined here (Retallack, 2019). Despite diagenetic additions and losses of organic carbon, the trend of surface enrichment of organic carbon remains apparent, even in soils that formed under strongly oxidizing conditions prior to burial. These results are consistent with other studies of paleosols where the surface enrichment of organic carbon was attributed to preservation of carbon from organisms living above and within the soil profile (Rye and Holland, 2000; Watanabe et al., 2004; Liivamägi et al., 2018; Liu et al., 2020). However, it is possible that addition of recent/modern organic carbon caused this enrichment, for example, by preferential groundwater flow and accumulation in the paleosurface of each profile. Results from this work cannot definitively rule out groundwater as a source of modern organic carbon, though it is unlikely that groundwater additions of organic carbon would have preferentially accumulated in the discreet, thin (10-20 cm), diffuse surface layers of the three buried soils.

3.5 Implications for Mars

Recent work has considered paleosols on Mars as potential high priority environments for *in-situ* biosignature investigation (Hays et al., 2017) and Mars Sample Return (Bishop et al., 2018a). This is because the composition and properties of paleosols preserve evidence of

paleoclimate, aqueous conditions, and life (Bishop et al., 2018a). A major finding of this study is that near-surface horizons of terrestrial paleosols appear to be a favorable location for SAM-EGA detection of organic carbon. Like modern soils, the surface layers of Mars-analog paleosols examined here show evidence of surface enrichment of organic carbon. Although the early diagenetic process of burial decomposition of organic matter has likely reduced the organic carbon content of these ancient soils by at least two orders of magnitude relative to modern soils (Broz, 2020), the enrichment of organic carbon in surface horizons (~0.03 wt. %) and subsequent depletion in deeper layers (<0.01 wt. %) was readily observable with a SAM-EGA analog instrument.

Results from this study have implications for interpreting the chemical and isotopic biosignature preservation potential of Al and Fe smectite-bearing weathering profiles on Mars. It is possible that clay minerals and/or amorphous phases in martian weathering profiles have imparted a similar control on the fate of organic carbon. However, putative martian weathering profiles have likely been subject to both galactic cosmic ray bombardment and the accumulation of oxychlorine salts that, together, have likely contributed to the degradation of organic matter in the top 1-2 m of the martian surface (Dartnell et al., 2007; Pavlov et al., 2012). This poses major challenges for the future detection of organic carbon in martian weathering profiles using current drilling techniques. Trace amounts of organic carbon may have been preserved in the Oregon paleosols (Table 2), but if putative martian paleosols have a Cretaceous exposure age comparable with Gale crater sedimentary rocks (Farley et al., 2013), millions of years of cosmic ray bombardment and interactions with oxychlorine salts may have led to the oxidation of a significant fraction of the organic carbon pool.

This work also provides an initial framework for investigation and sampling of martian weathering profiles should they be encountered by current or future landed missions. If possible, future *in-situ* analysis of putative weathering profiles should begin at the apparent ancient surface horizon (e.g., the buried topsoil layer) and sample down section into the unaltered protolith, similar to the sampling of a terrestrial soil profile. If the entire profile is not accessible for investigation (e.g., outcrop is at a topographic position inaccessible to the rover), the near-surface horizons of the profile, just below the overlying burial layer, should be considered the highest priority target for remote sensing, contact science, and collection of a drilled sample for

sample return to Earth. Two locations on Mars where current and future landed missions could encounter a paleosol profile are discussed below.

Mawrth Vallis

The compositional stratigraphy at Mawrth Vallis has been interpreted as a paleosol sequence (Horgan et al., 2012) or a laterite-like deep weathering profile (Liu et al., 2021a). In the rim of Muara Crater, a ~200 m stack of layered sedimentary rocks has spectral signatures consistent with pedogenic-like alteration of mafic sediments (Horgan, 2013), including Al/Fe smectites, Fe/Mg smectites, hydrated silica, and sulfates. As such, results from this study can help to constrain the organic preservation potential of putative weathering profiles from the Mawrth Vallis region. For example, results from this work showed that Al/Fe smectite-bearing paleosols that formed under strongly oxidizing conditions have preserved only trace amounts of organic carbon. Comparisons with terrestrial paleosols could therefore help to determine if weathering profiles at Mawrth Vallis are sites of enhanced organic preservation that should be targeted by future rover sampling campaigns. However, it should be noted that Eocene-Oligocene (42-28 Ma) eastern Oregon paleosols are an incomplete Mars analog due to several fundamental differences. For example, the source of organic carbon within the paleosols is primarily from microbial and/or plant biomass and represents a complex consortium of life above and within the soil profile. These irrevocable differences preclude direct comparisons between Earth and a presumably lifeless early Mars. Large differences in age (Oligocene [33 Ma] versus Noachian [4.1-3.7 Ga]) also have implications for diagenesis. The Oregon paleosols have experienced a range of minor to moderate diagenetic alteration including illitization of smectite, zeolitization and celadonization all resulting from alteration to clinoptilolite facies (Retallack et al., 2000; Horgan, 2016), but it is currently unclear if similar diagenetic alteration has affected potential paleosol sequences on Mars.

There are also major differences in the oxidation state of the atmosphere during subaerial weathering on Earth and Mars. The Oregon paleosols formed under a thoroughly oxidizing atmosphere but at present the oxidation state of an early Mars atmosphere is not well constrained (Ramirez et al., 2014). Leaching of Fe^{2+} in putative martian paleosols at Mawrth Vallis has been inferred from spectral weathering indices and are altogether consistent with an anoxic, reducing atmosphere during the early Noachian (Liu et al., 2021a). Furthermore, there may have also been

major differences in the pH of fluids participating in hydrolytic weathering of volcaniclastic sediments. The Oregon paleosols formed via pedogenic weathering with circumneutral-pH fluids, but subaerial alteration on Mars could have preceded with acidic, H_2SO_4 and HCl-rich surface waters as a result of volcanic outgassing of H_2 and SO_2 (Liu et al., 2021a, 2021b). Both scenarios would presumably affect the organic preservation potential of rocks that contain sedimentary organic matter.

Lastly, the organic carbon component of the Oregon paleosols and the resulting preservation and degradation mechanisms may not be the same on Mars, but it is possible that putative paleosols at Mawrth Vallis have mineralogy analogous to terrestrial paleosols and thus have a similar mineralogical control on the fate of organic carbon. If targeted for future exploration, these deposits could provide detailed information about climate and the duration of aqueous alteration throughout the Mawrth Vallis region, and they may represent sites of enhanced organic preservation that could be targeted by future rover sampling campaigns.

Jezero Crater

Spectral signatures of Al-bearing clay minerals and/or silica deposits that could have formed in subaerial environments were detected approximately 3 km from the Perseverance rover landing site at Jezero Crater. Across Jezero's western delta and northern fans, there are strong and ubiquitous orbital detections of Al-bearing clay minerals and/or silica that could be either detrital or authigenic in origin (Horgan et al., 2020). The strongest signatures across the western delta are associated with features that resemble point bar deposits and are consistent with formation in subaerial and/or seasonally waterlogged paleoenvironments (Horgan et al., 2020). These deposits could represent subaerial paleoenvironments and include individual paleosol profiles, which may have accumulated reduced carbon in near-surface horizons. If targeted for *in-situ* examination by *Perseverance* rover, these deposits could provide critical information about the climate and duration of delta activity at Jezero Crater (Horgan et al., 2020) and they could be a potential high-priority location for the preservation of chemical and isotopic biosignatures.

Conclusions

The objectives of this study were a) to determine whether the organic carbon content of ~33-million-year-old paleosols can be detected with a thermal and evolved gas analyzer

configured to operate like the SAM-EGA instrument onboard *Curiosity* Mars rover, and b) use radiocarbon (^{14}C) dating to constrain the age of organic carbon in bulk paleosol samples. Radiocarbon dating of organic carbon in four paleosol samples revealed the presence of recent and/or modern exogenous organic carbon. Samples from 10 - 20 cm were dated to ~6,200 years BP and had a fraction modern (FM) value of ~0.4, while a single deeper sample collected from 43 cm into the outcrop had a radiocarbon age of ~14,600 years BP and ~0.16 fM. The presence of radiocarbon in paleosols could have resulted from the addition of small amounts of modern organic carbon that mixed with ^{14}C-free endogenous organic carbon. Alternatively, a diagenetic event between 6-14 Ka could have introduced exogenous organics, possibly through groundwater alteration and/or precipitation-driven leaching of dissolved organic carbon. Application of a two-endmember mixing model (Equation 1) to the $D^{14}C$ values of bulk samples values provided supporting evidence for the hypothesis that paleosols from the site contain small amounts of modern organic carbon. The amount of modern carbon ($D^{14}C$= 0‰) that could have been added to a pool of Oligocene-age carbon ($D^{14}C$ = -999‰) was determined to range from ~0.5 – 3% of the total organic carbon in each sample. These results highlight a new approach for constraining the age and sources of organic matter in terrestrial paleosols.

SAM-EGA-like characterization of paleosols showed evolutions of CO, CO_2, and organic fragments. Coevolutions of CO_2 and organic fragments at ~400° C suggested the presence of refractory organic carbon. However, like other oxidized terrestrial paleosols of Cenozoic age and older, only trace amounts (<0.1 wt. %) of organic carbon was detected, which most likely was a result of diagenetic decomposition of organic matter over geological time scales. Many samples examined in this work typically contained very low amounts (~0.01 wt. %) of organic carbon, but these low values were nevertheless detectable by SAM-like evolved gas analysis of bulk samples. These results suggest the organic fraction of potential martian weathering profiles may be detectable with evolved gas analysis, even if organic concentrations are low.

A major result of this work was that organic carbon was concentrated in near-surface horizons of paleosols while deeper horizons were depleted in organic carbon. Like modern soils, these ancient soils were enriched in organic carbon in near-surface horizons, and it appears that this trend persisted in these samples despite burial decomposition of organic carbon over geological time scales. Alternatively, modern carbon could have leached into the outcrop, but it is unlikely such organic contamination would preferentially accumulate in the surface layers of

each successive buried soil profile. Enrichment of organic carbon in the original surface horizons of buried weathering profiles on Mars may therefore constitute a putative chemical biosignature. This work demonstrates that analytical techniques similar to SAM-EGA can detect trace amounts of organic carbon in complex pedogenic mineral matrices. The search for past life on ancient land surfaces of Mars should include targeting Martian weathering profiles for *in-situ* biosignature investigation and Mars Sample Return.

Additional Information

Acknowledgements

This work was performed on and adjacent to the ancestral homelands of the Numu, Cayuse, Umatilla, Walla Walla, and Confederated Tribes of the Warm Springs who were present before western settlement. Many thanks to Elizabeth Rampe and Paul Niles for the opportunity to work on this project and for providing research direction during a summer internship. This work was completed as part of a PhD dissertation supervised by Lucas C.R. Silva and Greg Retallack. Xiaomei Xu performed radiocarbon dating and greatly assisted with data interpretation, both of which were integral to this work. Megan Barrington and Barry Hughes assisted with fieldwork and entertained thoughtful discussion. Anais Roussel, Angela Olsen, Marshall Styczinski, Paul Regensberger and Joe Caggiano reviewed early versions of the manuscript. Funding to A.P.B. from the National Science Foundation, Geological Society of America, The Clay Minerals Society, The Society of Sedimentary Geology, and the Central Oregon Geoscience Society aided in the completion of this project.

Author Contribution Statement

A.P.B and J.V.C designed the study, performed all laboratory analyses and drafted the manuscript. J.V.C, D.W.M, P.D.A, and B.S contributed to data analysis and interpretation. B.H.H identified similarities between Mars and Oregon paleosols, led fieldwork, and assisted with data interpretation. L.C.R.S provided radiocarbon analyses and interpreted the data. J.V.C, P.D.A, B.S, D.W.M, and L.C.R.S supervised the project. A.P.B drafted all figures. All authors contributed to the manuscript.

Author Disclosure Statement

No competing financial interests exist.

Data Availability Statement

All data supporting the conclusions can be found within the article and in the following repository: Broz, 2022. All raw data to reproduce EGA traces are included in the supplementary dataset (Broz, 2022).

4 References

Alekseeva, T. V, Zolotareva, B.N., and Kolyagin, Y.G., 2019, Nonhydrolyzable Part of Soil Organic Matter in Buried and Modern Soils: Eurasian Soil Science, v. 52, p. 632–643, doi:10.1134/S1064229319060024.

Amundson, R., 2018, Meteoric water alteration of soil and landscapes at Meridiani Planum, Mars: Earth and Planetary Science Letters, v. 488, p. 155–167, doi:10.1016/j.epsl.2018.02.012.

Apesteguia, M., Plante, A.F., and Virto, I., 2018, Methods assessment for organic and inorganic carbon quantification in calcareous soils of the Mediterranean region: Geoderma Regional, v. 12, p. 39–48, doi:10.1016/j.geodrs.2017.12.001.

Archer, P.. et al., 2014, Abundances and implications of volatile-bearing species from evolved gas analysis of the Rocknest aeolian deposit, Gale Crater, Mars: Journal of Geophysical Research : Planets, p. 237–254, doi:10.1002/2013JE004493.Received.

Beaty, D.W., Grady, M.M., Mcsween, H.Y., Sefton-Nash, E., Carrier, B.., Altieri, F., and Al., E., 2019, The potential science and engineering value of samples delivered to Earth by Mars sample return: Meteoritics & Planetary Science, v. 671, p. 667–671, doi:10.1111/maps.13232.

Bestland, E.., 1997, Alluvial Terraces and Paleosols As Indicators Of Early Oligocene Climate Change (John-Day Formation, Oregon): Journal Of Sedimentary Research, v. 67, p. 840–855, doi:10.1306/D4268653-2B26-11D7-8648000102C1865D.

Bestland, E.A., 2002, Fossil Andisols identified with mass-balance geochemistry (Oligocene John Day Formation, Oregon, U.S.A.): Journal of Sedimentary Research, v. 72, p. 673–686, doi:10.1306/021802720673.

Bishop, J.L. et al., 2018a, Potential high priority subaerial environments for Mars sample return: Proceedings of the Second International Mars Sample Return Conference, v. 2071, doi:2018LPICo2071.6043I.

Bishop, J.L., Fairén, A.G., Michalski, J.R., Gago-duport, L., Baker, L.L., Velbel, M.A., Gross, C., and Rampe, E.B., 2018b, Surface clay formation during short-term warmer and wetter conditions on a largely cold ancient Mars: Nature Astronomy, v. 2, p. 206–213, doi:10.1038/s41550-017-0377-9.

Bishop, J.L., Gross, C., Danielsen, J., Parente, M., Murchie, S.L., Horgan, B., Wray, J.J., Viviano, C., and Seelos, F.P., 2020, Multiple mineral horizons in layered outcrops at

Mawrth Vallis, Mars, signify changing geochemical environments on early Mars: Icarus, v. 341, p. 113634, doi:10.1016/j.icarus.2020.113634.

Bishop, J.L., Loizeau, D., Mckeown, N.K., Saper, L., Dyar, M.D., Des, D.J., Parente, M., and Murchie, S.L., 2013, What the ancient phyllosilicates at Mawrth Vallis can tell us about possible habitability on early Mars: Planetary and Space Science, v. 86, p. 130–149, doi:10.1016/j.pss.2013.05.006.

Bishop, J.L., and Rampe, E.B., 2016, Evidence for a changing Martian climate from the mineralogy at Mawrth Vallis: Earth and Planetary Science Letters, v. 448, p. 42–48, doi:10.1016/j.epsl.2016.04.031.

Broz, A.P., 2022, Detection of organic carbon in Mars-analog paleosols with thermal and evolved gas analysis [Data set]: Mendelay, doi:10.17632/bkvcff9dw8.1.

Broz, A.P., 2020, Organic Matter Preservation in Ancient Soils of Earth and Mars: Life, v. 10, doi:doi:10.3390/life10070113.

Broz, A.P., Clark, J.V., Archer, P.., Sutter, B., Tu, V.M., Silva, L.C.R., and Horgan, B.H.N., 2021, Radiocarbon dating of Mars-analog paleosols reveals contamination with exogenous organic carbon, *in* Terrestrial Analogs, v. 8094.

Broz, A.P., Clark, J., Sutter, B., Ming, D.W., Tu, V., Horgan, B., and Silva, L.C.R., 2022, Mineralogy and diagenesis of Mars-analog paleosols from eastern Oregon, USA: Icarus, v. 380, p. 114965, doi:10.1016/j.icarus.2022.114965.

Cannon, K.M., Sutter, B., Ming, D.W., Boynton, W. V., and Quinn, R., 2012, Perchlorate induced low temperature carbonate decomposition in the Mars Phoenix Thermal and Evolved Gas Analyzer (TEGA): Geophysical Research Letters, v. 39, p. 2–6, doi:10.1029/2012GL051952.

Carter, J., Loizeau, D., Mangold, N., Poulet, F., and Bibring, J., 2015, Widespread surface weathering on early Mars : A case for a warmer and wetter climate: Icarus, v. 248, p. 373–382, doi:10.1016/j.icarus.2014.11.011.

Danielson, J.., Bishop, J.., Usabel, G.S., Miura, J.., Sessa, A.., Wray, J.., Itoh, Y., Parente, M., and Murchie, S.., 2019, Characterization of outcrops containing “doublet” spectra at Mawrth Vallis, Mars: Lunar and Planetary Science Conference, v. 2019, p. 1–179, doi:10.1029/2008g.

Dartnell, L.R., Desorgher, L., Ward, J.M., and Coates, A.J., 2007, Martian sub-surface ionising radiation : biosignatures and geology ∗: Biogeosciences, v. 4, p. 545–558.

Dynarski, K.A., Bossio, D.A., and Scow, K.M., 2020, Dynamic Stability of Soil Carbon: Reassessing the “Permanence” of Soil Carbon Sequestration: Frontiers in Environmental Science, v. 8, doi:10.3389/fenvs.2020.514701.

Eigenbrode, J.L. et al., 2018, Organic matter preserved in 3-billion-year-old mudstones at Gale crater, Mars: Science, v. 360, p. 1096–1101, doi:10.1126/science.aas9185.

Farley, K.A., Malespin, C., Mahaffy, P., and Grotzinger, J.P., 2013, In Situ Radiometric and Exposure Age Dating of the Martian Surface — Supplementary Materials: Science Express, p. 1–9, doi:10.1126/science.1247166.

Fernández, J.M., Peltre, C., Craine, J.M., and Plante, A.F., 2012, Improved characterization of

soil organic matter by thermal analysis using CO2/H2O evolved gas analysis: Environmental Science and Technology, v. 46, p. 8921–8927, doi:10.1021/es301375d.

Fornaro, T., Steele, A., and Brucato, J.R., 2018, Catalytic/protective properties of martian minerals and implications for possible origin of life on mars: Life, v. 8, p. 1–41, doi:10.3390/life8040056.

François, P., Szopa, C., Buch, A., Coll, P., Mcadam, A.C., Mahaffy, P.R., Freissinet, C., Glavin, D.P., and Cabane, M., 2015, Magnesium sulfate as a key mineral for the detection of organic molecules on Mars using pyrolysis: Journal of Geophysical Research – Planets, p. 61–74, doi:10.1002/2015JE004884.Received.

Freissinet, C. et al., 2015, Organic molecules in the Sheepbed Mudstone, Gale Crater, Mars: Journal of Geophysical Research : Planets, v. 120, p. 495–514, doi:10.1002/2014JE004737.Received.

Fremd, T.J., 1996, Data Quality in Terrestrial Assemblages: Perspectives from Volcaniclastic Sequences of the John Day Basin, Oregon: The Paleontological Society Special Publications, v. 8, p. 131–131, doi:10.1017/s2475262200001337.

Guggenberger, G., and Kaiser, K., 2003, Dissolved organic matter in soil : challenging the paradigm of sorptive preservation: Geoderma, v. 113, p. 293–310, doi:10.1016/S0016-7061(02)00366-X.

Hays, L.E., Graham, H. V., Des Marais, D.J., Hausrath, E.M., Horgan, B., McCollom, T.M., Parenteau, M.N., Potter-McIntyre, S.L., Williams, A.J., and Lynch, K.L., 2017, Biosignature Preservation and Detection in Mars Analog Environments: Astrobiology, v. 17, p. 363–400, doi:10.1089/ast.2016.1627.

Horgan, B.H.N., 2013, Climate change and a sequence of habitable ancient surface environments preserved in pedogenically altered sediments at Mawrth Vallis, Mars., *in* Lunar and Planetary Science Conference, p. 3059.

Horgan, B., 2016, Strategies for Searching for Biosignatures in Ancient Martian Sub-Aerial Surface Environments: Biosignature Preservation and Detection in Mars Analog Environments, p. 7463, doi:10.1089/ast.2016.1627.

Horgan, B.H.N., Anderson, R.B., Dromart, G., Amador, E.S., and Rice, M.S., 2020, The mineral diversity of Jezero crater : Evidence for possible lacustrine carbonates on Mars: Icarus, v. 339, p. 113526, doi:10.1016/j.icarus.2019.113526.

Horgan, B., Bishop, L., Christensen, P.R., and Bell, J.F., 2012, Potential ancient soils preserved at Mawrth Vallis from comparisons with Eastern Oregon paleosols: Implications for Early Martian Climate: Third Conference on Early Mars, v. 7074, p. 12–13.

Horgan, B., Rutledge, A., and Rampe, E.., 2018, Clay mineralogy and crystallinity as a climatic indicator: Evidence for both cold and temperate conditons on early Mars: 46th Lunar and Planetary Science Conference, p. 3–4, doi:10.1029/2006.

Ivanov, M.A., Slyuta, E.N., Grishakina, E.A., and Dmitrovskii, A.A., 2020, Geomorphological Analysis of ExoMars Candidate Landing Site Oxia Planum: Solar System Research, v. 54, p. 1–14, doi:10.1134/S0038094620010050.

Kleber, M., Bourg, I.C., Coward, E.K., Hansel, C.M., Myneni, S.C.B., and Nunan, N., 2021, Dynamic interactions at the mineral–organic matter interface: Nature Reviews Earth and

Environment, v. 2, p. 402–421, doi:10.1038/s43017-021-00162-y.

Kleber, M., Mikutta, R., Torn, M.., and Jahn, R., 2005, Poorly crystalline mineral phases protect organic matter in acid subsoil horizons: European Journal of Soil Science, p. 717–725, doi:10.1111/j.1365-2389.2005.00706.x.

Kremer, B., Kaźmierczak, J., and Środoń, J., 2017, Cyanobacterial-algal crusts from Late Ediacaran paleosols of the East European Craton: Precambrian Research, doi:10.1016/j.precamres.2017.12.018.

Krull, E.S., and Retallack, G.J., 2000, 13C depth profiles from paleosols across the Permian-Triassic boundary : Evidence for methane release: GSA Bulletin, v. 112, p. 1459–1472.

Kurth, V.J., MacKenzie, M.D., and DeLuca, T.H., 2006, Estimating charcoal content in forest mineral soils: Geoderma, v. 137, p. 135–139, doi:10.1016/j.geoderma.2006.08.003.

De la Rosa, J.M., González-Pérez, J.A., González-Vázquez, R., Knicker, H., López-Capel, E., Manning, D.A.C., and González-Vila, F.J., 2008, Use of pyrolysis/GC-MS combined with thermal analysis to monitor C and N changes in soil organic matter from a Mediterranean fire affected forest: Catena, v. 74, p. 296–303, doi:10.1016/j.catena.2008.03.004.

Lehmann, J., and Kleber, M., 2015, The contentious nature of soil organic matter: Nature, p. 1–9, doi:10.1038/nature16069.

Lewis, J.M.T. et al., 2021, Pyrolysis of Oxalate, Acetate, and Perchlorate Mixtures and the Implications for Organic Salts on Mars: Journal of Geophysical Research: Planets, v. 126, doi:10.1029/2020JE006803.

Liivamägi, S., Rodoń, J., Bojanowski, M., Gerdes, A., Stanek, J.J., Williams, L., and Szczerba, M., 2018, Paleosols on the Ediacaran basalts of the East European Craton: a unique record of paleoweathering with minimum diagenetic overprint: Precambrian Research, doi:10.1016/j.precamres.2018.07.020.

Liu, J., He, H., Michalski, J., Cuadros, J., Yao, Y., Tan, W., Qin, X., Li, S., and Wei, G., 2020, Reflectance spectroscopy applied to clay mineralogy and alteration intensity of a thick basaltic weathering sequence in Hainan Island , South China: Applied Clay Science, p. 105923, doi:10.1016/j.clay.2020.105923.

Liu, J., Michalski, J.R., Tan, W., He, H., Ye, B., and Xiao, L., 2021a, Anoxic chemical weathering under a reducing greenhouse on early Mars: Nature Astronomy, doi:https://doi.org/10.1038/s41550-021-01303-5.

Liu, J., Michalski, J.R., and Zhou, M., 2021b, Intense subaerial weathering of eolian sediments in Gale crater, Mars: Science Advances, v. 7, doi:DOI: 10.1126/sciadv.abh2687.

Loizeau, D. et al., 2020, ExoMars 2020 Surface Mission: Choosoing a Landing Site: v. 2019, p. 2019–2020.

Loizeau, D., Mangold, N., Poulet, F., Bibring, J., Bishop, J.L., Michalski, J., and Quantin, C., 2015, History of the clay-rich unit at Mawrth Vallis, Mars: High- resolution mapping of a candidate landing site: Journal of Geophysical Research: Planets, p. 1820–1846, doi:10.1002/2015JE004894.Received.

Loizeau, D., Quantin-nataf, C., Carter, J., Flahaut, J., Thollot, P., Lozac, L., and Millot, C., 2018, Quantifying widespread aqueous surface weathering on Mars : The plateaus south of

Coprates Chasma: Icarus, v. 302, p. 451–469, doi:10.1016/j.icarus.2017.11.002.

Mahaffy, P.R. et al., 2012, The sample analysis at mars investigation and instrument suite: Space Science Reviews, v. 170, p. 401–478, doi:10.1007/s11214-012-9879-z.

Marin-Spiotta, E., Chaopricha, N.T., Plante, A.F., Diefendorf, A.F., Mueller, C.W., Grandy, A.S., and Mason, J.A., 2014, Long-term stabilization of deep soil carbon by fire and burial during early Holocene climate change: Nature Geoscience, v. 7, p. 428–432, doi:10.1038/ngeo2169.

Matthewman, R., Cotton, L.J., Martins, Z., and Sephton, M.A., 2012, Organic geochemistry of late Jurassic paleosols (Dirt Beds) of Dorset , UK: Marine and Petroleum Geology, v. 37, p. 41–52, doi:10.1016/j.marpetgeo.2012.05.009.

Mcadam, A.., Sutter, B., Archer, P.., Franz, H.., and Eigenbrode, J.., 2020a, The chemistry and mineralogy of the Glen Torridon clay-bearing unit from Mars Science Laboratory Sample Analysis at Mars: 51st Lunar and Planetary Science Conference, v. 2243, p. 60–74.

Mcadam, A.C., Sutter, B., Archer, P.D., Franz, H.B., Wong, G.M., Lewis, J.M.T., Eigenbrode, J.L., and Stern, J.C., 2020b, Constraints on the Mineralogy and Geochemistry of Vera Rubin Ridge , Gale Crater , Mars , From Mars Science Laboratory Sample Analysis at Mars Evolved Gas Analyses: Journal of Geophysical Research : Planets, p. 1–26, doi:10.1029/2019JE006309.

Miller, K.B., McCahon, T.J., and West, R.R., 1996, Lower Permian (wolfcampian) paleosol-bearing cycles of the U.S. Midcontinent: Evidence of climatic cyclicity: Journal of Sedimentary Research, v. 66, p. 71–84, doi:10.1306/D42682B6-2B26-11D7-8648000102C1865D.

Ming, D.W. et al., 2014, Volatile and Organic Compositions of Sedimentary Rocks in Yellowknife Bay , Gale Crater , Mars: Science Express, p. 1–15, doi:10.1126/science.1245267.

Navarro-González, R., Iñiguez, E., De La Rosa, J., and McKay, C.P., 2009, Characterization of organics, microorganisms, desert soils, and mars-like soils by thermal volatilization coupled to mass spectrometry and their implications for the search for organics on mars by phoenix and future space missions: Astrobiology, v. 9, p. 703–715, doi:10.1089/ast.2008.0284.

Noe Dobrea, E.Z., McAdam, A.C., Freissinet, C., Franz, H., Belmahdi, I., Hammersley, M.R., and Stoker, C.R., 2016, Characterizing the mechanisms for the preservation of organics at the Painted Desert: Lessons for MSL, Exo-Mars, and Mars 2020: 47th Lunar and Planetary Science Conference, p. Abstract #2796.

Pavlov, A.A., Vasilyev, G., Ostryakov, V.M., Pavlov, A.K., and Mahaffy, P., 2012, Degradation of the organic molecules in the shallow subsurface of Mars due to irradiation by cosmic rays: Geophysical Research Letters, v. 39, p. 5–9, doi:10.1029/2012GL052166.

PiPujol, M.D., and Buurman, P., 1994, The distinction between ground-water gley and surface-water gley phenomena in Tertiary paleosols of the Ebro basin, NE Spain: Palaeogeography, Palaeoclimatology, Palaeoecology, v. 110, p. 103–113, doi:10.1016/0031-0182(94)90112-0.

Plante, A.F., Fernández, J.M., Haddix, M.L., Steinweg, J.M., and Conant, R.T., 2011, Biological, chemical and thermal indices of soil organic matter stability in four grassland soils: Soil Biology and Biochemistry, v. 43, p. 1051–1058, doi:10.1016/j.soilbio.2011.01.024.

Poulet, F., Gross, C., Horgan, B., Loizeau, D., Bishop, J.L., Carter, J., and Orgel, C., 2020, Mawrth Vallis, Mars: A Fascinating Place for Future In Situ Exploration: Astrobiology, v. 20, p. 1–36, doi:10.1089/ast.2019.2074.

Ramirez, R.M., Kopparapu, R., Zugger, M.E., Robinson, T.D., Freedman, R., and Kasting, J.F., 2014, Warming early Mars with CO2 and H2: Nature Geoscience, v. 7, p. 59–63, doi:10.1038/ngeo2000.

Rampe, E.., Morris, R. V, Ruff, S.W., Dehouck, E., Achilles, C.N., Ming, D.W., Bish, D.L., and Chipera, S.J., 2014, Amorphous phases on the surface of Mars: Eighth International Conference on Mars, p. 1–2.

Raynaud, X., and Nunan, N., 2014, Spatial ecology of bacteria at the microscale in soil: PLoS ONE, v. 9, doi:10.1371/journal.pone.0087217.

Reardon, P.N., Chacon, S.S., Walter, E.D., Bowden, M.E., Washton, N.M., and Kleber, M., 2016, Abiotic Protein Fragmentation by Manganese Oxide: Implications for a Mechanism to Supply Soil Biota with Oligopeptides: Environmental Science and Technology, v. 50, p. 3486–3493, doi:10.1021/acs.est.5b04622.

Retallack, G.J., 2014, Paleosols and paleoenvironments of early Mars: Geology, v. 42, p. 755–758, doi:10.1130/G35912.1.

Retallack, G.J., 2019, Soil of the Past: Wiley Blackwell.

Retallack, G.J., Bestland, E.., and Fremd, T.., 2000, Eocene and Oligocene Paleosols of Central Oregon: Geological Society of America Special Paper, v. 344, p. 1–192, doi:10.1046/j.1365-3091.2001.0394c.x.

Retallack, G.J., and Krull, E.S., 1999, Landscape ecological shift at the Permian – Triassic boundary in Antarctica: Australian Journal of Earth Sciences, v. 46, p. 785–812.

Retallack, G.J., and Mao, X., 2019, Paleoproterozoic (ca . 1 . 9 Ga) megascopic life on land in Western Australia: Palaeogeography, Palaeoclimatology, Palaeoecology, v. 532, p. 109266, doi:10.1016/j.palaeo.2019.109266.

Retallack, G.J., Wynn, J.G., and Fremd, T.J., 2004, Glacial-interglacial-scale paleoclimatic change without large ice sheets in the Oligocene of central Oregon: Geology, v. 32, p. 297–300, doi:10.1130/G20247.1.

Rye, R., and Holland, H., 2000, Life associated with a 2 . 76 Ga ephemeral pond ?: Evidence from Mount Roe # 2 paleosol: Geology, v. 28, p. 483–486, doi:10.1130/0091-7613(2000)28<483:LAWAGE>2.0.CO;2.

Schmidt, M.W.I. et al., 2011, Persistence of soil organic matter as an ecosystem property: Nature, doi:10.1038/nature10386.

Sheldon, N.D., Retallack, G.J., and Tanaka, S., 2002, Geochemical Climofunctions from North American Soils and Application to Paleosols across the Eocene - Oligocene Boundary in Oregon Geochemical Climofunctions from North American Soils and Application to Paleosols across the Eocene-Oligocene Boundary in Or: The Journal of Geology, v. 110, p. 687–696, doi:10.1086/342865.

Sickman, J.O., DiGiorgio, C.L., Davisson, M.L., Lucero, D.M., and Bergamaschi, B., 2010, Identifying sources of dissolved organic carbon in agriculturally dominated rivers using

radiocarbon age dating: Sacramento-San Joaquin River Basin, California: Biogeochemistry, v. 99, p. 79–96, doi:10.1007/s10533-009-9391-z.

Silva, L.C.R., Corrêa, R.S., Doane, T.A., Pereira, E.I.P., Horwath, W.R., Silva, L.C.R., Corrêa, R.S., Doane, T.A., and Pereira, E.I.P., 2013, Unprecedented carbon accumulation in mined soils : the synergistic effect of resource input and plant species invasion: Ecological Applications, v. 23, p. 1345–1356, doi:10.1890/12-1957.1.

Smith, R.., Horgan, B., Rampe, E., and Dehouck, E., 2018a, The Composition of Amorphous Phases in Soils and Sediments on Earth and Mars: 49th Lunar and Planetary Science Conference 2018, p. 14–15.

Smith, R.J., Rampe, E.B., Horgan, B.H.N., and Dehouck, E., 2018b, Deriving Amorphous Component Abundance and Composition of Rocks and Sediments on Earth and Mars: Journal of Geophysical Research: Planets, v. 123, p. 2485–2505, doi:10.1029/2018JE005612.

Stern, J.C., Sutter, B., Freissinet, C., Navarro-González, R., Mckay, C.., and Archer, P.D., 2015, Evidence for indigenous nitrogen in sedimentary and aeolian deposits from the Curiosity rover investigations at Gale ...: PNAS, doi:10.1073/pnas.1420932112.

Sutter, B., Boynton, W. V., Ming, D.W., Niles, P.B., Morris, R. V., Golden, D.C., Lauer, H. V., Fellows, C., Hamara, D.K., and Mertzman, S.A., 2012, The detection of carbonate in the martian soil at the Phoenix Landing site: A laboratory investigation and comparison with the Thermal and Evolved Gas Analyzer (TEGA) data: Icarus, v. 218, p. 290–296, doi:10.1016/j.icarus.2011.12.002.

Sutter, B., Mcadam, A.., Mahaffy, P.., Ming, D.., Edgett, K.., Rampe, E.., Eigenbrode, J.., Franz, H.., and Freissinet, C., 2017, Evolved gas analyses of sedimentary rocks and eolian sediment in Gale Crater, Mars: Results of the Curiosity rover's sample analysis at Mars instrument from Yellowknife Bay to the Namib Dune: Journal of Geophysical Research : Planets, p. 2574–2609, doi:10.1002/2016JE005225.

Sweeney, K.E., Roering, J.J., and Ellis, C., 2015, Experimental evidence for hillslope control of landscape scale: Science, v. 349, p. 51–53, doi:10.1126/science.aab0017.

Szopa, C. et al., 2020, First Detections of Dichlorobenzene Isomers and Trichloromethylpropane from Organic Matter Indigenous to Mars Mudstone in Gale Crater , Mars : Results from the Sample Analysis at Mars Instrument Onboard the Curiosity Rover: v. 20, p. 292–306, doi:10.1089/ast.2018.1908.

Viviano-Beck, C.E. et al., 2014, Revised CRISM spectral parameters and summary products based on the currently detected mineral diversity on Mars: Journal of Geophysical Research: Planets, v. 119, p. 1403–1431, doi:10.1002/2014JE004627.

Watanabe, Y., Martin, J.E.., and Ohmoto, H., 2000, Geochemical evidence for terrestrial ecosystems 2.6 billion years ago: Nature, v. 408, doi:10.1038/35046052.

Watanabe, Y., Stewart, B.W., and Ohmoto, H., 2004, Organic- and carbonate-rich soil formation ~2.6 billion years ago at Schagen, East Transvaal district, South Africa: Geochimica et Cosmochimica Acta, v. 68, p. 2129–2151, doi:10.1016/j.gca.2003.10.036.

Ye, B., and Michalski, J.R., 2021, Precipitation-Driven Pedogenic Weathering of Volcaniclastics on Early Mars: Geophysical Research Letters, v. 48, p. 1–10, doi:10.1029/2020GL091551.

Zech, M., Kreutzer, S., Zech, R., Goslar, T., Meszner, S., Mcintyre, C., Häggi, C., Eglinton, T., Faust, D., and Fuchs, M., 2017, Comparative 14C and OSL dating of loess-paleosol sequences to evaluate post-depositional contamination of n-alkane biomarkers: Quaternary Research, v. 87, p. 180–189, doi:10.1017/qua.2016.7.

CHAPTER V

DISSERTATION CONCLUSION

The objectives of this dissertation were to a) identify the factors that have led to enhanced preservation of organic matter in terrestrial paleosols from throughout Earth's 3.7 billion year old geological record; b) determine if the mineralogy and alteration history of Eocene (33 million-year-old) paleosols from eastern Oregon can be identified with Mars rover-like instruments; and c) determine if trace amounts of organic carbon in the Oregon paleosols can be detected with evolved gas analysis (EGA), a technique currently employed by the NASA *Curiosity* Mars Rover to search for past signs of life on Mars. First, a data compilation of previously published organic matter content of paleosols spanning ~3 billion years of Earth history showed that soil redox state before burial was a major factor that led to enhanced preservation of organic matter in paleosols. However, clay mineralogy, amorphous phase abundance, diagenetic alteration and sulfur content were all determined to be significant factors related to the preservation of organic carbon.

Next, evolved gas analysis, visible/near-infrared (VNIR) spectroscopy, and x-ray diffraction (XRD) were found to be suitable techniques for constraining the mineralogy and alteration history of 33-million-year-old paleosols from Oregon. For a detailed comparison with Mars, the Earth-based evolved gas instrument used in this work was calibrated to operate like the Sample Analysis at Mars Evolved Gas Analysis (SAM-EGA) instrument onboard *Curiosity* Mars Rover. Pedogenic features identified with these techniques included mixtures of dioctahedral Al and Fe smectites (nontronite and montmorillonite); a clay mineral doublet feature observed with VNIR spectroscopy, possibly resulting from isomorphous substitutions within the crystalline structure of clay minerals; abundant microcrystalline hematite; destruction of sedimentary/primary bedding features; sub-meter scale differences in composition and color; and illuvial accumulation of clay minerals into subsurface horizons, all of which resulted from sustained (10^3-10^5 year) precipitation-driven pedogenic weathering of andesitic to rhyodacitic volcanic ash and tuff.

Diagenetic features observed with SAM-EGA, VNIR and XRD in paleosols included: 1) drab green surface horizons due to burial gleization of organic matter; 2) brick-red color from burial-induced dehydration of ferric oxides and hydroxides; 3) zeolitization of volcanic glass and/or poorly crystalline phases; and 4) significant mechanical compaction from burial by ~2 km of overburden. Results from this Chapter can help distinguish pedogenic weathering on Mars from other forms of aqueous alteration and diagenesis, as well as aid in current and future efforts to identify putative weathering profiles on Mars.

Finally, when the organic fraction of several Oregon paleosols were examined with EGA, very low amounts of organic carbon (~0.01 wt. %) in several samples were able to be quantified. Radiocarbon dating of bulk paleosol samples was followed by application of a two-endmember isotopic mixing model for radiocarbon activity. These techniques showed that the paleosol organic matter pool was likely composed of small amounts (0.5-3 %) of modern organic carbon. A source of this radiocarbon could have been leaching of dissolved organic carbon from the modern weathering zone that overlies the lithified, brick-like paleosol outcrops. This implies that paleosols may also contain a large fraction of ancient, radiocarbon-dead organic matter, but it is challenging to determine whether all of the ancient carbon has been preserved since soil formation and burial ~33 million years ago. Although the sources of paleosol organic carbon remain unclear in this work, the detection of trace amounts of organic carbon with a SAM-EGA analog instrument, whether that carbon is ancient or modern, suggests that this technique is suitable for detecting low levels of organic carbon in putative martian paleosols. In the case of encountering a strongly oxidized paleosol candidate on Mars (e.g., rich in Fe oxides), which are considered less-than-ideal targets for biosignature preservation relative to reduced paleoenvironments (e.g., rich in Fe^{2+} clay minerals), a SAM-EGA like instrument would presumably be able to detect trace amounts (<0.01 wt. %) of organic carbon if they were present in samples.

A major finding of this dissertation is that the near-surface horizons of terrestrial paleosols appear to be a favorable location for SAM-EGA detection of organic carbon. Like modern soils, the surface layers of Mars-analog paleosols examined here show evidence of surface enrichment of organic carbon because the ancient surface layers of each of the three soils had significantly higher organic carbon

content relative to deeper layers. Although the early diagenetic process of burial decomposition of organic matter has likely reduced the organic carbon content of these ancient soils by at least two orders of magnitude relative to modern soils, the enrichment of organic carbon in surface horizons (~0.03 wt. %) and subsequent depletion in deeper layers (<0.01 wt. %) was readily observable with a SAM-EGA analog instrument.

This work also provides an initial framework for investigation and sampling of martian weathering profiles should they be encountered by current or future landed missions. If possible, future *in-situ* analysis of putative weathering profiles should begin at the apparent ancient surface horizon (e.g., the buried topsoil layer) and sample down section into the unaltered protolith, similar to the sampling of a terrestrial soil profile. If the entire profile is not accessible for investigation (e.g., outcrop is at a topographic position inaccessible to the rover), the near-surface horizons of the profile, just below the overlying burial layer, should be considered the highest priority target for remote sensing, contact science, and collection of a drilled sample for sample return to Earth.

APPENDIX A

SUPPLEMENTAL MATERIAL FOR CHAPTER II

Table S1. Mars-relevant observable pedogenic features

Feature	Origin	Observability†	Preservation ‡	Interpretation ʊ
Morphological				
Sharp bedded top or massive bed	Rapid sedimentation (burial)	In-situ	Good	Rapid burial of uppermost soil layer
Disrupted and veined beds	Pedogenic haploidization	In-situ	Good	Pedogenic mixing by shrink and swell in surface (A) horizon
Ptygmatic folding of crack	Pedogenic negative strain	In-situ	Good	Volume loss by weathering or compaction by overburden
Vesicular structure	Pedogenic gas production	In-situ	Good	Potential microbial gas production in saturated soil
Gypsum nodules	Pedogenic salinization	In-situ	Poor	Acid-sulfate weathering of leaching of water-soluble salts to subsurface (By) horizon
Calcite nodules	Pedogenic calcification	In-situ	Poor	Accumulation of acid-soluble salts below weathered surface to calcic (Bk) horizon
Pyrite nodules	Pedogenic pyritization	In-situ	Good	Potential microbial sulfate reduction in gleyed subsurface (Bg) horizon
Periglacial features	Surface freeze and thaw	In-situ	Good	Sand or ice-filled frost fissure in soil surface (A) horizon
Gradational horizonation	Chemical weathering	In-situ	Good	Prolonged subaerial top-down leaching of sediments

Relict beds or basalt below massive bed	Remnants of unweathered parent rock	In-situ	Good	Parent materials of C horizon not yet obliterated by soil formation
Chemical				
Molar weathering depletion (mass transfer)	Mass loss of weatherable soil components	In-situ	Good	Removal of individual weatherable elements
Phosphorus depletion	Microbial activity in surface horizons	In-situ	Good	Potential biological utilization of phosphorus minerals
Chemical index of alteration	Changing ratio of alumina to bases	In-situ	Good	Metric for progress of hydrolytic weathering
Surface enrichment of reduced carbon	Biological activity or meteoritic infall	In-situ	Poor	Potential biological production or carbonaceous meteoritic dust
Mineralogical				
Dioctahedral phyllosilicates	Pedogenic alteration	In-situ, orbital	Good	Subaerial weathering with liquid water
Repeating layered phyllosilicate sequences	Successive soil development and burial	In-situ, orbital	Good	Potential sequences of superimposed paleosols
Hydrated amorphous phases	Alteration of vitric volcanic ash	In-situ, orbital	Good	Common phases in volcaniclastic soils and paleosols

† Describes observability on the surface of Mars at different spatial scales

‡ Describes scale of features and modes of detection

ʊ Pedological interpretation of features

APPENDIX B

SUPPLEMENTAL MATERIAL FOR CHAPTER IV

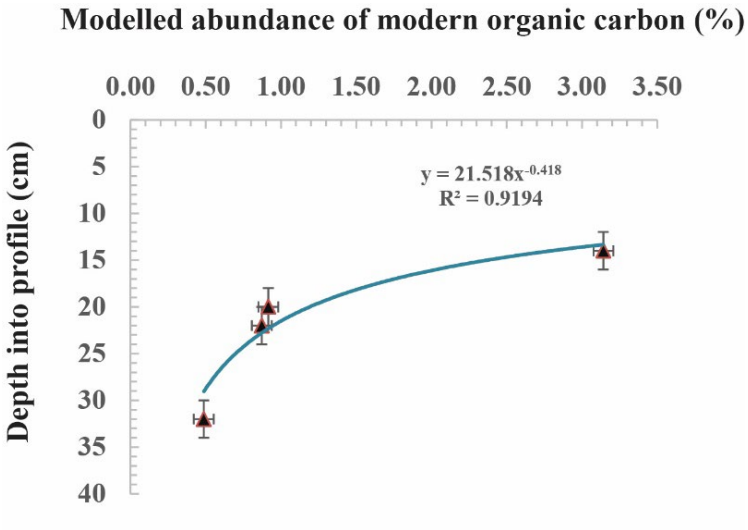

Figure S1. The modelled amount of modern organic carbon in bulk paleosol samples as a function of depth into the profile (outcrop). Note that depth refers to the horizontal depth into the outcrop where samples were taken from rather than the vertical depth in the stratigraphic section (see Methods)

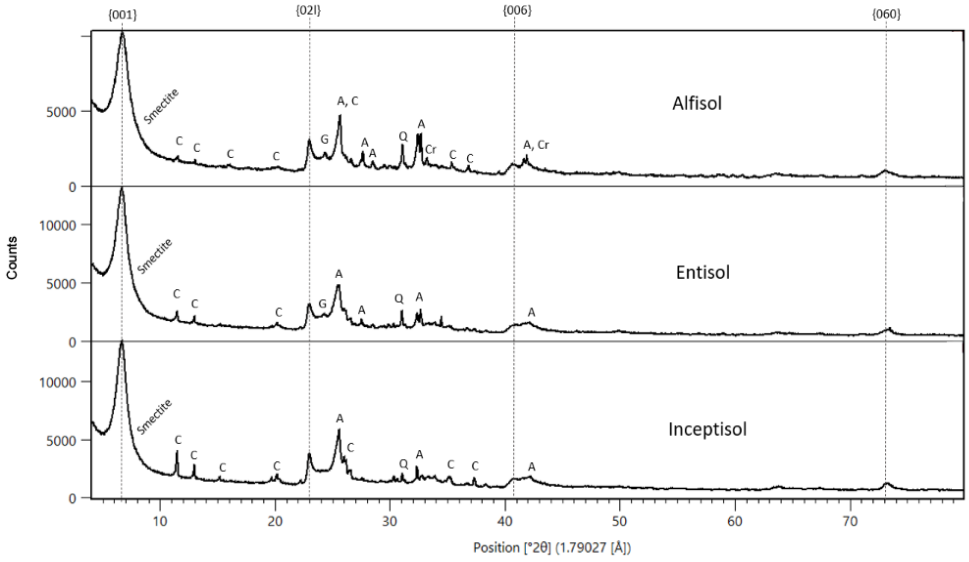

Figure S2. **X-ray diffraction patterns from the near surface (A-horizon) of three paleosols from the early Oligocene (33 Ma) middle Big Basin Member of the John Day Formation in eastern Oregon, USA. S=Smectite; G=Gypsum; A=Andesine; C=Clinoptilolite; Cr=Cristobalite; Q=Quartz.** Highlighted are the 001 and 02l smectite peaks; difference in 02l band position corresponds to a difference in octahedral occupancy.

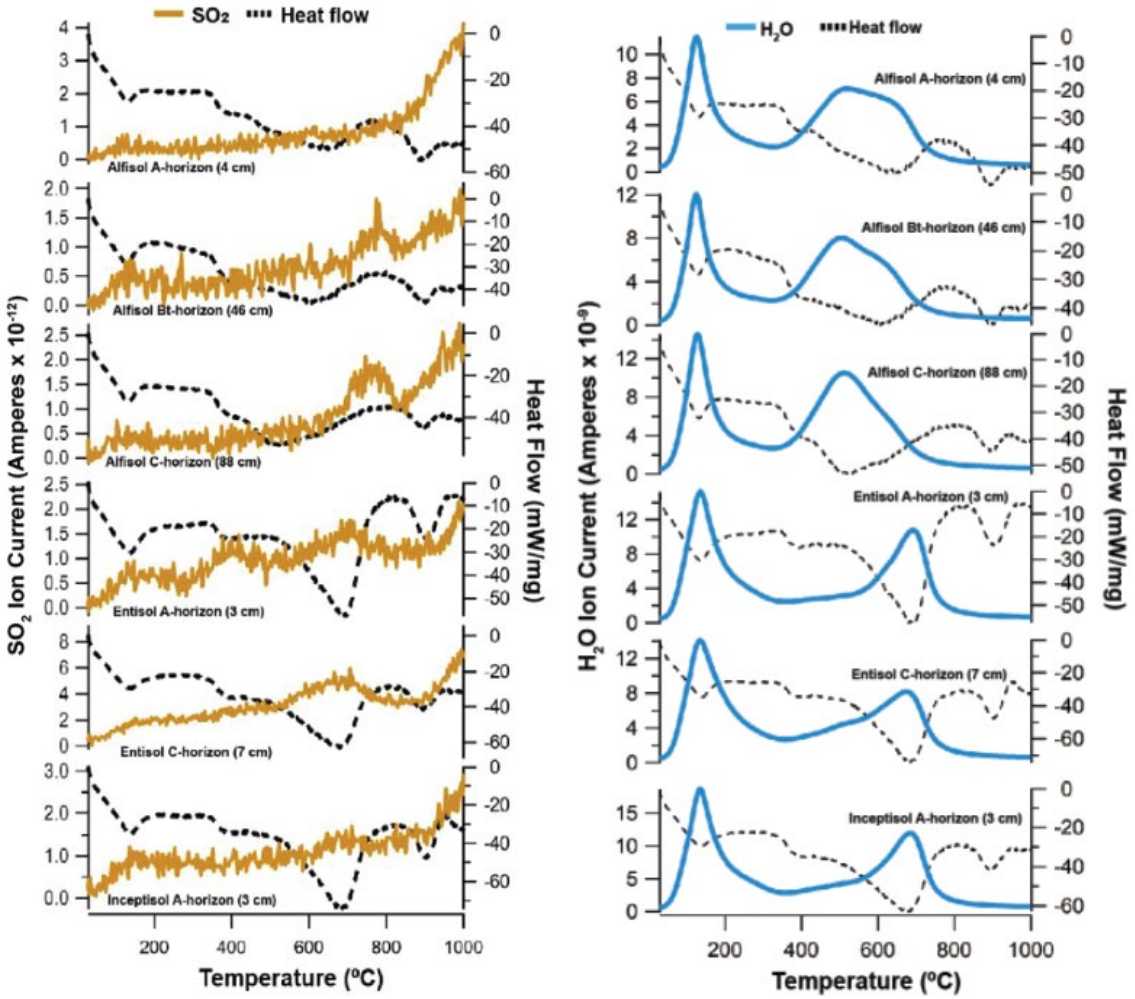

Figure S3. **Evolutions of SO_2 and H_2O from early Oligocene (33 Ma) paleosols from the John Day Fossil Beds National Monument, Oregon.** Yellow trace is SO_2 (m/z 64), blue trace is H_2O (m/z 18) and dashed trace is heat flow from differential scanning calorimetry (DSC). All analyses were conducted using helium as a carrier gas.

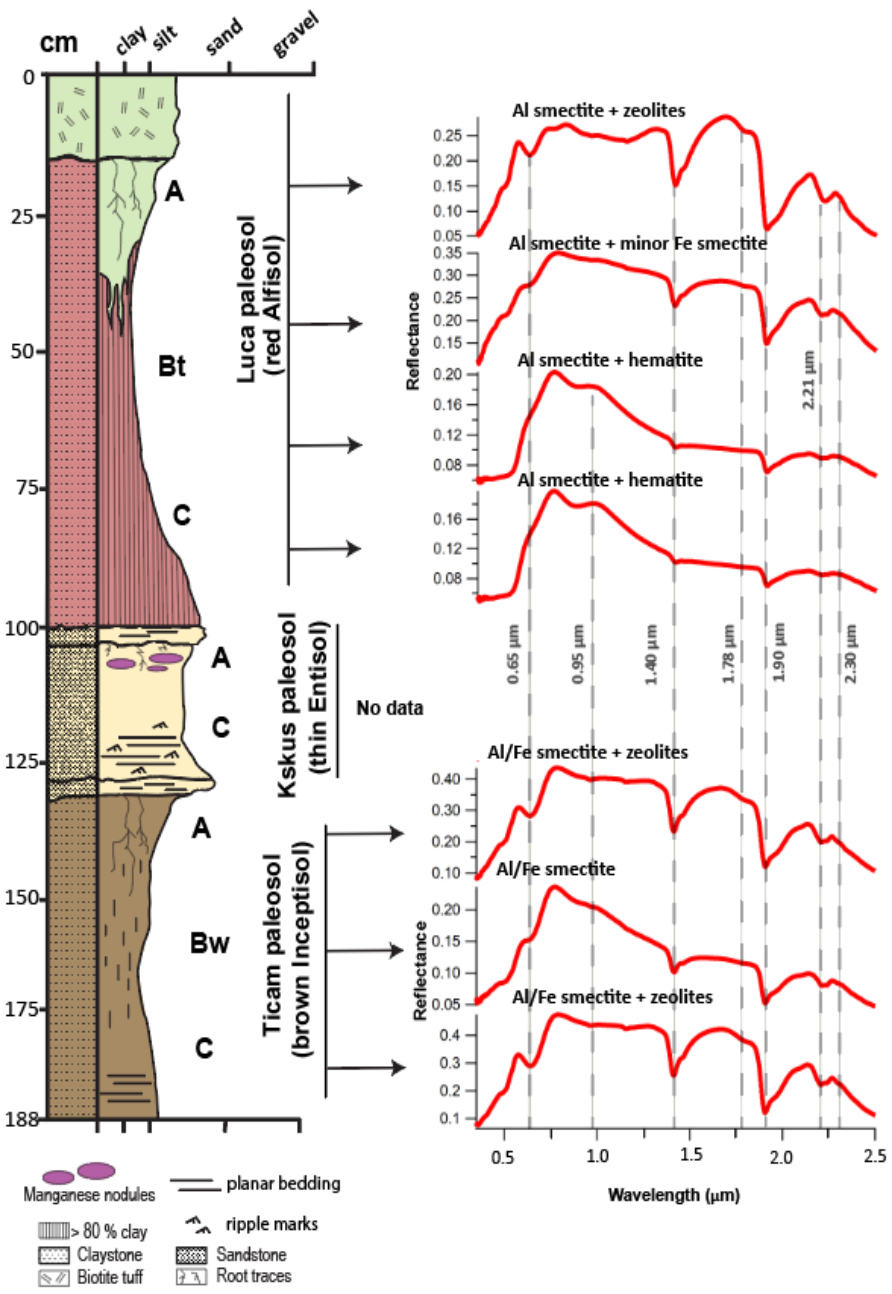

Figure S4. **Visible/near infrared reflectance (VNIR) spectra of two paleosols (Alfisol and Inceptisol) from the early Oligocene (33 Ma) middle Big Basin Member of the John Day Formation in eastern Oregon, USA**.

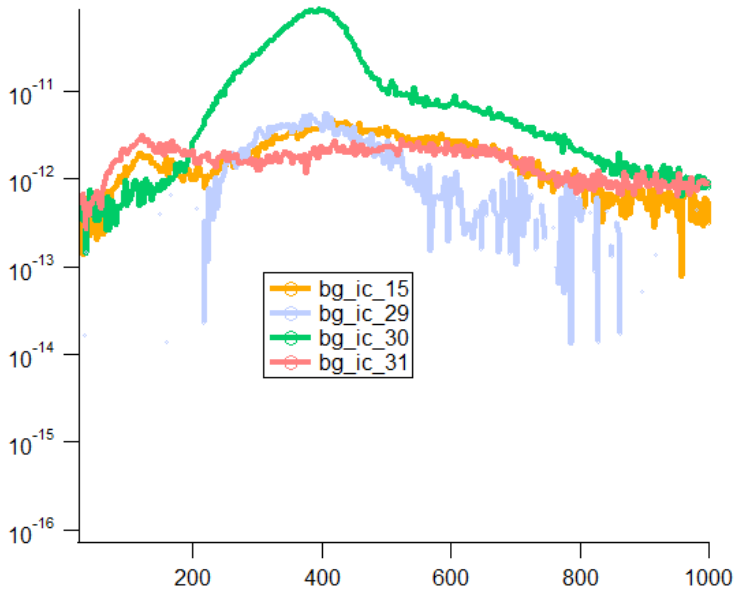

Figure S5. **Semi-log plot of the surface horizon (4 cm) of the Alfisol showing evolutions of *m/z* 15, 29, 30 and 31 (right).**

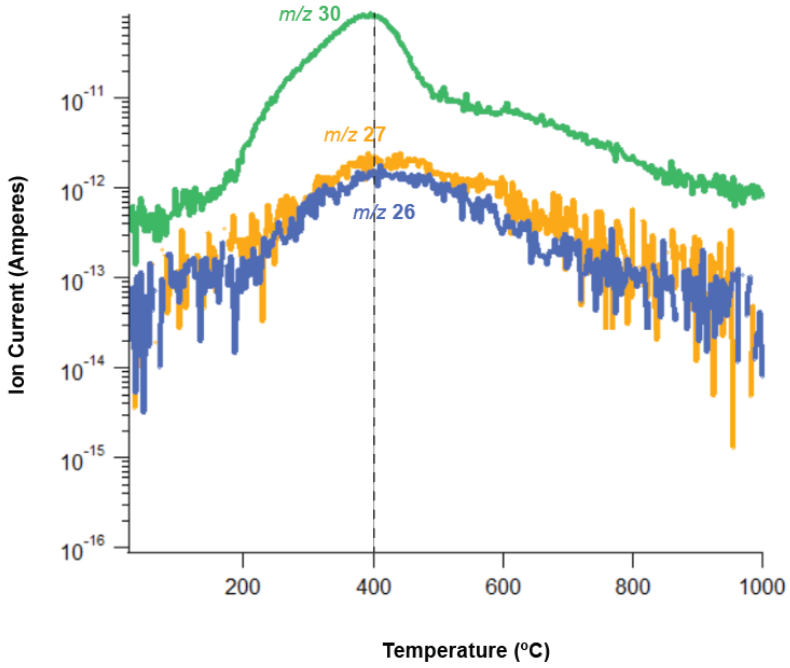

Figure S6. Semi-log plot showing evolutions of HCN (*m/z* 27, 26) and *m/z* 30 in the surface horizon (4 cm) of the Alfisol.